Application of Power to Gas (P2G) Systems in Danish Electric Distribution Networks

Aina Romaní Dalmau and David Martínez Pérez

MSc Thesis – Department of Energy Technology

Spring semester 2015

AALBORG UNIVERSITY
STUDENT REPORT

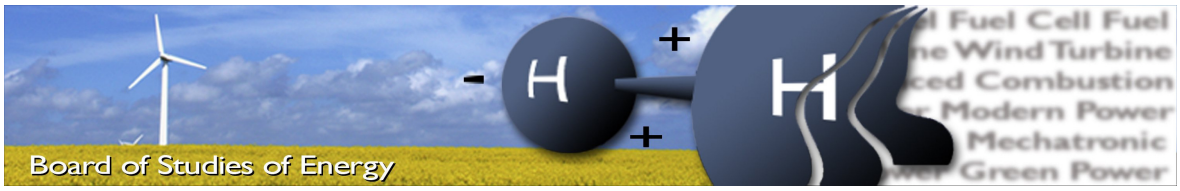

Title:	Application of Power to Gas (P2G) Systems in Danish Electric Distribution Networks
Semester:	3rd and 4th
Project period:	Master's Thesis
ECTS:	01/09/14 - 27/05/15
Supervisors:	Jayakrishnan Radhakrishna Pillai and Iker Diaz de Zerio Mendaza
Project group:	EPSH4-933

David Martínez Pérez

Aina Romaní Dalmau

Copies:	3
Pages, total:	152
Appendices:	A, B, C & D
Supplements:	CD

SYNOPSIS:

According to the latest energy policy, wind power share is expected to increase in order to allow Denmark to become fossil fuel free by 2050. This high wind power penetration is expected to introduce several challenges into the power system, such as large power imbalances or voltage rise. In order to tackle these issues, energy storage systems represent a possible solution for absorbing the wind power excess. Concerning the Danish case, the state-of-the art district heating and gas networks comprise perfect energy storage solutions. In this context, Power to Gas turns out to be an interesting option in order to inject the electricity excess into the gas network. This system is based on transformation of electricity to hydrogen by use of electrolyzers. The produced hydrogen can be directly injected into the gas grid or transformed into natural gas in an intermediate step. The present MSc Thesis focuses on testing the capability of an alkaline electrolyzer to deliver voltage regulation and energy management services to a typical Danish distribution grid with a high wind power penetration. The electrolyzer is integrated with the typical voltage regulation assets present in a distribution grid. One of the main targets of this project is to find a control strategy where the mentioned voltage regulation and energy management services coexist in a market environment.

By signing this document, each member of the group confirms that all participated in the project work and thereby all members are collectively liable for the content of the report. Furthermore, all group members confirm that the report does not include plagiarism.

Preface

This report has been written by group EPSH4-933 on the 3^{rd} and 4^{th} semester at the Department of Energy Technology at Aalborg University in the period from the 2nd of September 2014 until the 27th of May 2015. The purpose of this project is to analyze the technical impact of integrating a P2G system in a typical Danish medium voltage grid.

We as a group would like to thank our supervisors Iker Diaz de Zerio Mendaza and Jayakrishnan Radhakrishna Pillai for their guidance, patience and support throughout the development of this project. Additionally, we would like to express our gratitude to Carolina Carmo (INSERO Energy) and Jesper Bruun (Energinet.dk) for providing us with valuable information and data.

In this project the software DIgSILENT PowerFactory has been used to simulate an electrical distribution grid and its elements. Additionally, the software Matlab has been used to analyze data and execute calculations. The present report has been written using LaTeX.

Reader's Guide The used information in the present work has been found in literature, web pages and reports. The sources are cited through the report and can be found in the Bibliography. The method for referring to these sources is the IEEE citation style, which refers to the sources with a [number] by order of appearance. All references can be found on the CD, except the used books and websites. Additionally, tables, figures and equations are labeled with the number of the chapter.

The CD attached in the report contains the PDF of the project document, the relevant PowerFactory and Matlab files and the references that were available in PDF format.

Abstract

During the recent years, Denmark has progressively increased the share of renewable energy, which is expected to cover 100% of the total consumption by 2050. In this context, the electric distribution grid is expected to accommodate a high wind power penetration, which might lead to voltage rise. In order to simultaneously tackle this issue and make use of the excess wind power, energy storage systems turn out to be a possible solution. The Danish state-of-the art district heating and gas networks comprise perfect energy carriers for the mentioned purpose. Power to Gas consists of the transformation of electricity into hydrogen by use of electrolyzers; it might become the link between the electricity and gas networks.

The aim of this work is to assess the capability of a Power to Gas system to provide voltage regulation and energy management to a typical Danish distribution grid with a high wind penetration. For this purpose, the Distribution System Operator possesses an alkaline electrolyzer, which is integrated with the typical voltage regulation assets present in a distribution grid. Additionally, a control strategy is developed in order to provide the mentioned voltage regulation and energy management services in a market environment.

For this purpose, different analysis have been carried out with the software DIgSilent PowerFactory and Matlab, which include: an assessment of the steady state operation of the case study grid, a dynamic modeling of the grid elements, different dynamic simulations and the development of a market strategy. Firstly, the steady state operation was analyzed in order to assess the limits of the grid, to coordinate the voltage regulation assets and to determine the location and sizing of the electrolysis unit; furthermore, a hydrogen bleeding strategy was proposed. Secondly, dynamic models of a wind farm, a Combined Heat and Power plant, an On-Load Tap Changer and an alkaline electrolyzer have been presented, together with a simplification of the district heating and gas networks. Afterwards, dynamic simulations have been carried out for different scenarios, in order to evaluate the grid's voltage regulation capability and coordination as well as to test the hydrogen bleeding strategy. Finally, a market strategy has been developed in order to include both voltage regulation and energy management services while participating in the electricity wholesale markets.

The steady state analysis revealed that the distributed generation lead to a voltage rise up to $1.13p.u.$ during maximum generation and minimum load conditions. After testing the different voltage regulation strategies, the size of the alkaline electrolyzer has been determined to be of $6.525MW$ in order to bring the voltage within the limits established by the grid codes. The most significant finding during the dynamic modeling of the grid elements was the capability limitation of the alkaline electrolyzer during low operational temperature. The dynamic analysis of the voltage regulation strategy of the alkaline electrolyzer eliminated over/under- voltage in all buses and decreased losses around 50%; besides, it revealed that the gas network could not accommodate all the produced hydrogen. The market strategy managed to lower the price of the produced hydrogen from 2.19 to $1.43DKK/Nm^3$ and to decrease the active power export from 38.1 to $23.3MWh$ during the simulated week, while maintaining a similar voltage quality. The observed main draw back was an increment of the imported reactive power, from 343.4 to $437.6Mvarh$.

The most important finding of this project reveals that the Distribution System Operator can decide the price to pay for using the local generation to produce hydrogen, while maintaining the voltage within limits. This implies that the Distribution System Operator can decide the amount of energy to purchase according to the grid state and market prices, due to the flexible operation

of the different voltage regulation assets. However, a cost/benefit analysis must be done in order to implement Power to Gas technology in a profitable way. With a reduction of the currently expensive costs of the technology, its application could become economically feasible and could open the possibility to new business opportunities.

List of Figures

List of Tables

Nomenclature

Symbol	Unit	Description
β	$-$	Reactive power substitution rate
γ	$-$	Ratio of the specific heat capacities of a gas
ε	$-$	Heat exchanger efficiency
η_e	$-$	Efficiency of the electrolyzer
η_F	$-$	Faraday electrolysis efficiency
μ	$-$	Membership function
μ	$-$	Normal distribution average
ρ	kg/m^3	Air density
σ	$-$	Normal distribution typical deviation
ω	rad/s	Rotational speed
C_{max}	$W/°C$	Maximum heta capacity rate
C_{min}	$W/°C$	Minimum heta capacity rate
C_p	$-$	Performance coefficient
C_{p_cool}	$J/kg \cdot °C$	Specific heat of the cooling liquid
C_{p_e}	$J/kg \cdot °C$	Specific heat of the electrolyte
$C_{p_{H_2}}$	$J/kg \cdot °C$	Specific heat of hydrogen
C_r	$-$	Heat capacity ratio
C_t	m^2	Thermal capacitance of the electrolyzer
F	C/mol	Faraday constant
I	A	DC current in the electrolyzer
I_{xy}	A	Line current from bus x to y
J	s	Inertia
m_e	kg/s	Mass flow rate of the electrolyte
M_H	g/mol	Molar mass of hydrogen
m_{H_2}	kg/s	Hydrogen mass flow rate
n_c	$-$	Number of cells in the electrolyzer
n_{H_2}	mol/s	Production rate of hydrogen
P_i	bar	Pressure
P_{com}	W	Active power of the compressor
P_e	W	Active power of the electrolyzer
P_x	W	Active power of load X
PF	$-$	Power factor
Q_{com}	Var	Reactive power of the compressor
Q_{cool}	W	Heat demand for cooling
Q_{gen}	W	Internal heat generation of the electrolyzer
Q_{loss}	W	Total heat loss
Q_{max}	W	Maximum theoretical heat demand
Q_x	Var	Reactive power of load X
S	VA	Apparent power
T_i	$°C$	Temperature
T_{amb}	$°C$	Ambient temperature
T_e	$°C$	Temperature of the electrolyte
U	V	Voltage
u	$-$	Numerical output after defuzzification
U_{cell}	V	Voltage of the electrolyzer cell

U_e	V	Voltage of the electrolyzer
U_{rev}	V	Reversible voltage
U_{th}	V	Voltage threshold for the heat release process
v	m/s	Wind speed
V_{DG}	V	Voltage at the PCC of the DG
$\dot{V}$	Nm^3/h	Volume flow
V_n	V	Nominal voltage
V_x	V	Voltage of bus X
W_i	J/kg	Energy rate of the heat exchange
z	$-$	Number of electrons transferred in the reaction
Z_{xy}	Ω	Impedance of the line from bus x to y

Abbreviation	Description
AC	Alternate Current
AE	Alkaline Electrolyzer
$BESS$	Battery Energy Storage System
BRP	Balance Responsible Parties
CHP	Combined Heat and Power
CO_2	Carbon dioxide
DC	Direct Current
DG	Distributed Generation
$DFIG$	Doubly-Fed Induction Generator
DKK	Danish Krone
DPL	DIgSilent Programming Language
DSL	DIgSilent Simulation Language
DSM	Demand Side Management
DSO	Distribution System Operator
EHP	Electrical Heat Pumps
EM	Energy Management
ESS	Energy Storage System
EU	European Union
EV	Electrical Vehicle
$HRSG$	Heat Recovery Steam Generator
KOH	Potassium Hydroxide
LDC	Line Drop Compensation
MP	Minimum Power
M/R	Metering and Regulation
MV	Medium Voltage
OHL	Overhead line
$OLTC$	On-load tap changer
P	Proportional
$P2G$	Power to Gas
PCC	Point of Common Coupling
PEM	Proton Exchange Membrane
PF	Power Factor
PHS	Pumped Hydro Storage
PI	Proportional Integral
PID	Proportional Integral Derivative
PV	Photovoltaic
RES	Renewable Energy Sources
$SCADA$	System Control And Data Acquisition
SNG	Synthetic Natural Gas
SOC	State Of Charge
SOE	Solid Oxide Electrolyzer
SSM	Supply Side Management
TRF	Transformer
TSO	Transmission System Operator
VR	Voltage Regulation
VSC	Voltage Source Converter
$V2G$	Vehicle to Grid
WT	Wind Turbine
YSZ	Yttria-Stabilized Zirconia

Contents

1 Introduction

In this chapter the investigation done is contextualized, and the most relevant topics are presented. A short review introduces the current situation of renewable energy and discusses the possible solutions for their extensive implementation. The scope is further focused on the Power-to-Gas technology, as a promising storage in the Danish energy system. Besides, a literature review concerning the technical applications of this technology is presented. Subsequently, the scope and objectives of the project are stated, followed by the used methodology to solve the presented issues and finally the outline of the thesis.

1.1 Background

During the 20th century, energy demand has been covered by the relatively cheap and available fossil fuels. Nevertheless, the growing energy demand together with the increasing fuel prices are expected to bring along price uncertainty and dependence in countries without fuel resources. In this context, the Danish government has developed an energy strategy with the main target to become fossil fuel free by 2050, which also responds according to the growing international concern about CO_2 emissions and climate change [1].

According to this plan, Denmark has set the goal of covering half of its consumption with wind power by 2020. However, the intermittent nature of the wind will lead to the introduction of several challenges into the power system. Figure 1.1 shows an illustration that exemplifies the system imbalances for both present and 2050 scenarios.

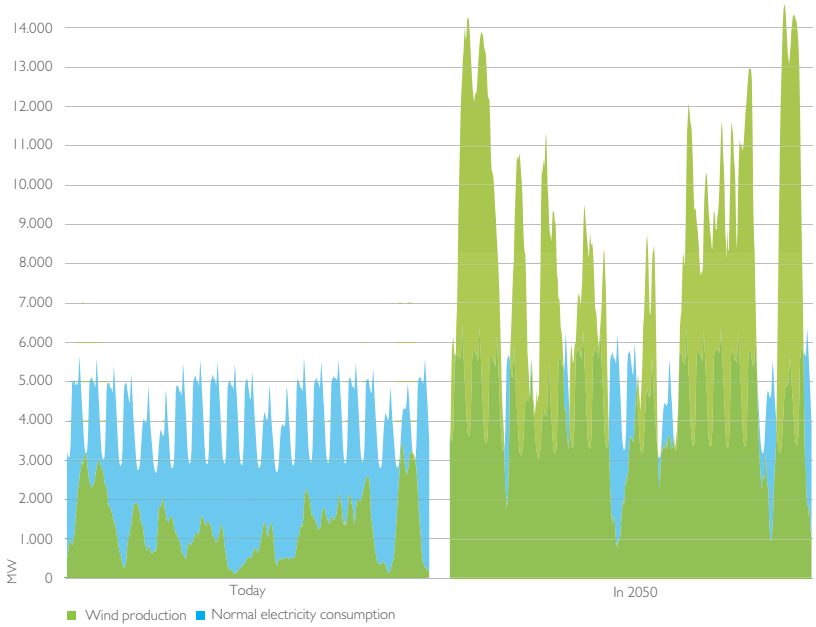

Figure 1.1: Wind power and load profile for the present and for 2050 in Denmark [2]

As it can be appreciated in some periods of the 2050 scenario, the wind power generation is expected to surpass the total consumption at the transmission level. Nowadays, according to [2], wind production exceeds demand around 100 hours/year, which is expected to significantly increase in the 2050 scenario. In the context of power regulation, the challenge is how to compensate the error between forecasted and actual wind power, which is around 7% for hour-ahead forecasts [3]. As wind power generation is expected to increase, as depicted in Figure 1.1, this will

lead to a bigger requirement of regulation power and reserve capacity by the Danish Transmission System Operator (TSO), Energinet.dk. Traditionally, in Denmark, regulation power has been supplied by dispatchable large-scale and small-scale Combined Heat and Power (CHP) plants and, mainly, international connections [2]. However, the decommissioning of the large-scale units will lead to a further decrease in the capacity of the reserves.

From the electric distribution level point of view, an increase of consumption and local production is expected. It is predicted that end users will replace their oil-fired boilers with heat pumps, their combustion engine cars by EVs and install solar panels on their roofs. This fact will lead to increased power flows in the medium and low voltage grids, specially during peak demand or low demand and high production periods, which could lead to line congestion and voltage issues. Furthermore, voltage rise in the Point of Common Coupling (PCC) of wind farms could be an additional issue when large units are connected to the distribution level. The presented problems have to be dealt by the Distribution System Operators (DSOs), who would have to invest in grid reinforcements. Figure 1.2 shows a combination of four different solutions in order to deal with the mentioned issues at both transmission and distribution level.

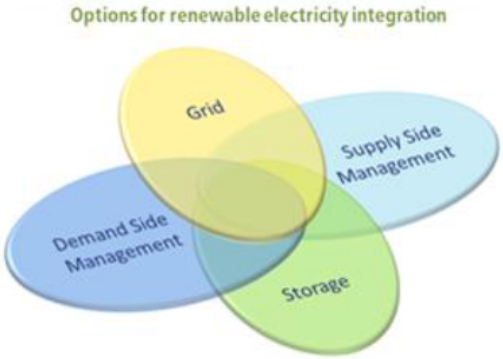

Figure 1.2: Possible solutions for the integration of Renewable Energy Systems (RES) [4]

One of the possible solutions, according to [4], is a reinforcement of grid interconnections. In that way, the reduction of line congestion can flatter prices, whereas reinforcing the weaker distribution grids can avoid line overloading. However, grid expansion requires high investments and a very long implementation process. Besides, it has been predicted that grid expansion cannot comprise a unique way to tackle the forthcoming challenges.

Demand Side Management (DSM) is another possible solution. It consists of adapting the customer's energy behavior depending on the condition of the grid. Load shifting from peak to off-peak periods will lead to a better utilization of the distribution capacity. Furthermore, the implementation of time varying prices, can lead to balance the overall system. The disadvantage is in the limited DSM capability, even considering the further implementation of electric vehicles (EV's) and heat pumps [4].

Another presented solution is Supply Side Management (SSM), which consists of enhancing the flexibility of power units in terms of frequent start-up and shutdown or quick response. Gas-fired power plants are the best suited to meet these requirements. However, this solution requires the modification of the existing power plants, and thus, requires a big investment.

Finally, Energy Storage Systems (ESS) appears to be a promising way to complement the previous three by matching generation with consumption and adding value to the excess of renewable energy [4]. They offer excellent capabilities, although they require a remarkable investment. Among the different large scale storage technologies available nowadays, Figure 1.3 and Figure 1.4 show their technical performance and the economical potential.

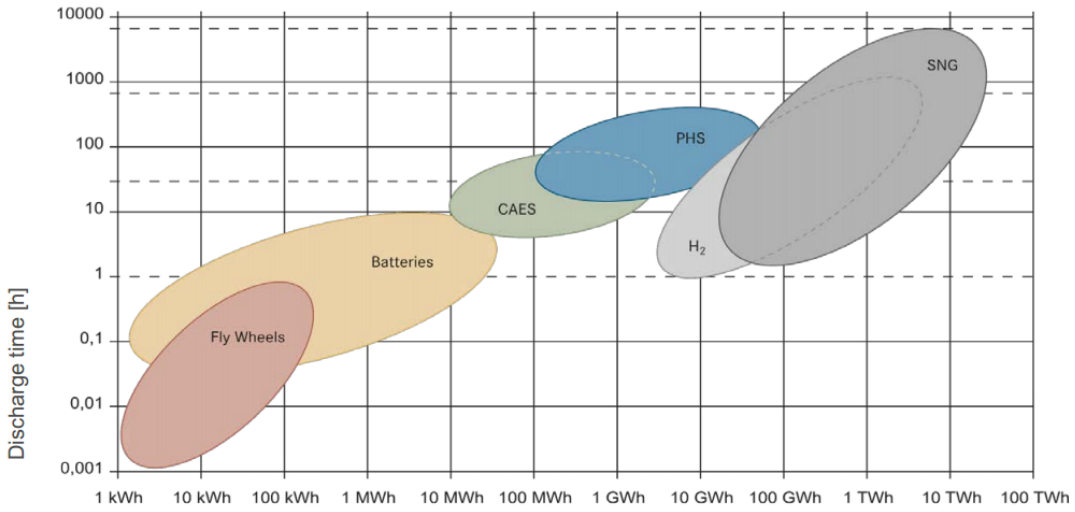

Figure 1.3: Technical comparison for both power and capacity of the different ESS [4]

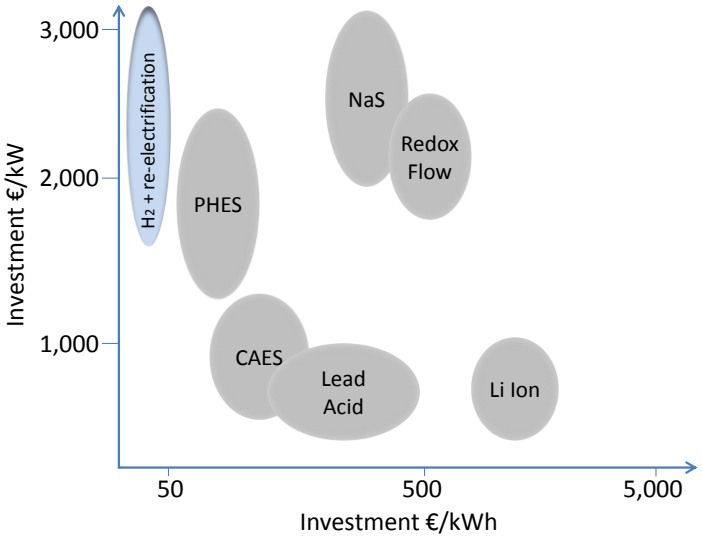

Figure 1.4: Economical comparison of the capacity of the different ESS [4]

According to [4], the technologies that have higher potential for long term storage regarding capability and investment are Power-to-Gas (P2G), synthetic natural gas (SNG), and pumped hydro storage (PHS). PHS is a mature technology and comprises the largest capacity among the ESS in Europe, although its implementation in Denmark is unfeasible due to geographical reasons. P2G is currently at research status and has a few implementations, mainly in Germany [5]. Nowadays the efficiency of P2G conversion is around 60%. Nevertheless, the attention gained lately by this technology responds to the high flexibility in the hydrogen management. Some examples of hydrogen management are re-electrification with fuel cells or gas turbines, utilization in industry and transport sectors, injection into the gas grid and conversion to synthetic natural gas (methane). However, the available technology presents some limitations regarding low re-electrification efficiency, which is around 40%, and the limited amount of hydrogen that the gas turbines and gas network can accommodate.

Furthermore, authors in [6] state that the current technology is not economically feasible today and it will probably not be, at least, before 2032. In order to make P2G more economically feasible, an improvement of the mentioned issues has to be achieved, which will suppose a technological

challenge [5] [4].

The implementation of P2G systems has already been addressed, mainly including a hydrogen storage and a fuel cell as the re-electrification carrier. [7] lists the opportunities of this technology in both isolated and distribution grids. Isolated systems based only on hydrogen and intermittent resources are able to run in a reliable way due to the hydrogen's long-term storage capacity, replacing the traditional diesel generators. The wind-H_2 system in the island of Utsira (Norway) is a good example of this application [8]. Moreover, authors in [9] included a supercapacitor in their wind-H_2 stand-alone system in order to mitigate wind power fast fluctuations that electrolyzer and fuel cell were not able to balance due to their limited dynamics. The same approach was taken by authors in [10], using a battery storage system (BESS) instead of the supercapacitor.

Regarding the opportunities in distribution grids, [7] states that the hydrogen application is less evident since the external grid provides the power to balance the local grid. Nevertheless, areas with large wind farms connected to rather weak grids could suffer active power curtailment [11], which could be avoided by means of a hydrogen storage system. In this context, authors in [12] formulate a power management control in order to obtain a desired active and reactive power output from a wind farm, obtaining an active dispatch out of an inherently passive generator.

Concerning the Danish case, the well developed gas network together with the upcoming wind power increase make a perfect scenario for the implementation of P2G technology. There is a unique potential of coupling the electricity system with the gas and district heating grids, as further explained in Section 2.3. The surplus of wind power can be converted into hydrogen using electrolyzers, which can be later injected into the gas network. The existing gas turbine CHP plants could use this hydrogen in order to convert it to both electricity and heat, being an alternative to the previously mentioned fuel cells as the re-electrification carrier.

Therefore the focus of this project is analyzing the possibility of DSOs to utilize a P2G system for energy management and voltage support purposes, injecting the produced hydrogen in the gas network. The term energy management is defined in this work as making use of the locally produced electricity, transforming it into hydrogen. Furthermore, DSOs which supply both electricity and gas to their customers, such as DONG Energy, could make a smart use of the electrolyzers. With the target of producing cheap hydrogen taking advantage of favorable spot market prices, electrolyzers could simultaneously deal with voltage issues from a congestioned distribution grid. An existing example of this application is VERDO, a Danish DSO that currently possesses a an electrolyzer. However, the hydrogen that is produced in this P2G plant is used in the metallurgic industry of the area.

1.2 Problem Formulation

The scope of this project is to analyze the technical impact of integrating electrolyzers in a typical Danish medium voltage grid. The analyzed scenario includes large wind power penetration and a CHP plant, both leading to power quality issues such as overvoltage at their Point of Common Coupling (PCC). These issues present disadvantages for the DSOs, having to invest on grid reinforcement. Instead, the grid's DSO integrates an alkaline electrolyzer to solve the voltage problems and, at the same time provide energy management services by means of absorbing any excess generated power.

The main aim of the present project is to develop an operation strategy that simultaneously allows an effective voltage regulation and energy management strategies. For this purpose, the operation of the alkaline electrolyzer is to be coordinated with the rest of the voltage regulation assets of the grid. Additionally, in order to produce cheap hydrogen, the participation of these units in

the electricity wholesale markets is analyzed as part of the energy management strategy. The produced hydrogen is assumed to be injected into the natural gas network of the DSO company, limited by the volume percentage restriction in the Danish gas network. Further re-electrification or heat generation from the produced hydrogen is not in the scope of this project.

1.3 Objectives

The main aim of the project is to analyze the feasibility of implementing P2G in a distribution grid and developing a market strategy that provides both voltage regulation and energy management services. This strategy intends to use the electrolyzers in combination with typical voltage regulation assets in order to support a high penetration of wind power from a Danish wind farm. The realization of this involves the following:

- Steady state analysis of the impact of integrating one or more electrolyzers in a typical Danish medium voltage grid as a mean of energy storage.
- Development of a dynamic model of the electrolyzer to provide voltage regulation, including its operational constraints and reactive power control.
- Development of simplifications of the district heating and gas networks, in order to assess their impact in the electrical distribution grid and the feasibility of the hydrogen bleeding strategy.
- Assess the capabilities and weaknesses of the electrolyzer in providing voltage regulation.
- Integrate the alkaline electrolyzer together with the typical voltage regulation assests of a distribution grid
- Technical analysis of the electrolyzer's participation in the Elspot, Elbas and regulation markets in order to develop a sub-optimal market strategy for the electrolyzer.
- Development of an operation strategy of the P2G system that integrates the market strategy together with an effective voltage regulation and energy management.

1.4 Methodology

The main tool for the development of this project has been DIgSILENT PowerFactory. Firstly, the steady state analysis of the case study grid has been realized in this program, performing load flow simulations which use Newton Raphson as a calculation method. The development of the dynamic models of several grid elements has also been implemented using this tool, employing DSL modules. Finally, RMS simulations have been utilized to assess their time-varying behavior. On the other hand, Matlab/Simulink has been used to analyze and create input data for the implemented grid in PowerFactory.

Regarding the applied methodology, it is summarized as following:

- A load flow analysis is performed in the case study grid to assess the capability of the implemented systems to provide voltage regulation under different situations. In this way a better understanding of the regulation capacity of this units is gained, as well as the grid behavior. Additionally, this analysis is utilized to determine the dimension and location of the implemented P2G system.

- The dynamic models of the elements of the case study grid are developed or enhanced. The regulating control of the units has been implemented by following voltage - power factor droops. Additionally, their coordination is set depending on voltage regulation priorities.
- Time-varying simulations have been used to represent the dynamic behavior of the system, comparing the different voltage regulating elements.
- An energy management strategy is developed, determining the operation of the P2G system depending on the grid situation and the market's price. This strategy is implemented using a fuzzy logic controller.

1.5 Limitations

The considered limitations of this project are the following:

- The operation of the switches of the case study grid is disregarded; thus, the analysis is carried out considering the topology of the grid to be radial.
- The model of the wind turbines is simplified to a passive generator, not taking into consideration the dynamics of the wind power curve, shaft and blade angle control.
- The model of the line drop compensation assumes as known both the loads and the CHP plant behavior.
- The modeling of district heating, gas network and hydrogen storage are very simplified. The associated delays related to their dynamics are not taken into account.
- It is assumed that the alkaline electrolyzer plant is situated in a remote place and thus, not able to be connected to the transmission gas network.
- The DSO is assumed to possess the necessary forecasting and decision making tools in order to implement the proposed market strategy.
- Load flow estimations are used in order to represent the error of real forecasts. They only include the wind power error.
- A complete cost/benefit analysis of the market strategy is not carried out.

1.6 Outline of the Thesis

The structure of the project consists of several chapters, they are summarized as it follows:

Chapter 1 - Introduction: In this chapter the background information of the chosen topic is introduced and contextualized according to the Danish case. The scope of the project and the considered limitations are presented. Moreover, the methodology used is explained.

Chapter 2 - State of Art: This consists of a literature review to investigate the most relevant topics for the project. These are presented in the form of a state of the art analysis. Being the main focus of the project, the electrolyzers as well as the Power to Gas (P2G) technology are presented. Additionally, the Danish electricity market is investigated. Finally, the characteristics of both the electrical distribution grid and gas network in Denmark are presented.

Chapter 3 - Integration of P2G in a Distribution Grid - Steady State Analysis: In this chapter the chosen distribution grid is modeled and analyzed in the software PowerFactory, performing load flow simulations. The integration of the new elements of the grid such as the OLTC, reactive power control of DGs and electrolyzers is presented in this chapter.

Chapter 4 - Dynamic Model Implementation in DIgSILENT PowerFactory: In this chapter the dynamic behavior of the wind turbines, CHP plant, OLTC and alkaline electrolyzer is modeled. The operation of each model is explained and verified.

Chapter 5 - Voltage Support from P2G Systems - Dynamic Analysis: The grid operation is analyzed with the implementation of the dynamic models presented in Chapter 4. The contribution of the several elements to provide voltage regulation is assessed and compared.

Chapter 6 - Energy Management from P2G - Dynamic Analysis: The market strategy for the energy management of the alkaline electrolyzers is presented in this chapter. Several simulations are included to show the new behavior of the system, comparing the results with the ones obtained in Chapter 5.

Chapter 7 - Conclusions and Future Work: The summary and conclusions of the project are presented in this chapter. Additionally, the possible future work based on this project is discussed.

2 State of Art

In this chapter a literature review of the most relevant topics of the project is presented. The Danish electricity grid and its market are analyzed; the smart energy system is introduced, followed by the district heating network and the structure of the gas network; and finally, the P2G technology is explained.

2.1 Danish Power System

The Danish power grid is divided in two areas: West Denmark and East Denmark. The first comprises the peninsula of Jutland and the island of Funen and is connected to Germany through an AC overhead line (OHL) and to Norway through several DC cables. The East Denmark region is connected to West Denmark and Germany through a DC cable and to Sweden through an AC cable. Consequently, West Denmark is part of the European grid and East Denmark is part of the Nordic grid. These two Danish systems are inter-connected through a DC cable since 2010, meaning they are asynchronous.

Furthermore, the Danish electricity grid is divided in two levels according to the voltage. These are Transmission, consisting of the networks from 400 kV to 60 kV, and Distribution, including networks from 60 kV to 0.4 kV [13].

2.1.1 Transmission Grid

The Danish transmission grid is owned and operated by Energinet.dk, a governmental company that has the role of Danish Transmission System Operator (TSO). Its main responsibilities are maintaining security of supply, planning and developing the transmission grid according to future scenarios, supporting green energy production technologies and balancing the production and consumption. Additionally, Energinet.dk is co-owner of the interconnections with Sweden, Norway and Germany.

Figure 2.1 illustrates the transmission grid in Denmark as it was in 2014. The different voltage levels in Denmark are 400, 220, 150 and 132. The type of connection, AC or DC, is also indicated.

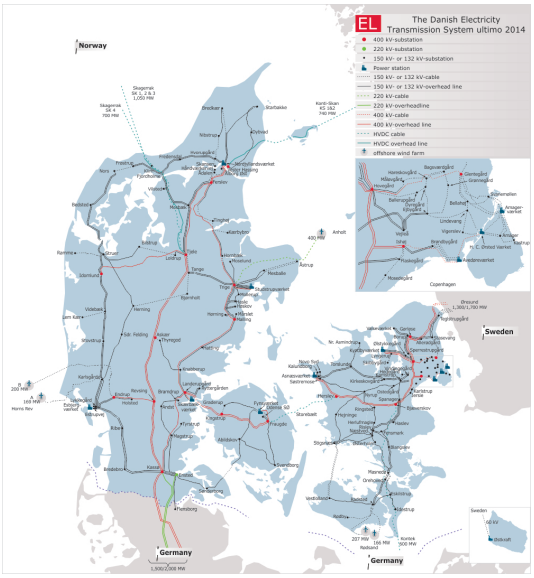

Figure 2.1: Existing Danish Transmission System in 2014 [13]

2.1.2 Distribution Grid

The distribution grid is the responsible to supply electricity to the end user, being their principal aim to provide reliable quality of supply to the customers. Its voltage levels range from 60 kV to 400 V. The different distribution systems in Denmark are operated by Distribution System Operators (DSO). Denmark has 92 different DSO, where the largest is DONG Energy, with more than 1.000.000 customers [14].

The distribution grids can be built according to different architectural topologies, which can benefit several aspects such as cost, supply reliability or robustness among others. The three different topologies are illustrated in Figure 2.2 and explained as following:

- Radial structure - Represents a feeder that consists of several buses connected to each other by one single line. It is the most used in rural areas due to its simplicity and low cost. However, if a fault occurs the rest of the feeder becomes compromised until it is cleared. This means that radial grids are less reliable in this aspect.
- Ring structure - As the name describes, the feeder has a circular structure where each busbar can supply two buses. In this way, if a fault occurs in any of the lines the security of supply can be maintained. One of the disadvantages is the increased cost of over-dimensioning the lines in order to transport a higher amount of load in case of fault.
- Meshed structure - This type consists of several interconnections with buses and other feeders and networks. Therefore it is the most complex and reliable topology of grid.

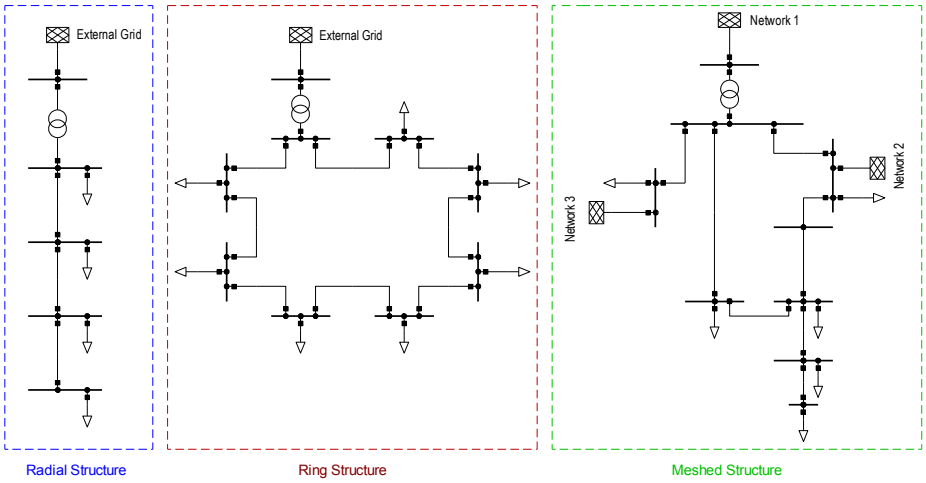

Figure 2.2: Single-line diagram of the different grid topologies

The distribution grids in Denmark presented many changes in the last decades. A great number of distributed generation (DG) units such as wind turbines and small CHP were introduced, presenting several challenges in the distribution grid. Traditionally the power flow was unidirectional, following the top-down principle. However. the introduction of DGs in the distribution grid created reversed power flow, over voltages, grid congestions, etc. On the other hand, the expected increase of electricity consumption can develop into under voltages.

2.1.3 Grid Codes

In order to ensure operation and protect the electrical grid and the elements that are part of it several technical regulations have to be followed. These are known as grid codes and consist

of guidelines that plant owners, grid owners and grid operators have to comply. As Denmark is the country taken into account in this project, the regulations to follow are mainly imposed by Energitilsynet, which is the Danish Energy Regulatory Authority, and Energinet.dk, as the TSO. These grid codes follow the European Standard EN 50160 for what concerns voltage quality.

The aim of this project is to analyze the implementation of an alkaline electrolyzer to provide voltage support to a medium voltage grid. Therefore, one of the main specifications is the allowed voltage deviation. As the previous sources mention, the voltage deviation in medium and low voltage is $\pm 10\%$. However, as low voltage analysis is not considered in this study, a deviation of $\pm 5\%$ will be taken into account for the studied medium voltage grid. Therefore the considered voltage limit ranges from 0.95 p.u. to 1.05 p.u..

Additionally, the generating facilities should also follow the TSO requirements regarding grid connection. These consist of specifications regarding the properties that the plants should have such as power factor variation for providing voltage regulation. The exact regulations depend on the type of generating units of the studied grid, therefore the ones taken into account in this project are presented in detail in Chapter 3.

2.2 Danish Electricity Market

The deregulation of the wholesale electricity market occurred in 1999. Since then, Danish market players are free to offer and purchase electricity among them, which has led to an increased free competition. The agreements are mainly made via Nord Pool, the common market for the Nordic countries and, less frequently, by bilateral trading. Regulating power is purchased by the TSOs in the Nordic Regulation Power Market. In Appendix A, the role of the different market players, the present Nord Pool markets (namely Elspot and Elbas) and the regulation and balancing power markets are further explained. References [15] [16] [17] [18] [19] are used to support this background information.

2.2.1 Future Markets

As previously stated in 1.1, the integration of RES in the distribution grid will present new challenges. A cheaper alternative to grid upgrade can be the creation of a new market to offer flexibility products to both TSO and DSOs. The Nordic Regulation Power Market is already a flexibility market, however it only offers services to the TSOs. A new flexibility market could offer products and settle prices in order to improve the congestion of the distribution grids and the balance of the transmission grid in a synergistic way. Figure 2.3 shows the integration of this new market with the different players. Whereas Energinet.dk and DSOs would buy these flexibility products, balance responsible parties (BRP) or aggregators would offer them in the market.

Figure 2.3: Markets for flexibility in the upcoming power system [20]

BRPs placed in congested distribution grids could gain extra benefit by taking part in the new market. For instance, a producer could decrease its output for avoiding lines overloading, if the market prices are attractive enough to change its schedule. In the context of this project, an electrolyzer placed in a distribution grid with high wind power penetration can provide voltage regulation and help avoiding local bottlenecks. When operated by the DSO, the target would be to correct the possible voltage deviation, minimizing the impact in the schedule.

2.3 Smart Energy System

Smart grids have been a broadly researched area during the last years, focusing mainly on making the electricity system more intelligent [2]. The growing interest in ESS (Energy Storage System) and the need of reducing the fossil fuel dependance in the whole energy system have brought along the novel aim of integrating together the electricity, gas and district heating systems in an intelligent way, expanding the concept of smart grid to smart energy system. Denmark has a really well developed electricity, gas and district heating systems, which makes it a perfect scenario for exploiting the synergies between these three forms of energy.

Electricity possesses the highest energy quality among the different forms of energy, with efficiencies above 90%. However, its main disadvantage is that it has to be consumed at the same instant it is produced, having almost no margin to be stored in this form of energy. Heat comprises the poorest form of energy due to its limited conversion capability and low conversion efficiency, although the efficiency in its obtainment is near 100%. Moreover, it is easily stored in the range of hours to days. Gas, namely natural gas and hydrogen, appears to have an intermediate energy quality; on the other hand, its storage capacity is high. Figure 2.4 represents a possible way to synergistically exploit these three forms of energy in the Danish context, taking into account their strengths and weaknesses.

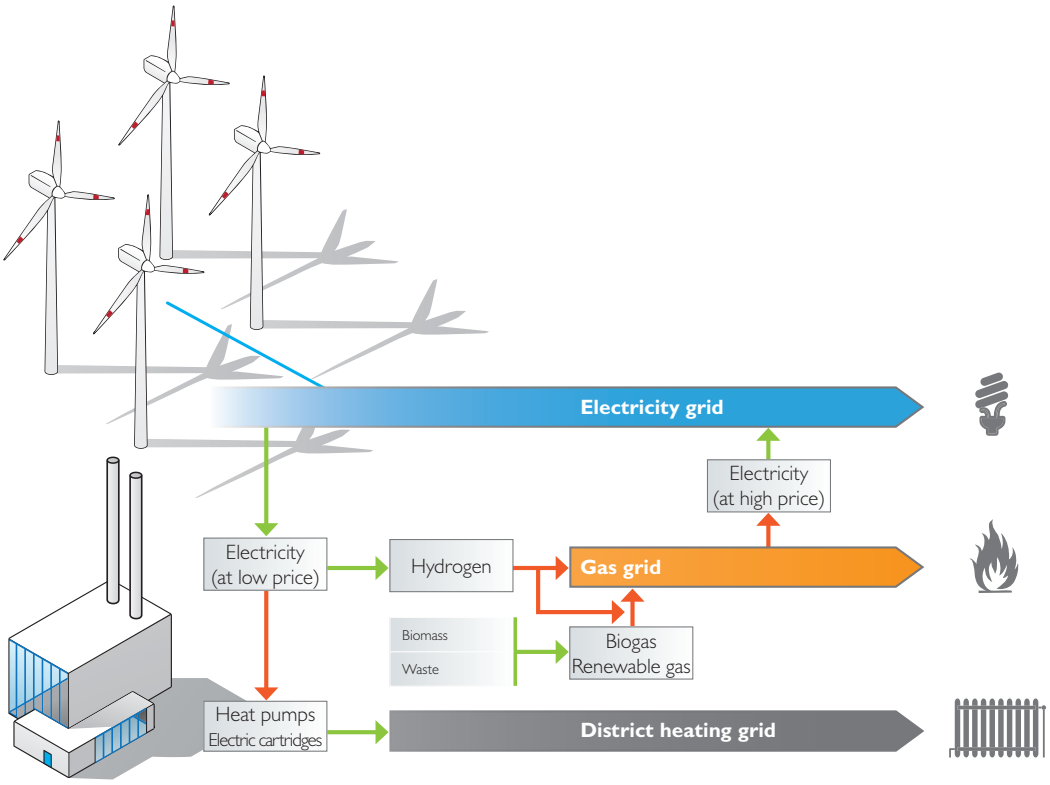

Figure 2.4: Diagram representing the integration of electricity, gas and district heating sectors [2]

The expansion of RES involves an increase of renewable electricity production. The high variability of wind or PV generation implies periods of lack or surplus of electricity. The excess of electricity could be transformed into hydrogen or heat, taking advantage of low spot prices. The responsible units for transforming electricity to heat are heat pumps and electrical cartridges, whereas electrolyzers are used to produce hydrogen. Taking into consideration the production of hydrogen, when renewable electricity cannot cover the demand, the deficit could be supplied by the re-electrification carriers, namely fuel cells and gas turbines.

In the context of the present work, the integration of the three energy sectors can be done by taking into consideration the implementation of a gas turbine CHP and an electrolyzer in a distribution grid. Nevertheless, the main focus will be assessing the impact of this integration into the electrical system. In the following sections, both Danish district heating and gas sectors will be further explained, as the electrical side has already been described in Section 2.1.

2.4 District Heating in Denmark

Denmark has been, for decades, the worldwide leader in district heating technologies. Heat is produced in a centralized and local scale, being transported to the end consumers through water pipes. Nowadays, around 63% of the Danish heat demand is supplied by its efficient district heating [21]. This heat is mostly produced in CHP plants, which consist of simultaneous production of both heat and electricity.

During 2012, 74.6% of the electricity production in Denmark was from CHP plants, whereas 73% of the produced heat was generated together with electricity [22]. The rest of the district heating demand was mainly produced with boilers and, in smaller amount, via electricity heating elements, namely electrical cartridges and heat pumps. These statistics show the high level of implementation this technology has in Denmark, both in the electricity and district heating systems. The scope of the present project regarding district heating will only fall within CHP plants, therefore, this will be the only technology further explained.

2.4.1 Combined Heat and Power (CHP)

As mentioned previously, CHP technology consists on producing heat and electricity simultaneously. The excess heat from conventional turbines is used in order to heat water, used in the industry and district heating. The use of waste heat leads to achieve higher efficiency and lower emissions, compared to separate production of electricity in a conventional thermal power plant and heat in a boiler. As an example, a 5MW combined cycle CHP has an overall efficiency of 75%, whereas the separate production for the same amount of heat and power has an efficiency of only 50% [23]. As previously explained, this technology has a high degree of implementation in Denmark. Table 2.1 shows the amount of CHPs and their installed capacity in 2013, where the higher amount of decentralized plants can be noticed.

Table 2.1: Amount of different CHP types and installed capacity in Denmark in 2013 [24]

Type of CHP	Number of units	Electricity capacity (MW)	Heat capacity (MJ/s)
Centralized units	32	6244	6301
Decentralized units	637	1890	2333
Autoproducers	301	540	1415

CHP units are mainly characterized by their prime mover, which determines their efficiency and heat to power ratio. The main prime movers are: steam turbines, gas turbines, reciprocating

engines, microturbines and fuel cells [23]. However, gas turbines is the only type considered in the present project.

In order to provide flexibility, heat and electricity are decoupled with other heating elements. These elements are heat storage and boilers (fuel-fired and electric). Excess heat is stored when electricity spot prices are high and operating the CHP plants is highly profitable. On the contrary, when electricity spot prices are low and producing electricity is not economically feasible, heat demand is covered by using the boilers or heat storage, if available [25].

Gas Turbines

The main characteristics of gas turbine generators are summarized in Table 2.2, giving the values of efficiency, nominal power and heat to power ratio:

Table 2.2: Characteristics of gas turbine generators [23]

Typical capacity (MWe)	Heat to power ratio	CHP efficiency (%)
0.5-300	0.6-1.1	66-71

The operation of gas turbines is based on the Brayton cycle, which consists of a compressor, a combustion chamber and an expansion turbine, as depicted in Figure 2.5. Air is first compressed and heated in the compressor, further heated in the combustion chamber by adding fuel and finally expansion takes place in the turbine, creating mechanical energy. This energy is used for driving both generator and compressor.

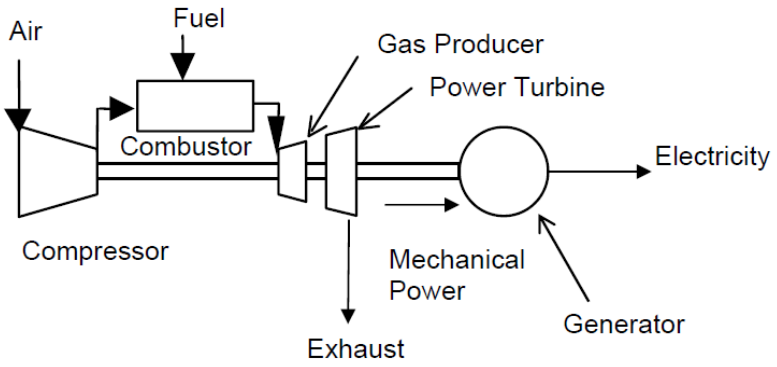

Figure 2.5: Basic Brayton cycle diagram [23]

An intercooling stage might be included before compression, in order to reduce the compressor's work. The high temperatures of exhaust gases can be used for different purposes. In case of CHP operation they are used to heat water, whereas for combined cycle a Heat Recovery Steam Generator (HRSG) is used in order to produce steam to run a steam turbine, increasing its electric efficiency [23].

Gas turbines have low emission levels, high reliability and short start-up time. The main disadvantage is their poor efficiency at low loading. Gas prime movers can run with multiple fuels: natural gas, synthetic gas, landfill gas and fuel oils. Besides, the first commercial units that use hydrogen as a fuel have already been implemented, as the installed unit in Berlin Brandenburg Airport by 2G CENERGY®[26] [23].

2.5 Danish Gas Network

Denmark is one of the few countries that is not dependent on natural gas, it has its own production of gas from the North Sea which is expected to continue until at least 2025 [27]. Furthermore, it exports gas to Sweden, Germany and The Netherlands. In 2013 the net production of natural gas was $4 \cdot 10^9 Nm^3$, of which 47% was exported [27].

The natural gas is transported to the mainland through offshore pipelines from the production placements in the Danish continental shelf. Two pipelines transport the gas to Denmark and another transports gas to The Netherlands. When the gas is onshore a treatment plant evaluates the quality of the gas. From there the gas is distributed to the customers, to storage facilities and to the neighboring countries [28].

The gas network is divided in two parts: transmission and distribution. First, the gas is transported at more than $50bar$ pressure. The distribution network brings the gas to the end-user, being transported at lower pressures [29].

The onshore gas transmission network is owned and operated by Energinet.dk. As shown in Figure 2.6, the pipelines transport the gas from north to south and west to east. Along the lines there are meter and regulation stations (M/R) which ensure that the pressure level is the adequate. Two subterranean storage facilities are available to ensure quality of supply: Lille Torup in North Jutland and Stenlille in Zealand, both owned by Energinet.dk [29].

Figure 2.6: The Danish transmission gas network in 2014 [30]

Gas Storage in Denmark

The limited natural gas supply coming from the North Sea results in a need of storage. In cold days the demand of natural gas can reach approximately $30-33 \cdot 10^6 Nm^3/day$, while the pipelines from the North sea can only transport about $22 - 24 \cdot 10^6 Nm^3/day$.

The storage facility of Lille Torup is placed in an underground salt dome. It consists of 7 storage cavities which range from 200-300 m high and 50-65 m wide. The total storage is $440 \cdot 10^6 Nm^3$, which corresponds to 2 months of gas consumption. Stenlille is an acquifer storage facility which consists of porous sandstone layers at 1500m depth. Its storage capacity is about $558 \cdot 10^6 Nm^3$. [31]

2.6 Power to Gas Technology

As explained previously in Section 1.1, P2G is a technology with high potential for long-term storage. Power to Gas consists of utilizing electrolyzers to convert electricity to hydrogen. The main characteristics of hydrogen are its low density and its high energy content per mass unit, the highest among all fuels. However, hydrogen is not found in its pure state, and it can only be produced from fossil fuels and water. The technology that is being investigated for its application with renewable energies is water electrolysis, the only sustainable source of hydrogen [32]. In the following, the different technologies of water electrolysis and some applications are presented.

2.6.1 Water Electrolysis Principles

Water electrolysis is a method that consists in applying direct current to water in order to separate its two elements: hydrogen and oxygen. The current circulates between the anode and cathode which are separated and submerged in electrolytes, a chemical substance that increases the ionic conductivity. A separator is placed in between the two electrodes to avoid the elements being mixed after the separation. Hydrogen is generated at the cathode, since is where the reduction reaction takes place; and the oxygen is generated in the anode, where the oxidation reaction occurs. The previous elements form what is known as the electrolysis cell, which are connected in series or parallel to form an electrolysis module [32]. The types of electrolyzers are distinguished by the electrolyte that is used, the three different types are the following:

Alkaline Electrolyzer (AE): Alkaline electrolyzers are the more developed type, being known for over 200 years [33]. This type of electrolyzer uses as electrolyte an aqueous solution. The most commonly used is potassium hydroxide (KOH) in solutions from 20-30 wt%, which offer the optimum conductivity and corrosion resistance values [34]. Their lifetime reaches approximately 15 years and the efficiency varies from 47% to 82% [32]. The advantages of alkaline electrolyzers are their robustness, long lifetime and their ability of producing large quantities of hydrogen [33].

Proton Exchange Membrane (PEM) Electrolyzer: The application of PEM electrolyzers started in the 1960s, and the first were commercialized in 1978 [32]. The electrolyte used is, as the name indicates, a proton exchange membrane or polymer membrane. The most used is perfluorosulfonic acid polymer, also known as Nafion^{TM} [35]. This type of electrolyzer, compared to the others, is very simple and compact [36], presenting efficiency levels from 48% to 65% [32].

Solid Oxide Electrolyzer (SOE): This type of electrolyzers were implemented in the late 1960s, being the last type of electrolyzers developed. They consist of high temperature electrolysis, from $600°C$ to $800°C$. Electrolysis is achieved by supplying steam to a porous cathode, which will be dissociated to oxygen and hydrogen when certain potential is applied [37]. The dense electrolyte that is normally used is yttria-stabilized zirconia (YSZ) due to its ability to withstand high temperatures and its good ionic conductivity [32]. The efficiency is higher than the other types of electrolyzer, however the technology is still under research [38].

Table 2.3 summarizes the types of electrolyzers according to their efficiency and maximum power:

Table 2.3: Comparation between the different electrolysis technologies [32]

Type of electrolyzer	Alkaline	PEM	SOE
Efficiency	47% - 82%	48% - 65%	$\sim$ 75%
Max. power (module)	3.5 MW	1 MW	few kW

2.6.2 Integration of Hydrogen in the Gas Network

The main issue of hydrogen production is its final use. The utilization of hydrogen for the transportation sector implies the construction of an infrastructure to distribute it [39]. Given this, a feasible solution is injecting it to the existing gas network [40]. However, there are restrictions regarding the materials of the pipelines and the energetic limitations of combining both gases [39]. In order to provide the same energy, the volume of hydrogen needed is three times of the natural gas [40], which limits the concentration of hydrogen in natural gas. However, the greatest limitation is due to the materials of the pipelines, storage units and equipment. The admissible concentration of hydrogen in present natural gas systems was studied in [41]. This study concluded that most elements of the gas network admit a concentration of 10% by volume of hydrogen. However, some elements could be deteriorated or cause adverse effects with such a high concentration of hydrogen. The most sensitive components are underground porous storage, steel tanks, gas engines and old gas turbines.

2.6.3 Power to Gas Applications

Historically, the two largest water electrolysis plants were installed in Norway, with approximately 135 MW each. The plants were supplied by hydro power, and the produced hydrogen was used for fertilizer production. However, these plants were closed down as hydrogen could be produced through other sources at a lower cost [42].

Nowadays, the focus on P2G plants is on re-utilizing the excess renewable production. Recently, these plants are being developed and installed in several countries for this purpose. Three projects are presented in the following:

BioCat Project: A new project called P2G-BioCat is being developed in Denmark, its objective is to design a commercial P2G facility to provide energy storage to the Danish energy system [43]. The project is coordinated by several companies, being the most important Electrochaea and Energinet.dk. In this case the surplus electricity from wind power is used to obtain hydrogen, which will be used to convert biogas into methane. A 1 MW water electrolysis plant, using an alkaline electrolyzer from Hydrogenics, will be installed in Spildevandscenter Avedøre, one of the largest waste-water treatment facilities. The final gas will be injected to the local distribution network and the co-products, oxygen and heat, will be recycled in the waste-water plant [44].

Falkenhagen (Germany): In 2013 the energy company E-ON installed a P2G plant in Falkenhagen, Germany. It consists of a $2MW$ alkaline electrolyzer that converts excess electricity from a wind farm to produce hydrogen. This hydrogen is injected at a rate of $360Nm^3/h$ to the natural gas network, at a volume rate of 2% [45].

Energie Park Mainz (Germany): A new P2G plant is planned to start operating in spring 2015 in the German city of Mainz. It consists of a 6 MW PEM electrolyzer, and therefore will be the largest plant operating on surplus electricity from wind power [46].

2.6.4 Conclusion

According to the presented literature review, it is known that the only types of electrolyzers that are commercialized nowadays are alkaline and PEM. However, the latter is still under development, while the alkaline electrolyzer can be considered as mature technology. As discussed in Sections 2.6.3 and 2.6.1, alkaline electrolyzer plants are available up to 135 MW, offering efficiencies from 47% to 82% and lifetime of 15 years. For this reason, the alkaline electrolyzer is the type that will be taken into consideration in this project. Moreover, a PowerFactory model of alkaline electrolyzer has been presented in [47], which can be used in this project with appropriate modifications.

3 Integration of P2G in a Distribution Grid - Steady State Analysis

In this chapter, the case study grid used to test the implementation of Power-to-Gas is presented. It includes the electrical distribution grid, which receives the main focus in this work, and a simplification of the district heating and gas networks. First, the electrical distribution grid architecture and the several elements that the grid includes are defined; namely lines, loads, transformers, wind turbines and CHP. Then, the simplifications of the district heating and gas networks are presented. Hence, the study case integrates the three energy systems, previously explained in Chapter 2.

After the grids are presented, a steady state analysis is performed to investigate its operating electrical strength, being the primary objective to evaluate the impact of high wind power penetration. This is done by analyzing the voltage and assessing the implementation of the previously mentioned electrical elements. In order to provide voltage support, an On-Load Tap Changer (OLTC) in the transformers and operating the wind turbines and CHP at lagging power factor are integrated. Finally, the implementation of an alkaline electrolyzer is tested to analyze energy management services and voltage support. It should be noted that this chapter does not include any dynamic behavior of these elements; these will be considered in the following chapters.

3.1 Grid Architecture

3.1.1 Electrical Distribution Grid

The aim of this project is to investigate the application of P2G in a typical Danish Medium Voltage (MV) grid with high wind power penetration. For this purpose an European benchmark model of a 20kV distribution grid is used [48]. As it can be observed in Figure 3.1, the grid consists of two feeders, each of them supplied by a 110/20 kV transformer. These feeders include several buses with loads that represent aggregated low voltage grids. The grid includes two types of generation units: wind turbines located in bus 8 and a CHP plant located in bus 9.

Table 3.1 summarizes the total generation and consumption in the mentioned grid in nominal installed power.

Table 3.1: Summary of the rated generation and loads in the grid

Installed power of generation and loads		
Generation	6 x wind turbines	12 MW
	2 x CHP units	5.92 MW
	TOTAL	17.92 MW
Loads	Residential loads	43.695 MVA
	Industrial loads	15.165 MVA
	TOTAL	58.86 MVA

The values and placement of the elements of the grid are based on [48], with exception of the ratings of the CHP plant and wind turbines. The CHP plant has been sized according to the heat demand that is committed to, explained later on in Section 3.1.2. The wind turbines have been upscaled to simulate a typical Danish grid with high wind power penetration. The data of all the

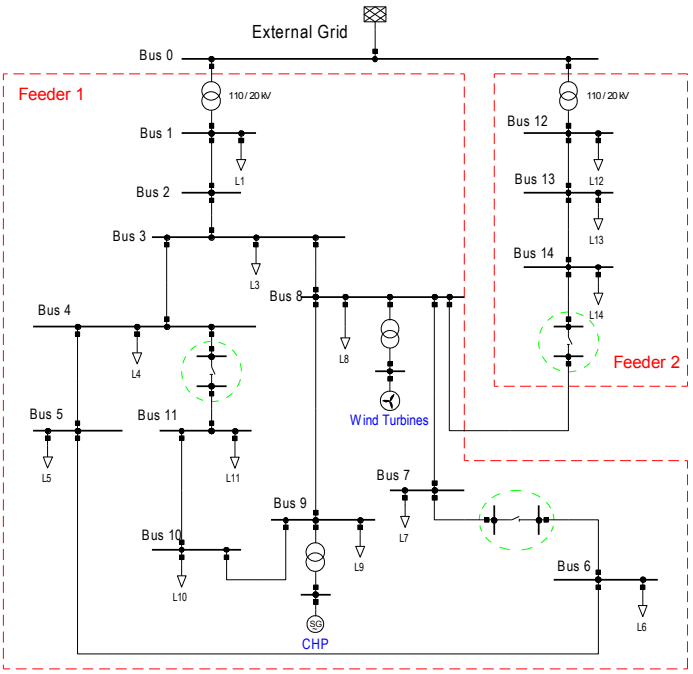

Figure 3.1: Single-line diagram of the benchmark MV grid [48]

elements of the grid can be found in Appendix B.1. Regarding the value of the loads, their rated power is specified in both Table B.4 and Table B.5. In order to represent their real behavior, each load follows a different load profile depending on their type and the season, as specified in Table B.4.

Two different seasons are taken into account for the simulation of these loads, these are winter and summer. Each of these scenarios has three different consumption curves representing residential loads and one for the industrial ones, as can be observed in figures 3.2 and 3.3.

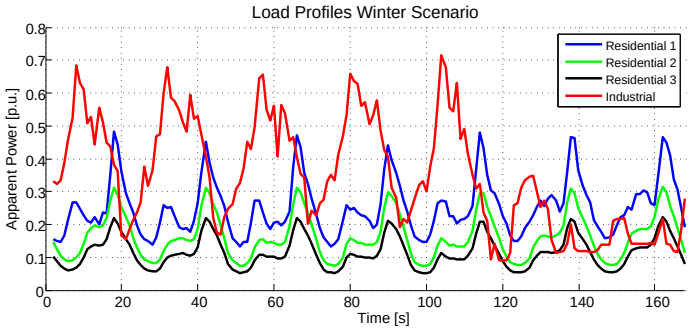

Figure 3.2: Industrial and residential load profiles during a winter week

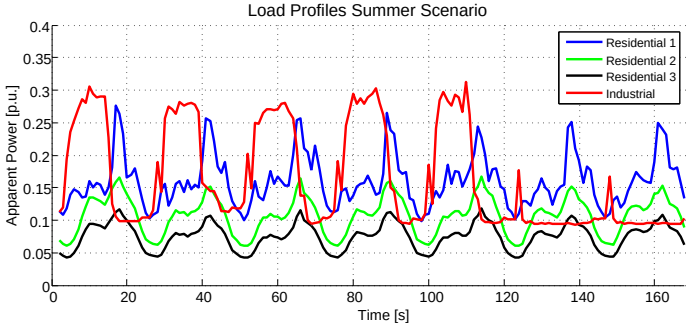

Figure 3.3: Industrial and residential load profiles during a summer week

According to [49], loads can be modeled as constant power, constant current or constant impedance. Table 3.2 shows the following modeling approximation for each type of load.

Table 3.2: Load type modeling approximations [50]

Feeder type	Constant P [%]	Constant Z [%]
Residential and commercial, summer peaking	67	33
Residential and commercial, winter peaking	40	60
Industrial	100	0

In order to simplify the load modeling in PowerFactory, both residential and industrial loads are aggregated in each bus. The ratio of constant power and constant impedance has been selected according to the percentages presented in Table 3.2 in proportion to the installed power of residential and industrial loads. The resulting load modeling for each bus can be observed in Table B.6 in Appendix B.1. It should be noticed that this is just an approximation, since the industrial and residential profiles presented in figures 3.2 and 3.3 are not the same.

Finally, the selected test system includes three coupling switches that are opened in normal operation, marked in green circles in Figure 3.1. This means that the grid can be analyzed as a radial network when these switches are opened, and as a meshed network when they are closed. The operation of these switches is normally used in distribution grids in order to improve reliability of supply and reduce power failure [51]. However, scenarios with closed operation of these switches are not covered in this project.

3.1.2 District Heating Network

As explained in Section 2.4, district heating is frequently supplied by local CHP plants. In the present study case it is assumed that the CHP plant provides district heating to 85% of the households electrically connected to Feeder 1, except load 1 as it represents the aggregation of several sub networks. For this purpose, Table B.4 in Appendix B.1 shows the rated power of the domestic load connected to each bus. Assuming that the average installed power of each household in a residential/rural area is 5 kVA, the number of households connected to buses 2-11 can be estimated, as shown in Table B.10, Appendix B.1. Therefore, district heating has to be provided to 660 households. The heat demand profile has been obtained by scaling obtained data from [52]. In order to calculate the heat demand that the CHP plant has to supply, an estimated 25% of district heating losses has been added to the calculated heat profile [53].

The study case CHP plant is assumed to have gas turbine units, as these are the most common in local district heating [24]. In order to flexibly decouple electricity and heat production, it is assumed to include a gas-fired boiler and a heat storage tank.

As further explained in Section 4.3.2, the dimensioning of the units has been carried out calculating the ratio between the yearly heat demand and the yearly produced heat at Skagen's CHP plant [54]. The resulting ratio has been applied in order to downscale Skagen's CHP unit to the present scenario. It should be noticed that the downscaled CHP has the same heat-to-power ratio of the Skagen unit, of 0.81. Table 3.3 shows the obtained values.

As the CHP plant output is decoupled from the heat demand that it has to supply, steady state analysis of the district heating network will be disregarded. A dynamic modeling and simulation of the latter should be performed in order to assess its influence on the electrical grid.

Table 3.3: Data of the CHP plant of Skagen and calculated data of the case study CHP [54] [55]

CHP Data	Skagen	Case Study
Yearly heat production/demand	$35857MWh$	$16315MWh$
CHP units electrical output	$13MW$	$5.9MW$
CHP units thermal output	$16MW$	$7.3MW$
Heat tank thermal capacity	$250MWh$	$114MWh$
Gas-fired boilers output	$37.5MW$	$17MW$

3.1.3 Gas Network

As introduced in Section 2.6.2, hydrogen injection into the gas network is expected to take an important role in the future Danish energy system [2]. Therefore, the use of the hydrogen is assumed for the present study case. The importance of modeling the gas network responds to assess the hydrogen injection limitation into it, which is expected to be a volume concentration of 10% in the near future [41]. In a similar way as for the heat demand, in order to decouple the hydrogen production from the operation of the CHP plant, a hydrogen storage is connected to the output of the electrolyzer. Its capacity is assumed to allow flexibility on a seasonal basis.

As it was not possible to find data of the study case gas network, it is assumed that the hydrogen is injected into the gas pipes feeding the CHP plant, which is expected to operate correctly with a 10% hydrogen concentration [56]. Figure 3.4 shows a sketch of the proposed hydrogen bleeding.

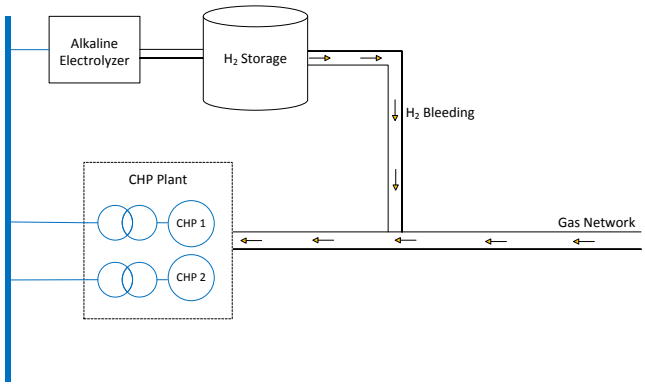

Figure 3.4: Sketch of the proposed hydrogen injection in the study case grid

The natural gas flow to the CHP plant has to be estimated in order to assess the hydrogen limitation. By knowing the CHP units and the gas boilers operation, their efficiencies and the calorific value of the natural gas, the natural gas flow can be calculated. Table 3.4 shows a realistic approximation of the mentioned parameters:

Table 3.4: Estimation of relevant parameters for calculating the natural gas consumption of the CHP plant [23] [57]

Parameter	Value
CHP units overall efficiency	70%
Gas boilers efficiency	80%
Natural gas calorific value	$12.1kWh/Nm^3$

The gas flow $[Nm^3/h]$ consumed by the CHP units ($\dot{V}_{CHP}$) and gas boilers ($\dot{V}_{boilers}$) can be estimated according to Eq 3.1 and Eq 3.2, where P_{heat} is the produced heat and P_{el} is the produced electricity.

$$\dot{V}_{CHP} = \frac{P_{el} + P_{heat}[MW]}{0.7} \cdot \frac{1Nm^3/h}{0.0121MW} \tag{3.1}$$

$$\dot{V}_{boilers} = \frac{P_{heat}[MW]}{0.8} \cdot \frac{1Nm^3/h}{0.0121MW} \tag{3.2}$$

The calculation of hydrogen production is done later in this chapter, after the electrolysis plant has been dimensioned. Nevertheless, the hydrogen injected into the gas network has to be assessed through dynamic simulations, since the storage decouples the hydrogen production and its injection.

3.2 Steady State Analysis

In this section, the behavior of the electrical distribution grid is analyzed by performing steady state simulations. This is done to determine the buses to be controlled by the tap changer, evaluate the need for reactive power compensation and, finally, determine the most convenient placing of the electrolyzer and its size. Hence, the evaluated scenarios are the following:

- Base Case: without OLTC, electrolyzer and unit power factor in wind turbines and CHP plant
- Implementation of OLTC: base case with OLTC in transformer
- Reactive Power Dispatch from Wind Turbines and CHP: previous case including reactive power capability from the generation units
- Implementation of the Alkaline Electrolyzer: previous case including a sized alkaline electrolyzers connected in the most favorable bus

Each of the previous scenarios is analyzed in the two worst case situations: Case 1 representing maximum generation and minimum load, and Case 2, representing no generation and maximum load.

In order to simplify the analysis, a time sweep of the winter and summer profiles has been carried out in both Case 1 and Case 2, and it was observed that the worst cases occur using the winter profile: the base load is similar for both seasons but the peak load is bigger in winter. Additionally, in winter the probability of having higher production than consumption is higher. Therefore, in order to simplify the analysis, both cases will be analyzed using the winter profile of the loads. The time sweep simulations are also used to determine the hour of the week that presents higher voltage deviation, being hour 121 for Case 1 and hour 105 for Case 2. The results of these simulations can be observed in Appendix C.

3.2.1 Base case

In this section the grid is analyzed without the influence of the electrolyzer load and the tap control of the transformers. The power factor of the wind turbines and CHP is assumed to be 1.

Case 1 - Maximum Generation

First, a typical cold and windy winter day is represented, in which both wind turbines and CHP produce at their rated power, 12 MW and 5.92 MW respectively. The simulation has been performed at hour 121, when the industrial loads are at their minimum (see Figure 3.3), which is the worst case scenario as previously mentioned. As it can be observed in Figure 3.5, the load flow simulation shows that buses 3 to 11 surpass the limit of 1.05 p.u., bus 9 being the one with higher overvoltage with a value of 1.135 p.u. The output of the CHP and wind turbines is bigger than the downstream loads, having an active power flow of 11.378 MW through TRF1 (Feeder 1) towards the external grid and Feeder 2. However, the reactive power flow goes from the external grid to the feeders, being 2.598 Mvar to Feeder 1.

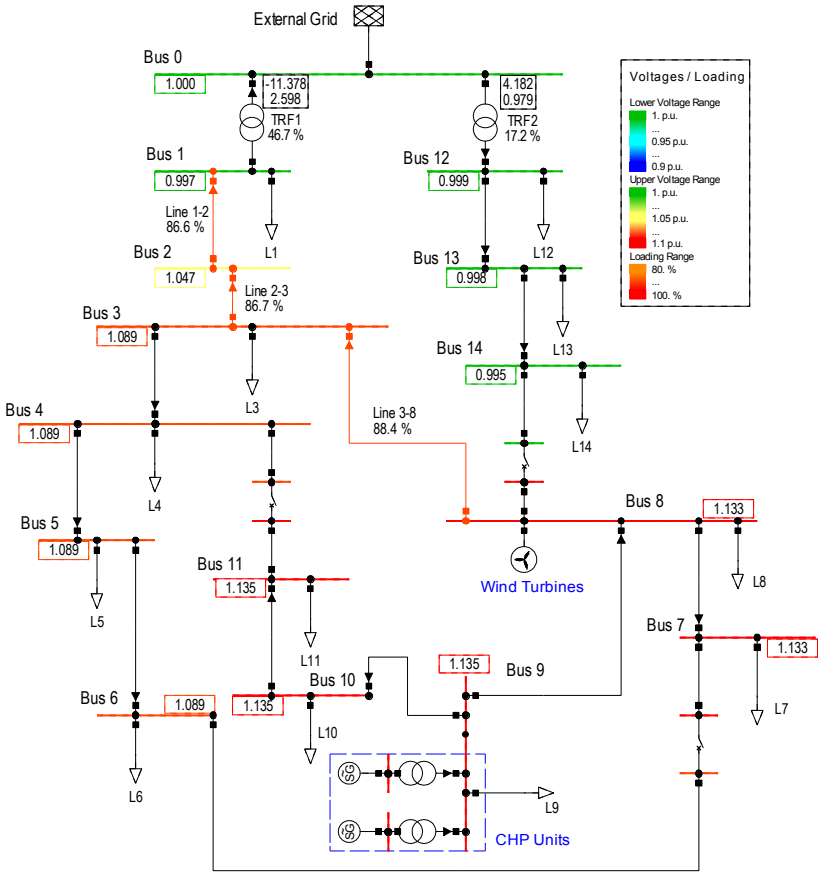

Figure 3.5: Load flow of the grid in DIgSILENT at maximum generation & without OLTC

It can be noticed that the loading of lines 1-2, 2-3 and 3-8 is above 80% as marked in orange color. It is observed that the most loaded one is the line connecting buses 3 and 8 with a value of 88.4%. This is due to the high amount of active power that is transferred from the CHP and wind turbines towards the external grid. The loading of the transformers are 46.7% for TRF1 and 17.2% for TRF2. Therefore, the grid is well dimensioned as its components can withstand the worst case scenario. Finally, the losses throughout the lines account for 2.18 MW and 1.64 MVAr in total.

Case 2 - No Generation

As a second case, it is assumed that neither CHP nor wind turbines produce electrical power. As previously mentioned, this case is analyzed at hour 105. In Figure 3.6 it can be observed that the voltage does not surpass 1 p.u. at any bus, being bus 7 the most affected by the voltage drop

with a value of 0.958 p.u.; although always within the allowed limits. The power flow is now from the external grid towards the two feeders, being 10.682 MW and 2.670 Mvar towards Feeder 1 and 8.801 MW and 2.533 Mvar towards Feeder 2.

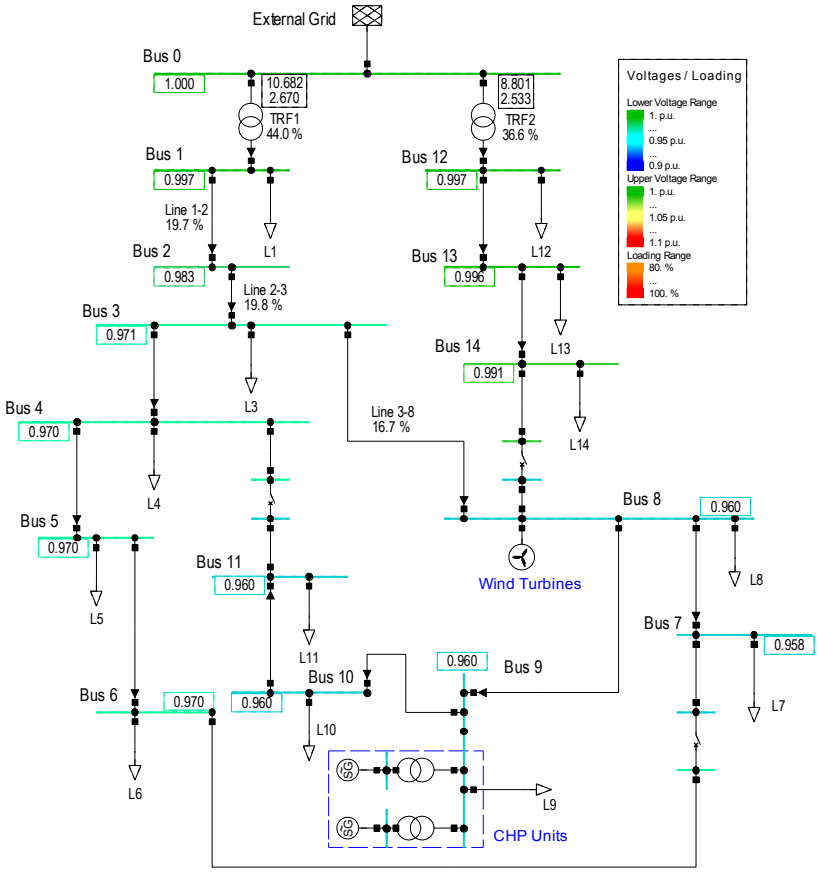

Figure 3.6: Load flow of the grid in DIgSILENT at minimum generation & without OLTC

In this case, the most loaded line is the one connecting bus 2 to 3 with a value of 19.8%. The transformer loading of Feeder 1 is 44.0%, whereas for Feeder 2 is 36.6%. Regarding the losses through the lines they are in this case 0.11 MW and 0.08 MVAr in total.

Summary

According to the previous two cases, the considered grid presents overvoltage in Feeder 1 when the power output of CHP and wind turbines is high. The allowed voltage limit is surpassed in buses 3 to 11, presenting higher overvoltage in bus 9 with 1.135 p.u.. During periods of no generation, bus 7 became the most affected one, with a drop of voltage to 0.961 p.u.. Therefore but 9 will be the chosen to set the control of the OLTC of Feeder 1 when overvoltage occurs, whereas bus 7 will be the reference for undervoltage cases. Regarding Feeder 2, it did not present any voltage or loading issues; therefore, it will not be taken into account in the rest of the project.

3.2.2 Implementation of On Load Tap Changer

As a key element in the voltage regulation of distribution grids, an OLTC is included in the transformer that links Feeder 1 with the external grid. This allows regulating the voltage output of the secondary terminal of the transformer according to the grid requirements. OLTCs usually include line drop compensation (LDC), which remotely controls the voltage at a predefined load

center. LDC is based on an internal impedance model that is adjusted to match the line impedance in order to estimate the voltage drop in the load center. This method is commonly dismissed by DSOs due to its more complicated operation and inaccuracy increase when implemented in a grid with intermittent generation [49] [58]. However, it has been proved that when LDC is used the size of DG that a grid can accommodate is bigger [59] and it avoids the investment on expensive communications.

Therefore, in this project it is assumed that the transformer uses LDC for estimating the voltages in buses 9 and 7, which have been proven to have the biggest overvoltage and undervoltage, respectively. For its implementation, it has been assumed that the voltage and current in the low voltage side of the transformer can be measured and the load currents can be estimated [58], as well as the current injected by the CHP plant. Furthermore, the generation located in bus 9 can be estimated as the difference of the previous currents. Eq. 3.3 and Eq. 3.4 show the voltage estimation, in [kV], for buses 9 (V_9) and 7 (V_7), respectively:

$$V_9 \simeq V_{tr} - Z_{13} \cdot I_{13} - (Z_{13} + Z_{38}) \cdot I_{38} - (Z_{13} + Z_{38} + Z_{89}) \cdot I_{89} \tag{3.3}$$

$$V_7 \simeq V_{tr} - Z_{13} \cdot I_{13} - (Z_{13} + Z_{38}) \cdot I_{38} - (Z_{13} + Z_{38} + Z_{87}) \cdot I_{87} \tag{3.4}$$

V_{tr} is the voltage measured in the secondary of the transformer, Z_{xy} is the impedance of the line between buses x and y and I_{xy} are the line currents from bus x to bus y. The latter are calculated, in [kA], as shown in Eq. 3.5, 3.6, 3.7 and 3.8:

$$I_{13} \simeq I_{tr} - I_1 \tag{3.5}$$

$$I_{38} \simeq I_{13} - I_4 - I_5 - I_6 \tag{3.6}$$

$$I_{89} \simeq I_9 + I_{10} + I_{11} - I_{CHP} \tag{3.7}$$

$$I_{87} \simeq I_7 \tag{3.8}$$

Where I_{tr} is the current measured in the secondary of the transformer, I_x is the current consumed by the load x and I_{CHP} is the forescasted current of the CHP.

It should be noticed that the load currents have been calculated from their active and reactive power forecast for a voltage of 1 p.u., obtaining an accurate estimation of the voltage profiles as shown later in Section 4.4. Since loads are modeled as part of constant impedance and constant power, representing precisely the voltage dependency of their currents would increase the complexity of the calculations. Load currents estimation, in [kA], is shown in Eq. 3.9, where V_n represents the nominal voltage of the grid, in this case 20 kV, and P_x and Q_x represent the forecasted active and reactive power of load x.

$$I_x \simeq \frac{P_x + jQ_x}{\sqrt{3} \cdot V_n} \tag{3.9}$$

Finally, the characteristics of the tap changer depend on the specific design of the transformer [60]. The typical number of tap positions of an OLTC is 32, ranging from $\pm 10\%$ [49]. However a number of 20 steps ranging from $\pm 4\%$ of the nominal voltage has been assumed, within the reference values in [61]. Furthermore, a deadband of $\pm 0.04 p.u.$ has been assumed for the voltage estimation of the LDC, in order to avoid excessive tap changes.

As stated in the previous scenario, the actual voltage in buses 9 and 7 will emulate the LDC estimation, in order to maintain the voltage within limits. It should be mentioned that bus 9 is selected to be the controlled bus during Case 1 and bus 7 for Case 2. Consequently, the OLTC will change its tap position in order to keep the mentioned voltages within limits. As stated in Section 2.1.3, the voltage limits set for the controlled buses are 0.95 p.u. to 1.05 p.u..

Case 1 - Maximum Generation

When the tap changer control is considered, the voltage in all buses decreases compared to the base case, however buses 3-11 are still above the limit of 1.05 p.u.. As it can be observed in Figure 3.7, the voltage of bus 9 dropped from 1.135 p.u. to 1.099 p.u. at hour 121. This improvement has been achieved by changing the tap position of TRF 1 to -10, decreasing the voltage of bus 1 to 0.957 p.u.. The active power flow from Feeder 1 towards the external grid and Feeder 2 is slightly reduced from 11.378 MW to 11.228 MW, due to increased losses. On the other hand, the reactive power flow from the external grid towards Feeder 1 has increased from 2.61 Mvar to 2.715 Mvar due to the same reason.

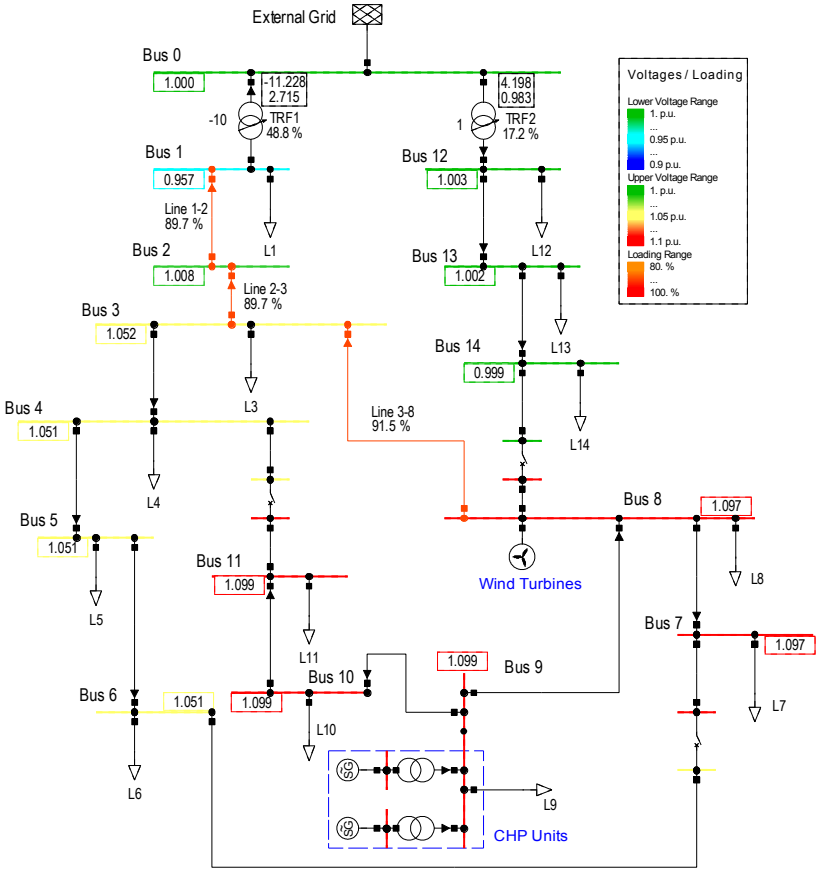

Figure 3.7: Load flow of the grid in DIgSILENT at maximum generation & OLTC

Regarding the loading of the lines, the most loaded one is line 3-8 with 91.5%. In this case, the total line losses account for 2.33 MW and 1.79 MVAr. This increase respect to the previous

scenario is due to higher current through the lines, as the generation and an important part of the loads are modeled as constant power.

Case 2 - No Generation

When the wind turbines and CHP do not produce any power, the tap position of TRF 1 changes to 3, increasing the voltage of the secondary by 1.2%. As in the previous section, the load flow has been performed at hour 105, as it is the most critical. The voltage at bus 7, the most susceptible to voltage drops as explained in the previous scenario, increased from 0.958 p.u. to 0.971 p.u.. Furthermore, the power flow from the external grid towards Feeder 1 increased from 10.682 MW to 10.771 MW and 2.67 Mvar to 2.685 Mvar due to the higher consumption of the voltage dependence loads. This can be observed in Figure 3.8.

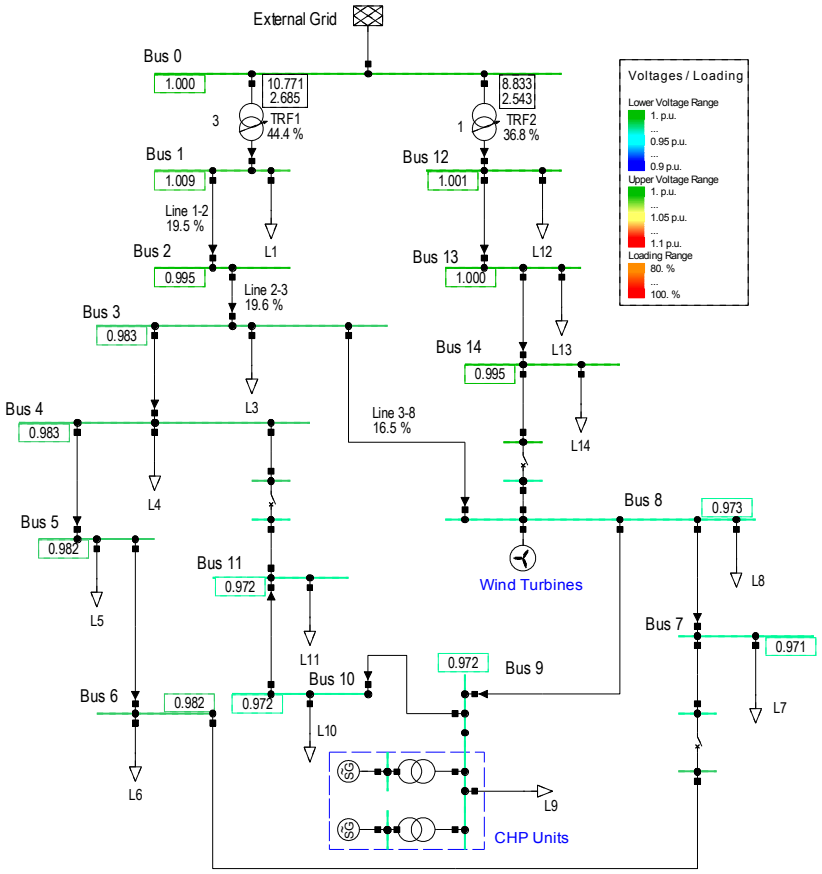

Figure 3.8: Load flow of the grid in DIgSILENT at no generation & OLTC

As in the previous scenario, the most loaded line is the one connecting bus 2 to 3 with a value of 19.6%. Regarding the line losses, the total value is 0.11 MW and 0.08 MVAr.

Summary

It can be concluded that the tap changer control presents a significant improvement in the buses of Feeder 1, although the overvoltage issues persist. Regarding the loading of the lines in Case 1, it has been observed that it was higher than in the previous scenario, although remaining below 100%. This increase was due to the voltage reduction while transporting the same apparent power. The improvement in voltage is summarized in Table 3.5.

Table 3.5: Comparison of critical voltages in Cases 1 and 2 with and without tap control

	Without OLTC	**With OLTC**
Case 1 - bus 9, h. 121	1.135 p.u.	1.099 p.u.
Case 2 - bus 7, h. 105	0.958 p.u.	0.971 p.u.

3.2.3 Reactive Power Dispatch of Wind Turbines and CHP

In the previous scenario it was observed that the tap changer was not able to correct the over-voltage during Case 1. In order to further decrease the voltage, the DSO has the option to send a command to both wind farm and CHP plant to supply reactive power regulation. As specified in [62], the plants should supply reactive power regulation according to the instructions from the local grid operator, as long as the operating limits specified by Energinet.dk's technical regulations are followed.

Therefore, in this section, the reactive power capability and capacity requirements of the wind turbines and CHP are presented.

Wind Turbines

In compliance with Energinet.dk's technical regulations for wind farms above 11 kW [63], wind turbine power plants between 1.5 MW and 25 MW should be able to receive any reactive power set-point within the hatched area in Figure 3.9:

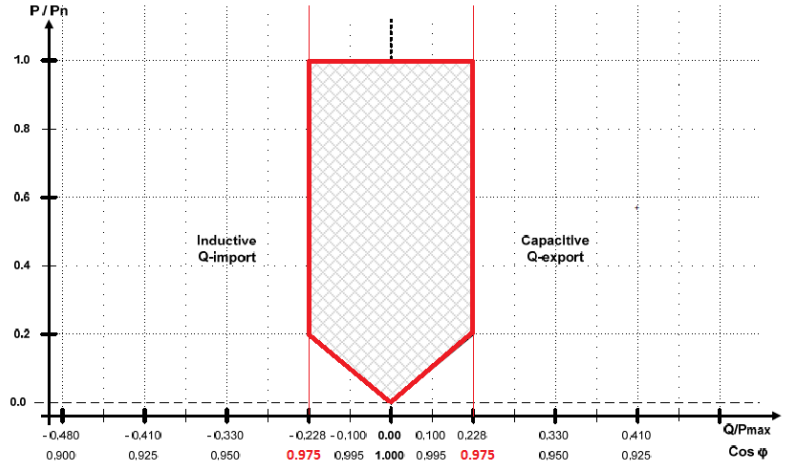

Figure 3.9: Reactive power requirements for wind power plants with a power output range between 1.5 and 25 MW [63]

As explained later in Section 4.2, the Vestas V80 2MW is the selected wind turbine model for the wind farm. Regarding its power factor range, it was found that the converter of the wind turbine is capable of varying it between 0.96 lagging and 0.98 leading [64]. As it can be observed in Figure 3.9, the inductive power factor requirement is fulfilled but the capacitive power factor requirement is not. Nevertheless, it will be assumed that the wind power plant has additional reactive power compensation which allows it to reach the requirement of 0.975 leading, as shunt capacitors.

Regarding the technical regulation dictated by the TSO in [63] section 5.9.3, it is stated that *"Control form and settings must be agreed with the electricity supply undertaking."* Therefore, it will be assumed that the DSO will be able to make use of the reactive power capability if

the voltage deviates from the allowed range. Hence, when the maximum active power output is reached (12 MW), the wind farm has the obligation of absorbing or producing up to 2.689 Mvar if any voltage issue arises. During no active power output, no reactive power requirement has to be fulfilled.

CHP

The technical regulation concerning thermal power plants bigger than 1.5 MW states that CHP plants should be capable of receiving any reactive power set-point within $-0.20 \leq tan\phi \leq 0.40$ at nominal maximum power [65]. Based on the reactive power requirements in the PQ curve of the synchronous generator of CHP units, it can be seen in Figure 3.10a and Figure 3.10b that it is within the limits of the machine.

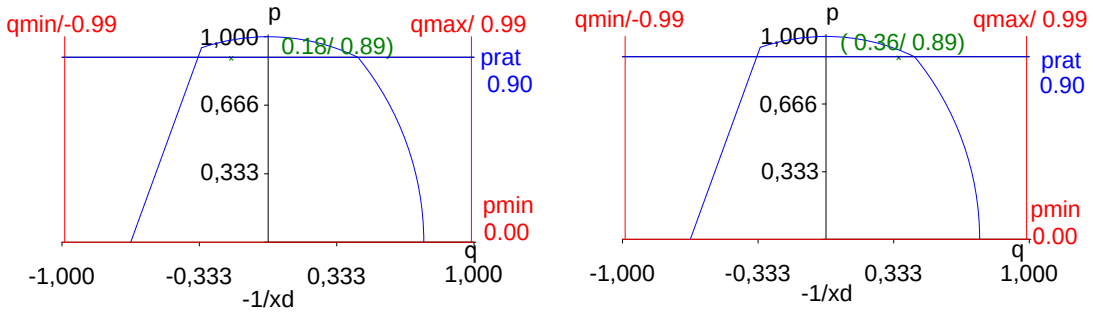

(a) Maximum active power and tan ϕ = -0.20 operation point

(b) Maximum active power and tan ϕ = 0.40 operation point

Figure 3.10: PQ capability curve of the CHP units' synchronous generator and requested operation points

Furthermore, according to [65], section 11.6, the CHP plant has the obligation of adjusting tan ϕ to the minimum (-0.20) if the voltage exceeds the maximum allowed and to the maximum (0.40) if the voltage goes below the minimum allowed. Hence, if any voltage issue arises, the CHP has the obligation of absorbing up to 1.18 Mvar or producing up to 2.36 Mvar when operating at the rated active power. When the active power output is zero, no reactive power requirements have to be fulfilled.

Coordination of OLTC, Wind Turbines and CHP

In order to provide voltage regulation, the reactive power of the DGs has to be controlled in a way that does not interfere with the controller of the OLTC. This means avoiding to operate the DGs in constant voltage mode when implementing a descentralized control [66], i.e. controlling the voltage of the bus they are connected to.

Instead, a modification of the DGs' power factor control strategy presented in [67] is implemented. This descentralized control consists of the following rules, which are depicted in Figure 3.11. It should be noted that the operation of the DGs is meant to follow the thick line.

- If V_{DG} goes below a lower threshold (V_{min}^{PFC}), the power factor adjusts to the lagging minimum (PF_{min})
- If V_{DG} goes above an upper threshold (V_{min}^{PFC}), the power factor adjusts to the leading minimum (PF_{max})
- If V_{DG} remains within the mentioned threshold, the power factor adjusts to the rated (PF_{PFC})

Where V_{DG} is the voltage at the PCC of the DG, V_{max}^{PFC} and V_{min}^{PFC} are the upper and lower voltage thresholds from which power factor modification takes place, and V_{max} and V_{min} are the upper and lower voltage grid limits respectively. Regarding the power factor, PF_{PFC} is the nominal power factor, PF_{max} is the leading minimum and PF_{min} is the lagging minimum.

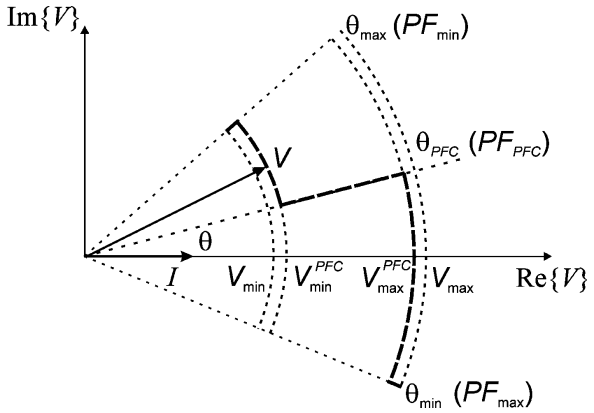

Figure 3.11: Vector diagram of the DG voltage and its injected current, according to the intelligent power factor control [67]

The modification introduced in the present study case includes a linear variation of the power factor from (V_{min}^{PFC}) to (V_{min}) and from (V_{max}^{PFC}) to (V_{max}) in order to have a smoother transition. The assumed parameters for the power factor controller are presented in Section 3.2.4

The settings of the OLTC remain unchanged respect to the previous scenario, with the voltage deadband set to $\pm 0.04 p.u.$. When the OLTC starts to operate, after the voltage surpasses the previously mentioned deadband, the reactive power of the DGs will have already reached its full capability; therefore, the applied decentralized control should not interfere negatively with the tap changer controller. The dynamic efficacy of this coordination will be tested in the dynamic simulations performed in Chapter 5, while its maximum steady state capability is tested in the present chapter. In the following, the improvement achieved by the explained reactive dispatch is presented for maximum generation and no generation cases.

Case 1 - Maximum Generation

In this case, the wind turbines and the CHP will absorb the maximum requested reactive power, 2.689 and 1.18 Mvar respectively, in order to bring the voltage within limits, while maintaining active the OLTC. In this case, the grid is analyzed at hour 121 when the worst case happens. The voltage has been further decreased; however, buses 7 to 11 still surpass the limit with a value of 1.066 p.u.. The active power flow through Feeder 1 towards Feeder 2 and the external grid is decreased from 11.228 MW to 11.09 MW, whereas the reactive power import of Feeder 1 is increased from 2.715 Mvar to 6.87 Mvar. Regarding the loading of the lines, the most loaded one is Line 3-8 with 96.6%; whereas the loading of TRF 1 is 54.9%. This loading increases due to the high reactive power import from the external grid. The absorption of reactive power presents a notable increase in the total line losses, being 2.60 MW and 2.06 MVAr. The loss increase respect the previous scenario is 0.29 MW and 0.29 MVAr.

Although the voltage levels improve, this significant increase of reactive power consumption is not beneficial neither for the DSO nor the TSO. In the case of the DSO, this leads to an important increase in losses. For the TSO, a significant increase in reactive power demand coming from many DSOs would require more investment on reactive power compensation and a reinforcement of the network; otherwise, the security of supply would be compromised by the increased risk of voltage collapse [68].

Case 2 - No Generation

As the wind turbines and the CHP have no obligation to provide reactive power when they do not operate, the results will remain unchanged respect to the improvement achieved by the tap changer.

Summary

In this section it has been proved that the absorption of reactive power from the wind turbines and CHP partially corrects the voltage drop, decreasing the voltage from 1.099 to 1.066 p.u., as it is summarized in Table 3.6. It was also observed that the total losses through the lines increased, therefore, the utilization of reactive power compensation is not desirable and it will be not be considered for the sizing of the electrolyzer. This fact assures that the voltage is kept within limits during steady state operation, without requiring reactive power absorption. Nevertheless, the dynamic behavior of the OLTC and AE might not be fast enough to correct short term voltage deviations. Hence, the reactive power capability will be left for voltage support in these extreme cases.

Table 3.6: Comparison of critical voltages in Cases 1 and 2 with only tap control and with both tap control and reactive power dispatch

	With OLTC	**OLTC & reactive power dispatch**
Case 1 - bus 9, h. 121	1.099 p.u.	1.066 p.u.
Case 2 - bus 7, h. 105	0.971 p.u.	0.971 p.u.

3.2.4 Implementation of the Alkaline Electrolyzer

As explained in subsections 3.2.2 and 3.2.3, the OLTC and reactive power could not bring the voltage within allowed limits. The grid presents overvoltage when both wind turbines and CHP are at maximum generation. The high amount of power that has to be transferred to the external grid leads to a high voltage drop from the generation to the external grid. This can be avoided by increasing the active power consumption in Feeder 1.

As explained in chapter 2, Power-to-Gas is an emerging technology that can be beneficial in grids with a high penetration of renewables. Therefore, an alkaline electrolyzer is connected into the grid in order to provide an effective voltage support and energy management. Only the OLTC is maintained active for the dimensioning purpose, as explained in the conclusiong of the previous scenario. Firstly, the placement and size of the electrolyzer will be determined; secondly, the coordination with the rest of the voltage regulation elements, namely OLTC and reactive power, is presented; then, the hydrogen produced is calculated; finally, the improvement in the grid is tested.

Unit Placement

Firstly, the location will be determined by means of load flow sensitivities and losses criteria. Load flow sensitivities determine how the change of generated/consumed power in different buses affects the variation of voltage in a certain bus. As previously mentioned in Section 3.2, the bus with the biggest overvoltage is bus 9. Therefore, load flow sensitivities have been carried respect to bus 9 at hour 121, the one presenting the biggest overvoltage. The buses that affect the most to a voltage variation in bus 9 are buses 11, 10 and 9 with sensitivity values of 0.00724 p.u./MW and 0.00789 p.u./Mvar. Among the three possibilities, the location that leads to lower losses is

bus 9. This is because buses 10 and 11 do not have generation; thus, the power flow is always from bus 9 towards them. Consequently, placing the electrolyzer in either bus 10 or bus 11 would increase the mentioned power flow through these lines, leading to increased losses. Besides, bus 9 is the bus where the CHP plant is connected to, making it physically more feasible to inject the hydrogen into its gas pipes. Hence, this bus is the chosen one for placing the electrolyzer. Figure 3.12 illustrates the new structure of the grid, including the electrolyzer in bus 9.

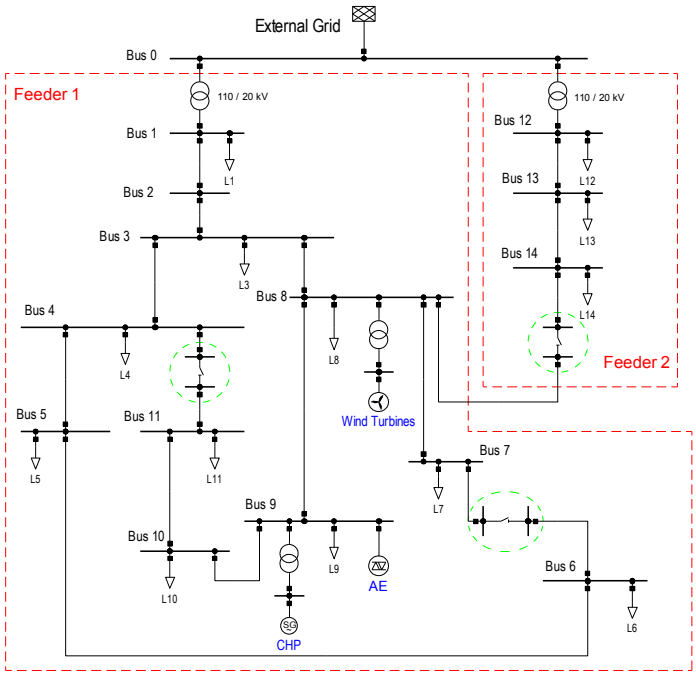

Figure 3.12: Single-line diagram of the grid including alkaline electrolyzer load

Unit Sizing

After the location has been determined, the size of the electrolyzers is calculated. This will be done maintaining the module size presented in [47], therefore the modeled AE units amount to 0.355 MW plus 0.08 MW for the compressor. It should be noted that the electrolyzer is merely sized for the considered study and the main target is to bring back the voltage within limits and to provide energy management. An optimal sizing should be done according to annual analysis, taking into account losses, economical aspects and hydrogen demand.

The sizing is calculated at the worst case scenario, Case 1 at hour 121. The OLTC is considered but not the reactive power absorption, as explained in the summary of 3.2.3, which leads to a bigger sizing than if the latter was considered. Hence, the advantages of proceeding in such way are the avoidance of reactive power absorption and a bigger energy management capability.

The voltage in bus 9 was found to be 1.099 p.u. and therefore at least 0.049 p.u. needs to be corrected to bring the voltage within allowed limits. The previously calculated load flow sensitivities of bus 9 gave a value of $0.00724 p.u./MW$ for the active power. As a fast calculation, the active power necessary in order to correct a voltage deviation of 0.049 p.u. can be estimated according to Eq. 3.10:

$$P_{required} \simeq \frac{\Delta V_9}{\frac{\Delta V_9}{\Delta P_9}} = \frac{0.049 p.u.}{0.00724 p.u./MW} = 6.77 MW \tag{3.10}$$

Where $\frac{\Delta V_9}{\Delta P_9}$ is the load flow sensitivity of bus 9 and ΔV_9 is the voltage deviation that has to be corrected. It should be noted that the varying sensitivity value has been approximated to the provided one, calculated for Case 1 during hour 121. As the modeled electrolyzer unit is 0.435 MW in total, 15 units are selected, accounting for a total nominal power of $6.525MW$. It is introduced in the grid as a constant power load, as further explained in Section 4.5.

Coordination of OLTC, Wind Turbines, CHP and AE

As explained in Section 3.2.3, the reactive power is not taken into account for the sizing of the electrolysis unit. However, its coordination is included with the OLTC and AE as it will be used in extreme situations. Furthermore, it is explained that the coordination of the three units is necessary to avoid interference with their performance. Hence, the decentralized coordination strategy presented in 3.2.3 is adapted to integrate the electrolyzer, which operates following a voltage - active power droop during arising overvoltages. It should be added that the electrolyzer is assumed to incorporate a power converter, with a size of 0.355 MVA, which also allows reactive power control. Hence, the latter is additionally controlled according to a voltage - reactive power droop, but only active during undervoltage situations.

Figure 3.13 shows the proposed control for the absorbed active power and produced reactive power of the AE. The blue line represents the reactive power control, whereas the green represents the active power control. The pink area highlights the allowed voltage limits.

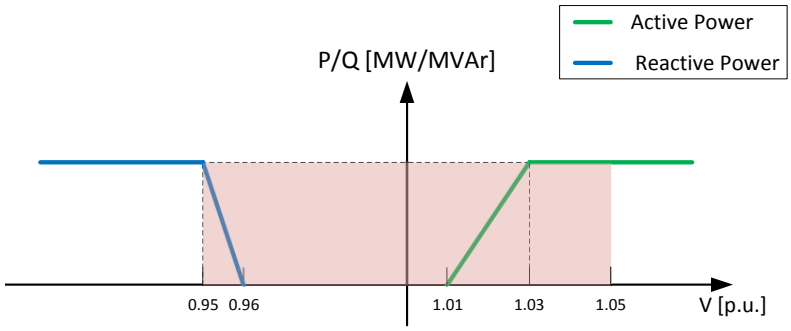

Figure 3.13: Voltage - power droop control of the AE

The priorities for the voltage control coordination is assessed as follows: firstly, when the voltage surpasses 1.01 p.u. the AE starts regulating, secondly, if the voltage reaches 1.03 p.u. the OLTC regulation is included and finally, the DGs' reactive power is triggered when 1.04 p.u. is exceeded. As explained in Section 3.2.3, this is done by setting the deadbands in an intelligent way. The implemented coordination can be appreciated graphically in Figure 3.14. It should be noticed that the usage of reactive power is intended to be minimized by using it only when the voltage is close to the allowed limit.

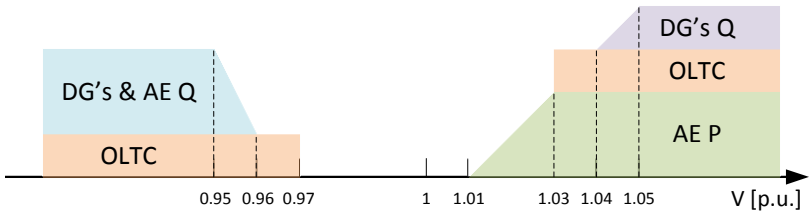

Figure 3.14: Coordination of the OLTC, power factor controller and the AE

Hydrogen Production

Once the electrolyzer is sized, the produced hydrogen can be calculated. The electrolyzer model presented in [47], further developed in Chapter 4, calculates the hydrogen output, $\dot{m}_{H_2}$ in $[mol/s]$. Hence, the total produced hydrogen volume flow, $\dot{V}_{H_2}$ in $[Nm^3/h]$, can be calculated according to Eq 3.11.

$$\dot{V}_{H_2} = \sum_{n=1}^{15} \dot{m}_{H_2}[mol/s] \cdot \frac{3.6 \cdot 10^3 s}{1h} \cdot \frac{22.4 Nm^3}{10^3 mol} \tag{3.11}$$

Eq 3.1, 3.2 and 3.11 will determine how the 10% volume concentration limitation will limit the hydrogen injection. This is assessed in the dynamic simulations performed in Chapter 5. Following, the electrical implementation of the electrolyzer will be tested in two cases; i.e. maximum and no generation.

Case 1: Maximum Generation

As for the previous scenarios, a load flow simulation is performed during maximum generation at hour 121. The OLTC remains active whereas the reactive power does not. As it can be observed in Figure 3.15, after placing a load of $6.525MW$ in bus 9 all the buses present voltage within limits, where the highest voltage found is 1.050 p.u. in buses 7 to 11. The active power export of Feeder 1 decreased to 6.229 MW, whereas the reactive power import also decreased to 1.589 Mvar.

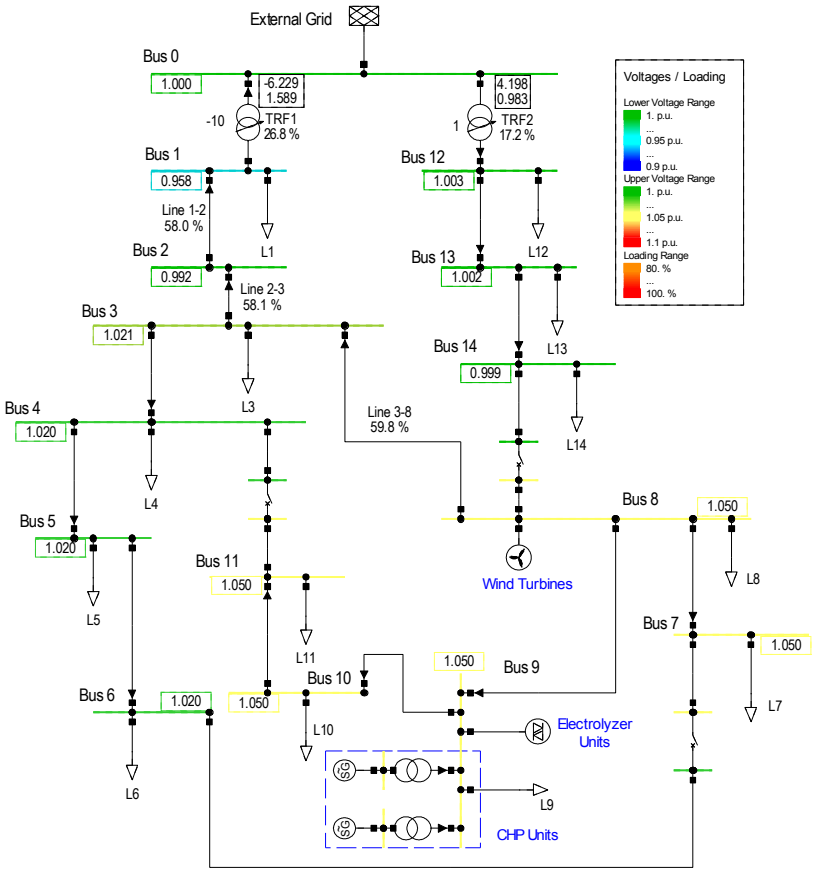

Figure 3.15: Load flow of the grid in DIgSILENT at maximum generation, OLTC and 6.525 MW of electrolyzers

Regarding line losses, the introduction of the electrolyzers leads to an improvement, being now 0.98 MW and 0.66 MVAr. The produced power is now consumed locally, which decreases power flow along the lines and, consequently the losses. Furthermore, the loading rate of the transformers and lines is also reduced. The loading of TR1 before implementing the electrolyzers was 54.9% and now decreased to 26.8%. Regarding the lines, the one with highest loading is now line 3-8 with 59.8%, being 96.6% in the previous scenario.

Case 2: No Generation

The electrolyzers represent an additional load to the grid; hence, the voltage drop has to be checked during no generation case and maximum electrolyzer load in case it is below the lower boundary. The load flow simulation is performed at hour 105, when the loads are at their peak. Figure 3.16 shows that the bus with highest voltage drop is bus 7 with a value of 0.927, surpassing the lower boundary. Furthermore, buses 7-11 present a voltage below the admissible limit. This means that the operation of the electrolyzers is constrained by a lower voltage limitation. Regarding power flow import in Feeder 1, it increases up to 18.378 MW and 3.711 Mvar.

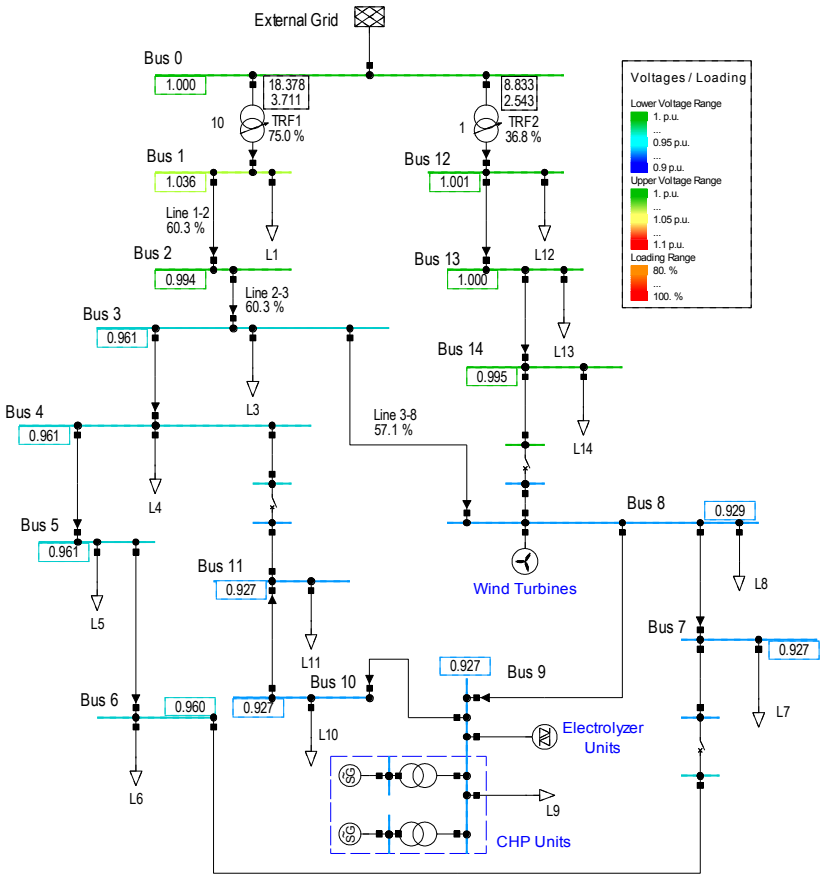

Figure 3.16: Load flow of the grid in DIgSILENT at no generation, OLTC and 6.525 MW of electrolyzers

In this case, as the external grid has to supply a higher consumption the loading of the lines and transformer has increased respect to the previous scenarios. Being the loading of TRF1 75.0% and line 1-2 and 2-3 60.3%. The total line losses are also higher with a value of 1.03 MW and 1.07 MVAr.

In order to estimate the maximum amount of power the electrolyzers can consume without causing an undervoltage in bus 7, Eq. 3.12 is applied. It should be noted that the voltage in the mentioned

bus should increase by 0.023 p.u..

$$P_{max} = P_{rated} - \Delta P = P_{rated} - \frac{\Delta V_7}{\frac{\Delta V_7}{\Delta P_9}} = 6.525 - \frac{0.023 p.u.}{0.0124 p.u./MW} = 4.67 MW \tag{3.12}$$

Where P_{max} is the maximum power the electrolyzer can consume, P_{rated} is the nominal power of the electrolyzer at full power, ΔP is the amount of power that will produce the desired change of voltage, ΔV_7 is the desired change of voltage and $\frac{\Delta V_7}{\Delta P_9}$ is the load flow sensitivity of bus 9.

After reducing the load of the electrolyzers 6.525 MW to 4.67 MW it is found that the voltage in bus 7 is 0.95 p.u., being the rest of the buses voltage above the lower boundary.

Summary

In this section, the size and location of the electrolyzer have been determined assuming active OLTC and no reactive power absorption from the DGs. It has been found that 15 electrolyzer units are necessary in order to bring the voltage within allowed limits. In Case 1 they bring back the voltage to 1.05 p.u. and in Case 2 they lower the voltage down to 0.927 p.u., below the admissible limit. Therefore, these units should be only utilized to absorb excess power from the wind turbines and CHP. The following table 3.7 summarizes the steady state voltage results, compared to the ones obtained in the previous scenario.

Table 3.7: Comparison of critical voltages in Cases 1 and 2 with reactive power dispatch and with 6.525 MW of electrolyzers, both with tap control

	Q dispatch & OLTC	**Adding 15 AE units**
Case 1 - bus 9, h. 121	1.066 p.u.	1.050 p.u.
Case 2 - bus 7, h. 105	0.971 p.u.	0.927 p.u.

Besides the voltage regulation, the implementation of the alkaline electrolyzer leads to a decrease in losses and an important reduction of the exported active power through Feeder 1. This means that it is able to perform energy management, i.e. utilizing the local generation for producing hydrogen.

3.3 Conclusions

The results of the steady state analysis are summarized and illustrated in this section. Figures 3.17 and 3.18 show the voltage of every bus of Feeder 1 in the different analyzed scenarios. The results of the Base Case analysis shows that the high penetration of distributed generation (wind turbines and CHP) leads to violating the maximum allowed voltage, whereas the minimum boundary is never surpassed. Initially, the highest voltage during Case 1 was 1.135 p.u. at bus 9 and in Case 2 the lowest was 0.958 p.u. at bus 7. The overvoltage was partially corrected by the OLTC of the substation transformer, although remaining above the allowed limits. In order to further decrease the overvoltage, the wind turbines and CHP were asked to absorb reactive power, however, this measure was not enough.

Finally, electrolyzers were integrated in the grid in order to correct the remaining overvoltage after the application of OLTC. Therefore, reactive power compensation was not considered in this scenario. According to load flow sensitivities and losses criteria, bus 9 was the chosen one to connect them to. For the sizing of electrolyzers, 15 modules of 0.435 MW were selected in order

to bring the voltage within limits and provide energy management services. It should be noticed that, during Case 2 the operation of the 15 AE units produce undervoltage, as shown in 3.18. Therefore, the maximum power that the electrolyzers can consume is 4.67 MW.

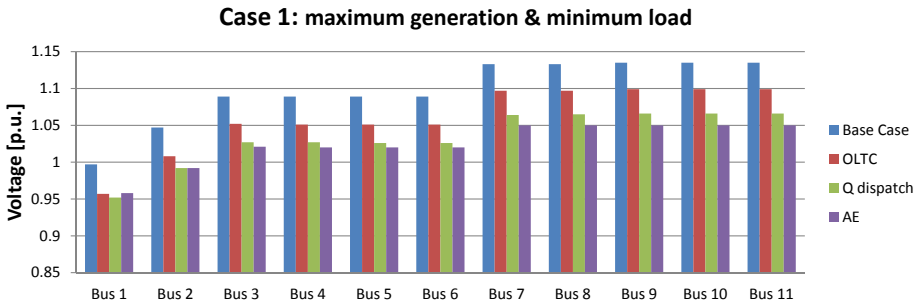

Figure 3.17: Voltage results of the performed load flows during Case 1

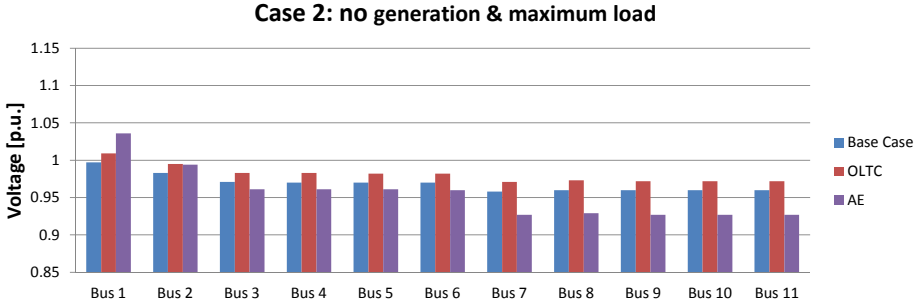

Figure 3.18: Voltage results of the performed load flows during Case 2

The capability of the grid to accept the described measures to provide voltage support has also been analyzed. As illustrated in figure 3.19, it can be observed that in Case 1 the loading of the lines and transformer reaches high values. The worst scenario in terms of loading rates occurs when the generating units, wind turbines and CHP, absorb reactive power. The highest loading value occurs at line 3-8 being 96.6%, which is due to the increased transmitted power through the lines. Regarding the integration of alkaline electrolyzers, it can be observed that the line loading decreases as the the generated power is consumed locally. However, when there is no local generation the loading increases as the transmitted power through the lines is higher in order to supply the AE load.

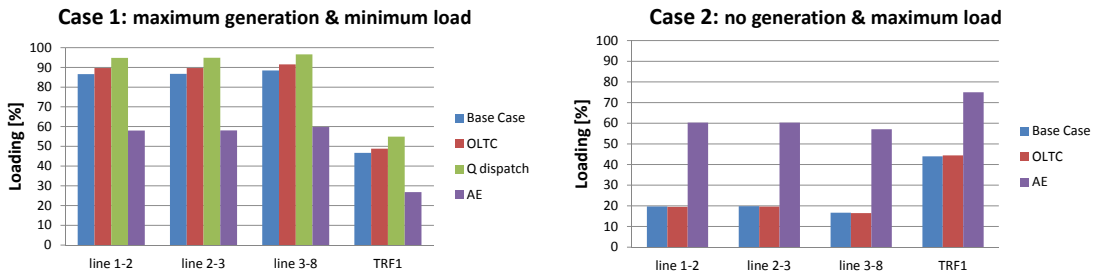

Figure 3.19: Line and transformer loading results of the performed load flows during (a) Case 1 and (b) Case 2

The direction of the active and reactive power flow in Feeder 1 can be observed in Figure 3.20,

where a positive value means power import from the external grid and a negative value means power export to the external grid. In Case 1, the decrease of exported power is observed when the electrolyzer is implemented, as the power produced by the DG is utilized to produce hydrogen and, at the same time provide energy management services. However, in Case 2, the increase of imported power is higher than in the previous cases, as the AE load is added to the residential and industrial loads.

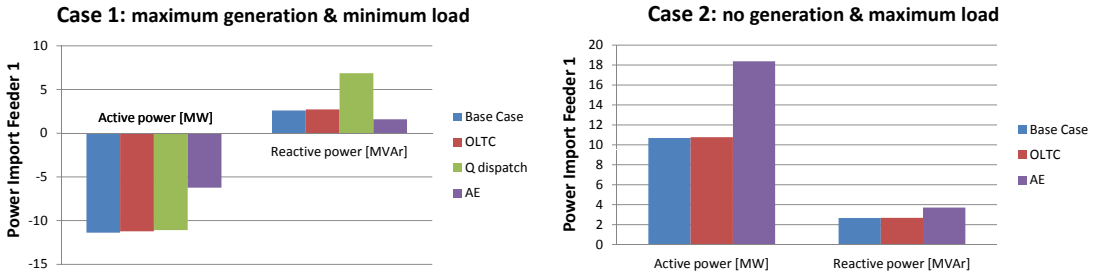

Figure 3.20: Active and reactive power import of Feeder 1 during (a) Case 1 and (b) Case 2

Finally, the total losses through the lines are presented in figure 3.21. It is observed that even though the voltage is corrected, a significant increase in the line losses appeared when including OLTC and reactive power compensation reaching 2.60 MW and 2.07 MVAr. However, in Case 1 the losses are compensated when the alkaline electrolyzers are included decreasing by 0.53 MW and 0.44 MVAr. Regarding Case 2, the line losses increase when the electrolyzer is included, since the power to supply it comes from the external grid.

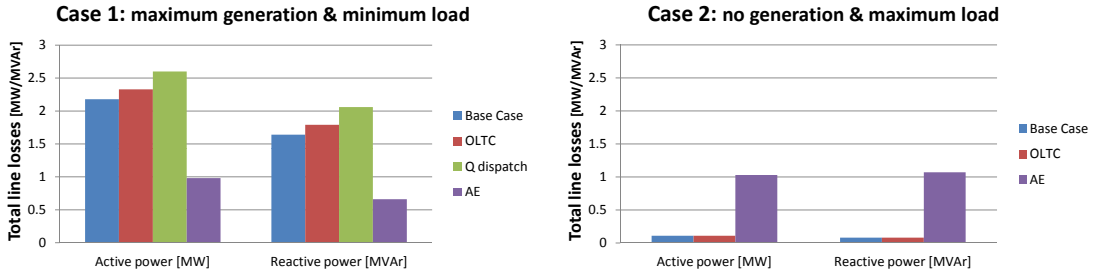

Figure 3.21: Total line loss results of the performed load flows during (a) Case 1 and (b) Case 2

In this chapter, it has been proved that the introduction of an alkaline electrolyzer enables the purpose of providing energy management services and voltage regulation by absorbing the excess production of the distributed generation. However, in order to decrease losses, its operation should be defined according to the grid requirements and adapted to the local generation, i.e. the CHP plant and wind turbines.

As the loading of the different components is below the maximum during the worst case scenarios, its analysis will be disregarded in the dynamic simulations. Focus will be placed on the voltage magnitude, losses and active and reactive power export from Feeder 1. Furthermore, it should be highlighted that the limitations of the electrolyzer to consume active power was not taken into account in this chapter. As mentioned in [47], the operation temperature of the electrolyzer limits its capacity to produce hydrogen and, therefore, to consume active power. The dynamic behavior of the OLTC, wind turbines, CHP plant and electrolyzers is presented in Chapter 4, in order to assess the capability of the electrolyzers to perform the mentioned regulation.

4 Dynamic Model Implementation in DIgSILENT PowerFactory

In this chapter, the dynamic behavior of the different elements of the study case is modeled. The models will be developed and simulated in DIgSILENT PowerFactory, and later introduced into the case study grid that was presented in Section 3.1. The elements that possess an inherent dynamic behavior are the loads, wind turbines, CHP, the OLTC and the alkaline electrolyzer.

Table 4.1 summarizes the type of owner and control of the mentioned dynamic elements. As the owners of the the wind turbines and CHP are private producers, the DSO is only able to control their power factor (pf) in case that voltage issues arise, as previously explained in Section 3.2.3. Hence, their active power output depends on different criteria: wind speed in the case of the wind turbines, heat demand and electricity price in the case of the CHP.

Both the alkaline electrolyzer and OLTC are owned by the DSO, thus these elements are modeled into more detail, as their output can be freely modified by the latter. Nevertheless, the operation of the OLTC and the electrolyzer might be constrained by their inherent characteristics. For the OLTC this is the daily tap changes limitation, due to reliability issues, whereas for the electrolyzer is its operating temperature [47].

It is common for some DSOs to own part of the distribution gas networks such as DONG Energy in Denmark [69]. Therefore, the DSO can make profit of the hydrogen produced by the electrolyzer and, at the same time, provide voltage regulation and energy management services to the electrical grid.

Table 4.1: Owners and available control for the DSO of different elements of the grid

	CHP	**Wind Farm**	**OLTC**	**Electrolyzers**	**Loads**
Owner	Private Owner	Private Owner	DSO	DSO	Private Owners
DSO Control	pf control if voltage issues	pf control if voltage issues	Full	Full	None

As previously explained in Chapter 3, the CHP plant is assumed to run on natural gas and to provide district heating to part of the customers of the analyzed grid. Furthermore, the hydrogen produced by electrolysis is assumed to be injected into the gas network in a limited rate of 10% of volume. The dynamic modeling presented in this chapter will help to understand both the electrical behavior of the elements mentioned in Table 4.1 and their interactions with the district heating and gas networks, through the CHP plant and electrolyzer.

4.1 Modeling of the Loads

As explained in Section 3.1, the loads follow predefined profiles presented in Figures 3.2 and 3.3. For the dynamic simulation, the aggregated load profiles for each bus are inputted as a measurement file to the grid element. The dynamic behavior of each load is defined by internal model of PowerFactory, where the user can customize the percentage of static load (constant impedance) and dynamic load. The characterization of the loads has already been explained in Section 3.1 and the different ratios are presented in Table B.6.

4.2 Modeling of the Wind Turbines

The aim of this project is to simulate a Danish electrical distribution grid with high wind penetration. For this purpose, the modeling of the behavior of a wind farm is necessary as their behavior might lead to technical issues, as the voltage rise presented in Chapter 3. Therefore, a reasonably accurate power output of the wind farm is presented in this section, in order to precisely simulate the potential issues.

The wind farm output is calculated from a time series of wind speed data. Dynamic modeling of the latter is not included since the control of the wind farm is not on the scope of this project. Due to this limitation, the wind turbines will be modeled as an active and reactive power time series coming from a static generator.

According to [70], the Vestas V80 2MW is one of the most common models installed on-shore. Therefore, it has been the selected model for the present project. Table 4.2 shows the relevant characteristics of the chosen wind turbine:

Table 4.2: Relevant characteristics of the Vestas V80 2MW turbine [71]

Generator type	**Asynchronous with variable speed**
Rated power	2 MW
Cut-in wind speed	4 m/s
Rated wind speed	16 m/s
Cut-out wind speed	25 m/s
Rotor diameter	80 m
Hub height	67 m

Once the turbine model has been selected and its relevant characteristics are known, the wind power output from the wind farm can be calculated, as summarized in Figure 4.1 where the applied software for each step is also mentioned.

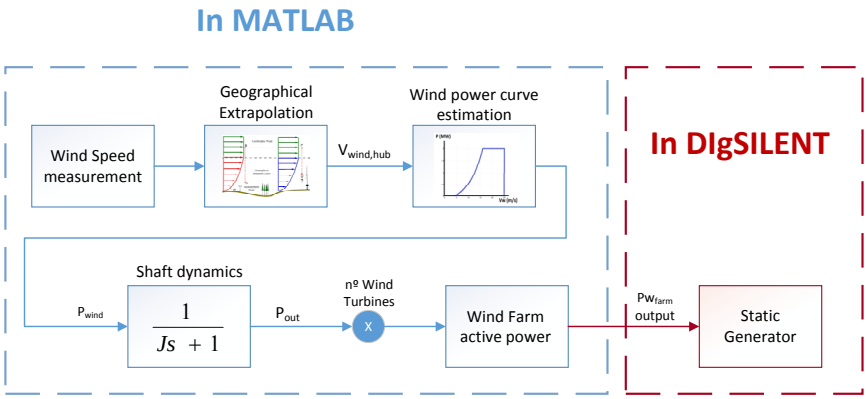

Figure 4.1: Wind farm active power calculation from wind speed measurement

Firstly, the obtained wind speed has to be adapted from the measurement point to the hub height; next, the wind power extracted from the obtained wind speed is calculated through the wind power curve; finally, the obtained wind power is inputted through a delay block emulating the shaft dynamics and multiplied by the number of wind turbines that compose the wind farm. The final wind farm active power output is sent to DIgSILENT PowerFactory and forwarded to a static generator.

4.2.1 Wind Speed Adaptation

Wind speed measurements for a summer and a winter week have been taken from [72], with a sampling of $10s$. The measurements have been taken at a height of $12m$ and not at the hub height, therefore a wind speed conversion has been done using the method presented in [73]. The detailed explanation of this method is summarized in Appendix B.2. The result of this conversion is that the obtained wind speed measurement has to be scaled by the factor of 2.108 as expressed in the following equation:

$$v_2(67m) = 2.108 \cdot v_1(12m) \tag{4.1}$$

Where $v_2(67m)$ represents the wind speed at the hub height, 67 m, and $v_1(12m)$ represents the wind speed at the measurement point, 12 m.

4.2.2 Wind Power Curve

Once the wind speed time series is adapted to the hub height, the power output of the turbine is calculated throughout the wind power curve. For this purpose the cut-in, rated and cut-out wind speeds included in Table 4.2 are used, obtaining three different power outputs:

- If wind speed $< 4m/s$ or wind speed $> 25m/s \longrightarrow P = 0$
- If $4m/s <$ wind speed $< 16m/s \longrightarrow P = 0.5 \cdot \rho \cdot Cp \cdot \frac{\pi D^2}{4} \cdot v^3 \cdot 10^{-6}$ [MW]
- If $16m/s <$ wind speed $< 25m/s \longrightarrow P = 2$ MW

Where v is the wind speed in m/s, P is the output active power of the wind turbine, ρ is the air density in kg/s, and Cp is the power coefficient.

It should be remarked that the Cp applied has been assumed to be constant, with a value of 0.1586. It was calculated in order not to produce discontinuities in the power curve when the wind speed is $16m/s$. Figure 4.2 compares the obtained power curve with the one provided by the manufacturer. As it can be appreciated, the approximation can be considered good enough for the purpose of this project.

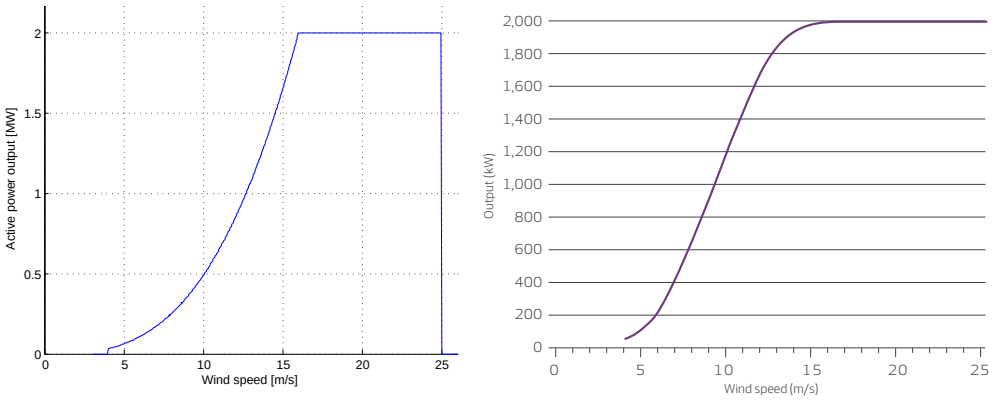

(a) Estimated wind power curve **(b)** Wind power curve provided by Vestas [71]

Figure 4.2: Comparison between the estimated wind power curve (left) and the provided by the manufacturer (right)

4.2.3 Shaft Dynamics and Wind Farm Active Power Output

In order to approximate the shaft's dynamics, the previously obtained power vector is introduced to a time delay block with Matlab Simulink. An inertia value of $J = 8.04s$ was observed in a DIgSilent PowerFactory template for a 2 MW doubly-fed induction generator (DFIG) wind turbine, as the Vestas V80 2MW, and therefore has been assumed for this purpose. Since the wind farm is composed by six wind turbines, this output has been multiplied by this number. The transfer function applied in this step can be appreciated in Figure 4.1. Neglecting losses, the obtained power is the active power produced by the six wind turbines.

4.2.4 Integration in DIgSilent PowerFactory

In order to integrate the obtained wind power into DIgSilent Powerfactory, a measurement file with the previously presented values was created, forwarding an active current setpoint (i_d) to a static generator model. Since the voltage is expected to vary during the simulations, the i_d signal has to be adjusted proportionally to the voltage (in p.u.) so the power output from the wind turbine does not vary proportionally to the voltage fluctuations. Hence, the voltage of the bus where the wind turbines are connected to, i.e. bus 8, is used in order to perform this correction in the Voltage Adjustment block. Furthermore, a reactive current setpoint ($i_{q_{ref}}$) coming from the reactive power control, explained in Section 3.2.3, is forwarded to the static generator. Figure 4.3 shows the composite model created for this purpose.

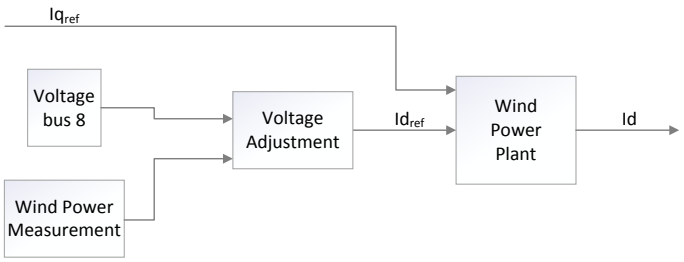

Figure 4.3: Composite model for the wind farm power output

After running simulations for the selected weeks, the wind farm active power output was obtained. Figures 4.5 and 4.4 show the power generation, for the selected winter and summer weeks, respectively.

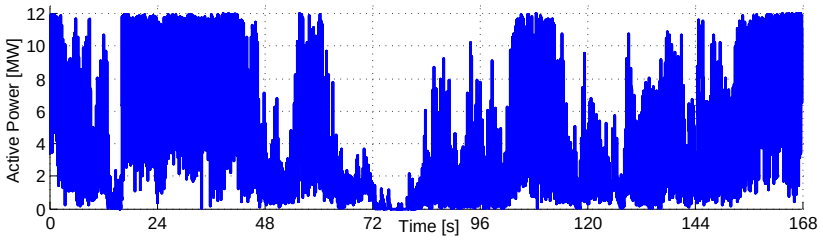

Figure 4.4: Wind active power output during the winter week [72]

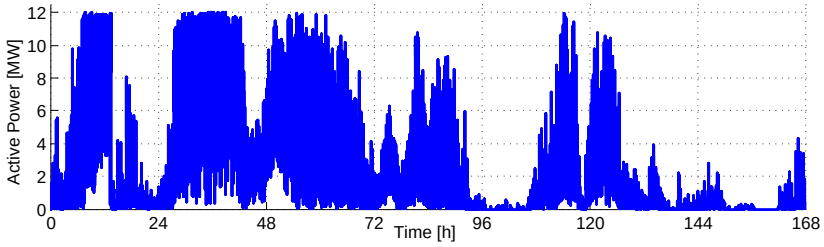

Figure 4.5: Wind active power output during the summer week [72]

Reactive Power Control

The reactive power control introduced in Section 3.2.3 is modeled and explained in the following. For this purpose, the voltage of the PCC (i.e. bus 8) is taken for implementing the mentioned control, sending the reactive current reference ($i_{q_{ref}}$) to the composite model explained in Figure 4.3. Figure 4.6 shows the composite frame of the reactive power control, where i_d is the output active current signal of the wind farm model.

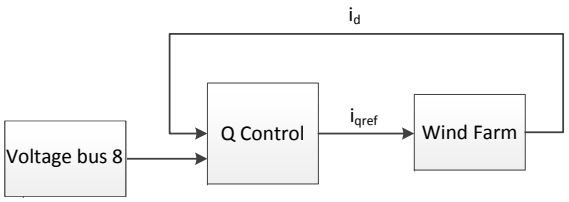

Figure 4.6: Composite model for the wind farm reactive power control of the wind farm

The Q control block is further explained in Figure 4.7. The V-pf droop block implements the power factor controller explained in Section 3.2.3, whereas the Power factor to i_q block takes the power factor set-point and the actual i_d current output in order to calculate the $i_{q_{ref}}$ set-point. U represents the current voltage at bus 8, U_{ref} is the reference voltage, i.e. 1 p.u., and therefore U_{diff} is the difference between the previous two.

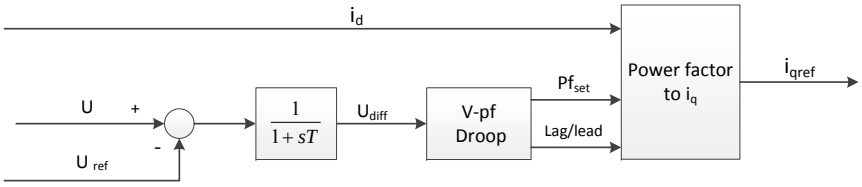

Figure 4.7: Block diagram of the reactive power control of the wind farm

It should be noticed that the reactive power control is not tested, maintaining a unity power factor for the simulation results presented in Figures 4.4 and 4.5. Instead, it will be implemented in Chapter 5 since the settings are changed according to the studied case (with or without AE).

4.3 Modeling of the CHP Plant

As explained in Section 3.1.2, the district heating of the case study grid is supplied by a gas-fired CHP plant. The present CHP plant is assumed to possess two CHP gas turbine units, gas-fired boilers and a heat storage tank. The rated power of the CHP units (accounting for the two units), boilers and the capacity of the heat storage tank have been presented in Table 3.3 in Chapter 3. The objective of this section is to assess how the district heating demand affects the electrical behavior of the CHP plant, by obtaining a realistic electrical power output from the latter.

As stated in [25], the ultimate target of the CHP plant is to meet the heat demand and at the same time obtain a high revenue. Therefore, in order to determine whether the operation of the CHP units is profitable the Elspot and up-regulation prices are used. When the CHP units are offline, the heat demand is supplied by the heat storage and/or the boilers. The composite frame developed for the CHP plant is showed in Figure 4.8. It includes the two CHP units, the heat storage, the heat demand and the decision-making block of the CHP units' and boiler's set-points, which depend on the current Elspot and up-regulation prices.

Regarding input signals to the CHP units, Pf_{set} determines the value of the power factor of

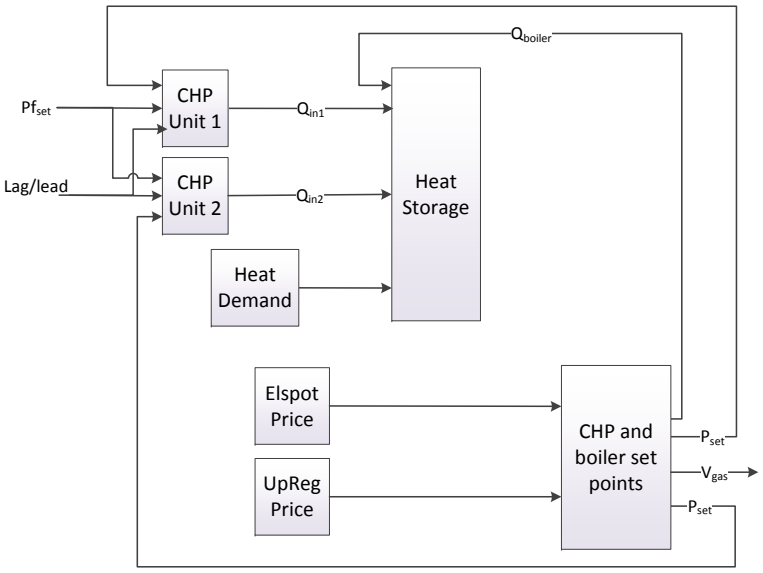

Figure 4.8: DIgSILENT PowerFactory composite model of the CHP plant

the generators and $lag/lead$ specifies whether it is lagging or leading. Q_{in} represents the heat produced by the CHP units and Q_{boil} represents the heat produced by the gas-fired boilers, both signals being inputted to the Heat Storage. The Elspot and Up-regulation prices are sent to the block "CHP and boiler set-point", which decides how the CHP plant operates. The obtained active power setpoint P_{set} is sent to each CHP unit, and the volume of natural gas required $\dot{V}_{gas}$ is measured.

In the following, the composite model of the case study CHP plant is explained.

4.3.1 CHP Units

The CHP unit block is modeled in another composite model. It consists of a generator, excitation system and prime mover/governor. These models, as well the composite frame, have been taken from the available library in PowerFactory and are described in Appendix B.3. Nevertheless, two contributions have been made in order to adapt the composite frame to the CHP use.

The first addition is the Power to Heat block, which estimates the heat output of the unit Q_{in} by applying the power to heat ratio to the produced active power P_t from the Turbine Generator. The other contribution is the the Power Factor block, which receives the active and reactive power produced by the generator, P and Q respectively, and the power factor command from the reactive power control through the signals $P_{f_{ref}}$ and $lag/lead$, as explained in Section 3.2.3. This modifies the set-point of the excitation voltage v_{cs} accordingly and inputs the final excitation voltage v_e to the generator. This control is achieved throughout a PI controller, as illustrated in Appendix B.3. Finally, the nominal apparent power S_{nom}, the nominal power factor $cos\theta$ (both parameters of the machine) and the rotational speed of the generator ω are sent to the turbine governor. The explained frame can be observed in Figure 4.9.

The power factor control is included in order to emulate the way the local CHP plants control their reactive power. During normal operation the power factor is assumed to be one, unless they receive a command from the DSO. Figure 4.10 shows the test of the power factor controller when the CHP units are operated throughout the week. It can be observed that the reactive power is kept close to zero at every moment.

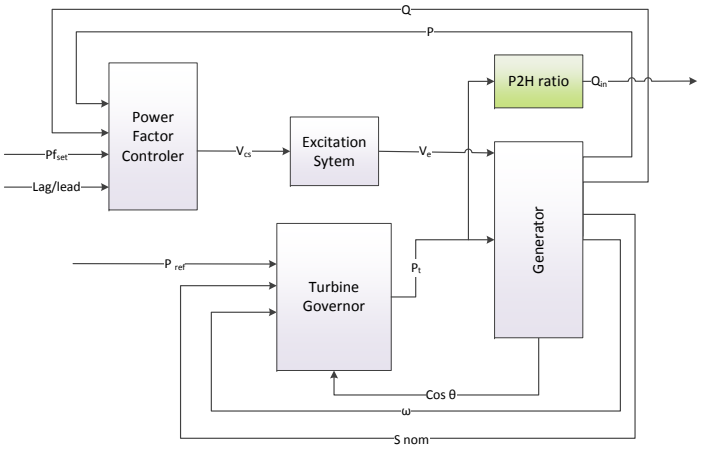

Figure 4.9: Modified composite model for the CHP units

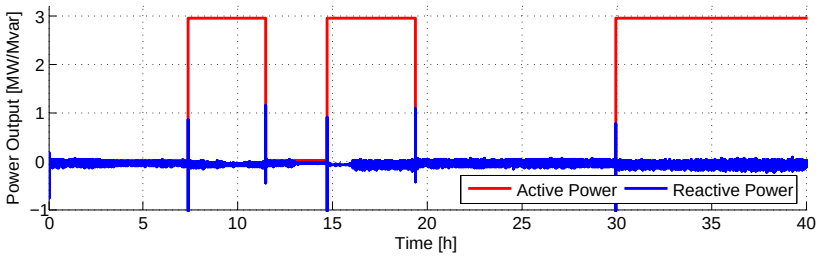

Figure 4.10: Active and reactive power output from a CHP unit

Reactive Power Control

In the following the reactive power control that forwards the power factor set-point to the CHP units is explained. The control is based on the voltage-power factor controller explained in Section 3.2.3. The composite frame of this reactive power control is shown in Figure 4.11. It measures the voltage in the PCC (i.e. bus 9), implements the mentioned voltage-power factor controller and sends the power factor set-point to the CHP units.

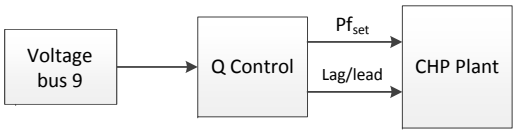

Figure 4.11: Composite model of the CHP plant reactive power control

The Q control block is further explained in Figure 4.12. The V-pf droop block implements the power factor controller explained in Section 3.2.3.

Figure 4.12: Block diagram of the Q control block of the CHP

It should be noted that the reactive power control is not tested, maintaining a unity power factor for the simulation results presented in this section. Instead, it will be implemented in Chapter 5 since the settings are changed according to the studied case (with or without AE).

4.3.2 Heat Demand

The heat demand slot includes a measurement file of the heat to supply during each hour, accounting for the 660 customers heat demand profile plus a 25% of losses, as explained in Section 3.1.2.

4.3.3 Heat Storage

As stated in 2.4.1, most part of the CHP plants have a heat storage in order to decouple heat and electricity production. This system consists of a water tank which receives a heat input (Q_{in}) from the CHP units and boiler, and has a heat output (Q_{out}), in order to meet the heat demand. For each of the mentioned heat production units and consumption, the water is assumed to follow a closed circuit, therefore the mass flow rates from/into the storage can be considered equal. Hence, the volume of water in the storage can be assumed to be constant. The model of the Heat Storage slot is presented in Figure 4.13.

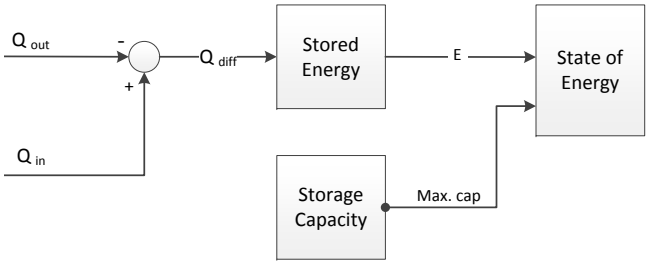

Figure 4.13: Model of the heat storage block of the CHP

Besides the heat inputs and output, there is also a heat loss through the walls of the tank, which has been assumed to be neglectable. Once the input and output heat are known, the thermal energy in the tank (E) can be calculated according to equation 4.2:

$$Q_{in} - Q_{out} = \frac{dE}{dt} \tag{4.2}$$

Finally, the state of energy of the tank [%] is calculated, from the stored energy and its maximum storage capacity.

4.3.4 Set-Points of the CHP Units and Boiler

This subsection includes the scheduling of the CHP plant, in which the heat demand is met at the lowest possible cost. Besides, it includes an estimation of the natural gas consumption according to its operation. In order to emulate the output of the CHP units as realistically as possible, the behavior of Skagen's CHP plant has been observed during the analyzed winter and summer weeks. Figure 4.14 shows, for the winter week, the heat output from the CHP units and the current Elspot and up-regulation prices, whereas Figure 4.15 shows the state of energy of the storage tank.

It can be observed that each of the three CHP units of the Skagen plant are either disconnected or operating at full power. Furthermore, it can be appreciated that the units start working at full power when the Elspot price surpasses $250DKK$, approximately. During this period the plant also receives the residual heat from two industries, fulfilling the heat demand thanks to the flexibility the heat storage provides. Besides, the heat storage remains at the same level after the week. This indicates that the thermal energy provided by the CHP units and both industries perfectly

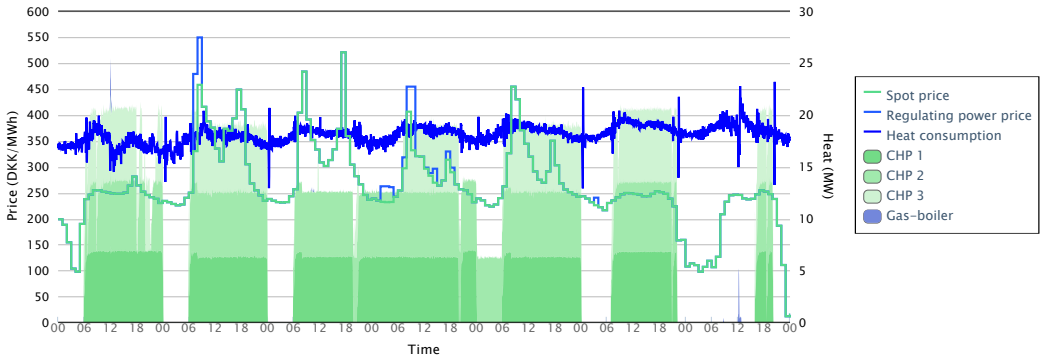

Figure 4.14: Skagen's CHP units output during the winter week

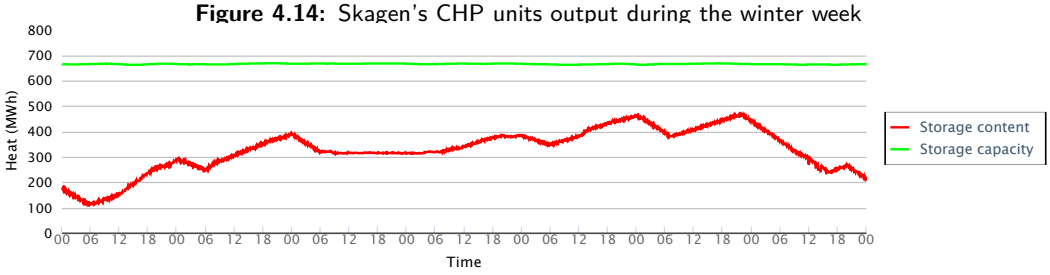

Figure 4.15: Skagen's tank's state of energy during the winter week

fulfills the heat demand energy. Therefore, in this project, the gas-fueled boilers will replace the function of the residual heat in the Skagen plant.

A Matlab script was created in order to evaluate the thermal demand the boiler has to supply throughout the week, assuming the CHP units operate at full power when Elspot or up-regulation prices go above $250DKK$. It was found that the thermal demand would be fulfilled by operating the boiler at 5.2 MW, in case the CHP units are offline. The obtained schedule of the CHP plant can be observed in Figure 4.16, whereas the heat storage state of energy is represented in Figure 4.17.

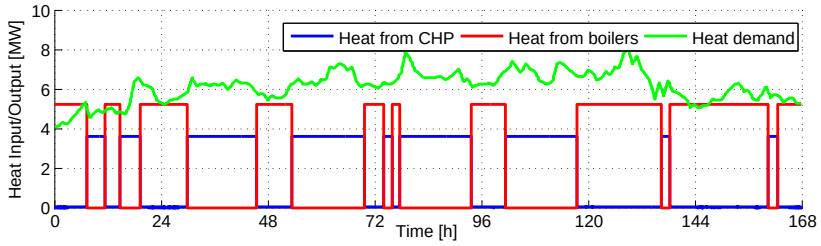

Figure 4.16: Heat demand, generated heat from boilers and generated heat from one CHP unit in the winter week

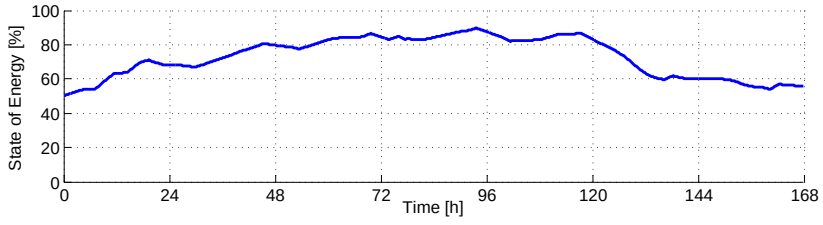

Figure 4.17: State of energy of the CHP's heat storage

As it can be observed, even with a simple operation of the boilers, the heat demand is met and the storage level is kept within limits assuming an initial condition of 50%. This shows the practical feasibility of this schedule without analyzing the dynamics. A more optimal operation of the boilers is out of the scope of this project.

For what concerns the summer week, the operation of the Skagen CHP plant is shown in Figures 4.18 and 4.19.

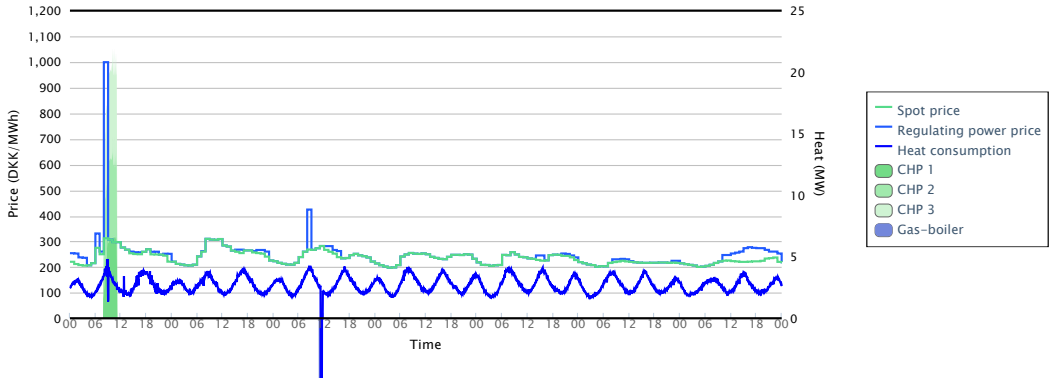

Figure 4.18: Skagen's CHP units output during the summer week

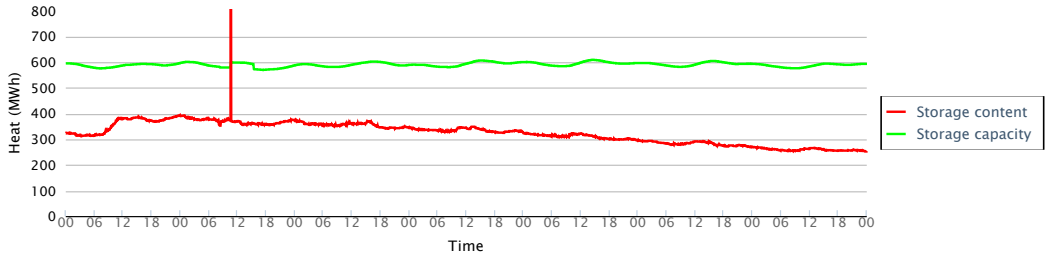

Figure 4.19: Skagen's tank's state of energy during the summer week

It can be observed that Skagen's CHP units are only operated for a few hours, where the Elspot and up-regulation prices were at the highest point of the week, above $300DKK$. During the rest of the week the heat demand was supplied by the residual heat from the industries and the heat storage. In a similar way as for the winter week, it will be approximated that when the Elspot or up-regulation prices go above $300DKK$, the implemented CHP units will operate at full power. Executing the same Matlab script, it was observed that the CHP units provide, approximately, the whole thermal demand throughout the week. Hence, the boilers do not have to operate. The obtained scheduling of can be observed in Figure 4.20, whereas the heat storage state of energy is represented in Figure 4.21.

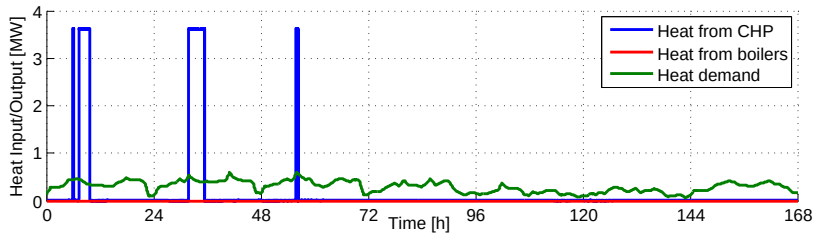

Figure 4.20: Heat demand, generated heat from boilers and generated heat from one CHP unit

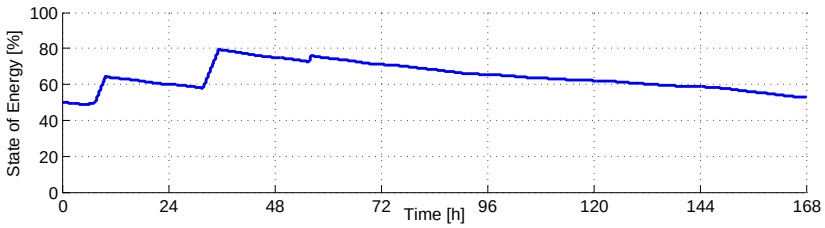

Figure 4.21: State of energy of the CHP's heat storage

As for the winter week, the heat demand is fulfilled and the storage is kept within limits, showing the feasibility of the obtained operation schedule.

Once the behavior of the CHP is known, its natural gas consumption can be estimated. For this purpose, Eq. 3.1 and 3.2, presented in Section 3.1.3, are implemented within the set-point blocks of the CHP units and boiler. Figures 4.22 and 4.23 show the gas consumption, in $[Nm^3/h]$, during the winter and summer weeks, respectively.

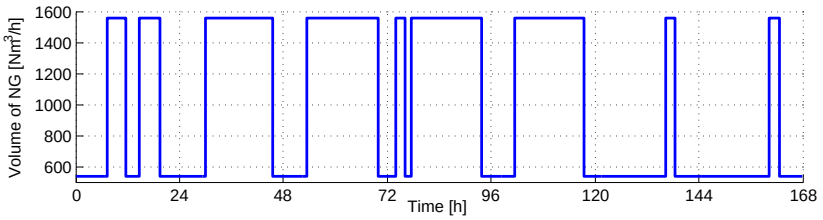

Figure 4.22: Gas consumption of the CHP in $[Nm^3/h]$, during the winter week

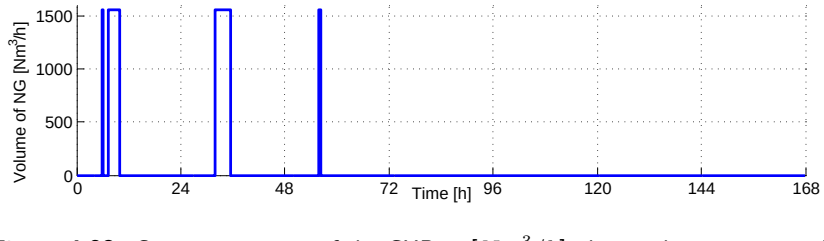

Figure 4.23: Gas consumption of the CHP in $[Nm^3/h]$, during the summer week

4.4 Modeling of the Line Drop Compensation and Tap Changer Controller

As shown in Chapter 3, the OLTC was able to correct the voltage in bus 9 from 1.134 p.u. to 1.098 p.u.. A realistic modeling of the LDC and the tap changer controller will determine how effective is the OLTC at regulating the voltage during a dynamic simulation. The applied OLTC controller frame can be observed in Figure 4.24. The LDC estimates the voltages in buses 7 and 9, v_7 and v_9, which are inputted to the Tap Changer Controller, as well as the current tap position. The new tap position is sent to the Sample and Hold block, which is the responsible to send the final tap position signal to the transformer of Feeder 1 (TRF1) every 60 seconds, as determined by the Clock.

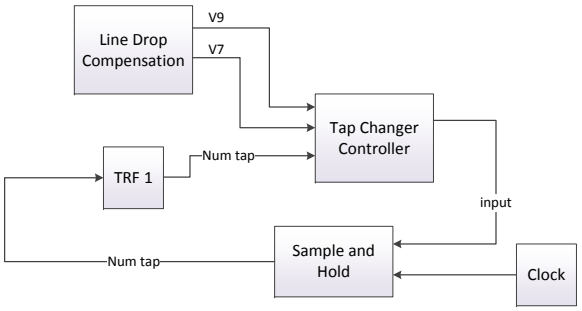

Figure 4.24: Composite frame of the OLTC controller

As explained in Section 3.2.2, the voltage in nodes 7 and 9 is estimated by the LDC. Its composite frame, included in the OLTC controller frame, is showed in Figure 4.25. The estimation of these voltage are obtained by using the equations presented in Section 3.2.2.

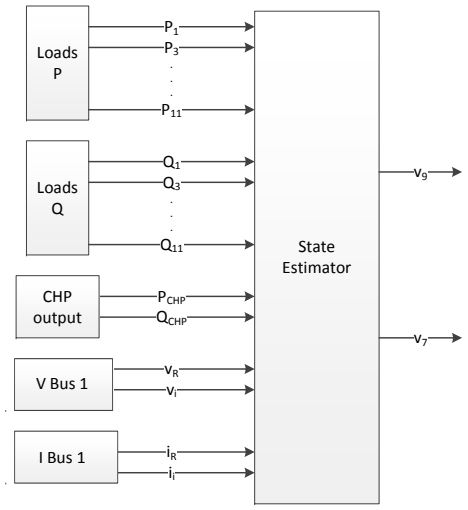

Figure 4.25: Composite frame of the Load Drop Compensation

The State Estimation block receives the active power and reactive power forecast from all the loads in Feeder 1, $P_{1\rightarrow 11}$ and $Q_{1\rightarrow 11}$, and from the CHP plant, P_{CHP} and Q_{CHP}. Additionally, the measured voltage and current in bus 1 are also used for the calculation, R and I being their real and imaginary parts.

For the loads, the forecast represents the actual consumption for a voltage of 1 p.u.. In the case of the CHP plant, the forecast is assumed to be its actual output, taking into account that its active power output can be predicted according to the electricity prices and that the way the reactive power is controlled is known. Within the State Estimation modeling, the LDC equations presented in Section 3.2.2 are implemented in order to estimate the voltage in buses 9 and 7. The accuracy has been tested for a 24 hour simulation, obtaining an error average of 0.00085 p.u. for bus 9 and 0.00023 p.u. for bus 7. It can be concluded that the accuracy is good enough for the purpose of triggering a tap change.

Moving to the Tap Changer Controller block, in Figure 4.24, it takes the LDC voltage estimations from buses 7 and 9 and the current tap position from the transformer TRF1. The logical sequence that leads to a tap change, forwarded to the sampler, is explained as follows:

- Voltage measurement is compared with 1 p.u.
- Positive and negative voltage deviations are compared with a deadband
- If the positive deviation of v_9 is bigger and the current tap position is not in the lower limit, the controller sends a command to reduce one tap
- If the negative deviation of v_7 is bigger and the current tap position is not in the upper limit, the controller sends a command to increase one tap
- The output of the controller is the new tap position if a tap change has been commanded or the old tap position if it has not

In order to limit the rate of tap changes the output of the controller is sampled and forwarded to the transformer TRF1 as the desired tap position. Besides, this signal has also been taken in order to count the number of tap changes throughout the simulation. As stated in [74], increasing the number of tap changes per day reduces the lifetime of the OLTC. Due to the high wind penetration the voltage is expected to fluctuate significantly, leading to a high amount of tap changes if the

settings of the controller are not correctly adjusted. [61] states that, in normal grid conditions, the tap changer should be operated between 10 and 20 times per day. Therefore, the number of tap changes will be kept below 140 during the week simulations in Chapter 5. In order to achieve this, the sampling rate was set to 60 seconds whereas the deadband is modified in each scenario according to its voltage regulation priority. A test of the controller is presented in the following. Figure 4.27 shows the current tap position according to the voltage in bus 9, presented in Figure 4.26, during a 24 hour simulation.

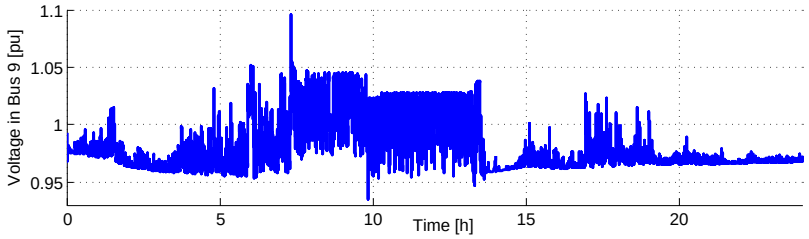

Figure 4.26: Voltage in bus 9

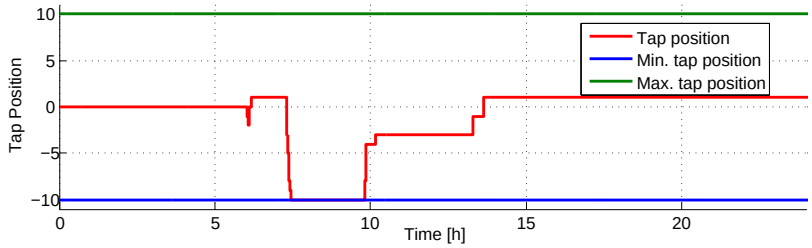

Figure 4.27: Current tap position of TRF1

4.5 Modeling of the Alkaline Electrolyzer

In order to integrate the Power to Gas technology in the case study grid, the implementation of the alkaline electrolyzers is presented in this section. As stated in Chapter 3, the owner and controller of this component is the DSO of the grid. The main purpose of their implementation is to provide voltage regulation and energy management services, by absorbing the surplus power of the wind turbines. Furthermore, it is expected to participate in the wholesale markets in order to produce cheap hydrogen. At the same time, the hydrogen produced will be injected to the gas network respecting a constraint of maximum 10% of volume, as stated in section 2.6.2.

As mentioned in section 3.2.4, 15 electrolyzer modules are utilized in the present work. In the following, the control of these units and their implementation in PowerFactory is presented. Firstly, the composite frame shown in Figure 4.28 is used.

As it can be appreciated, the voltage in the PCC of the AE, i.e. bus 9, is measured in order to determine, in the Dispatch slot, the active and reactive power set-points, P_{in} and Q_{in}, of each electrolyzer module. These signals are sent to the AE frame which determines the active and reactive power outputs from the electrolyzer module (P_e and Q_e), the compression power (P_{comp} and Q_{comp}) and the produced hydrogen ($\dot{V}_{H_2}$). These values are multiplied by the selected number of modules in the present work, i.e. 15 units.

Finally, the resulting active and reactive power from both electrolysis and compression are forwarded to constant power loads, which link the modeling with the electrical grid. The total

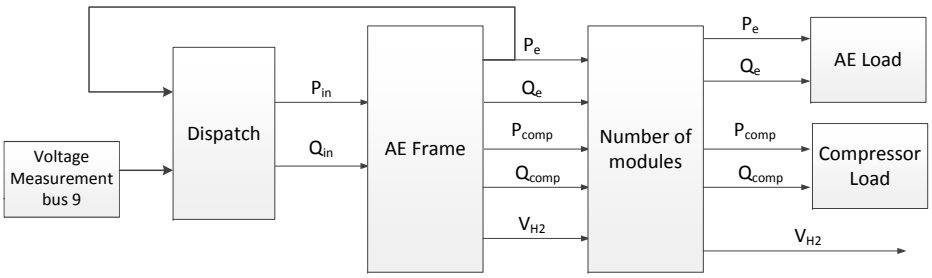

Figure 4.28: Composite frame of the control, modeling and grid implementation of the 15 electrolyzer modules

produced hydrogen is sent to the hydrogen storage, explained further on in this chapter. From the previous explanation of Figure 4.28 it can be inferred that the most important slots are the Dispatch, which determines how the electrolyzers are controlled, and the AE Frame, which contains the dynamic behavior of the electrolyzer. In the following, these two slots are explained in detail.

4.5.1 Active and Reactive Power Dispatch

The block diagram of the Dispatch slot is presented in Figure 4.29. Its structure is very similar to the applied in the reactive power control of the wind turbines and CHP plant. The voltage deviation (U_{diff}) is calculated, U being the measured voltage at bus 9 and U_{ref} 1 p.u.. This signal is sent to the V Droop after a first order delay of 10 s has been added, in order to facilitate the convergence of the simulation. The V Droop slot calculates the active power set-point from the voltage deviation by means of a droop, as explained in the voltage control coordination presented in section 3.2.4. The same applies for the reactive power set-point.

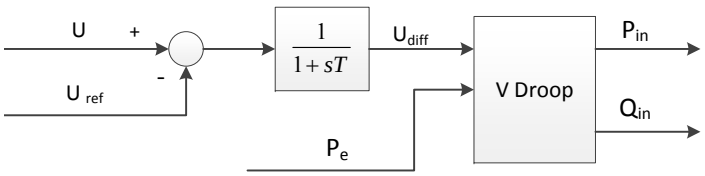

Figure 4.29: Block diagram of the active and reactive power control of the 15 electrolyzer modules

Nevertheless, an addition to this coordination has been made. As explained in [47], the operating temperature of the electrolyzer determines its capacity to consume active power; hence, there might be periods where the actual active power consumption cannot meet the set-point and risk of overvoltage appears. In order to avoid these plausible situations, if the voltage is bigger than 1.04 p.u. the electrolyzer is commanded to absorb reactive power according to Eq. 4.3.

$$Q_{absorb} = \beta \cdot (P_{in} - P_e) \tag{4.3}$$

Where P_{in} is the given active power setpoint, P_e is the actual active power consumed and β is the substitution rate, presented in [75], which is selected to be the ratio between the reactive and active power voltage sensitivities of bus 9. Theoretically, by applying this rate, the effect in the voltage of the absorbed reactive power would be the same as the active power that cannot be consumed. In a similar way as the reactive power controller of the wind farm and CHP plant, the control of the electrolyzer set-points will be tested in Chapter 5.

4.5.2 Alkaline Electrolyzer Frame

In the following, the model of the electrolysis module applied in the case study is presented. It is based on the mathematical model developed by [34] and the PowerFactory model described in [47]. The first describes the AE model, dividing it in three submodels: thermodynamic, electrochemical and thermal; whereas the latter developed a model that implements the previous alkaline electrolyzer model in the software PowerFactory, including a compressor for storing the produced hydrogen in higher pressures. In order to calculate the hydrogen produced, Eq. 3.11 (section 3.2.4) has been added into the electrochemical submodel. Additionally, an adaptation for achieving reactive power control has been done in order to emulate the power converter interface, which allows independent active and reactive power control. The model has been simplified and does not include the detailed description of the power converter and DC busbar. The data of this model can be found in Appendix B.4.

Figure 4.30 illustrates the composite frame, which gives an overview of the several elements taking part in the model. It consists of several slots representing the reactive power measurement, load control and the alkaline electrolyzer model.

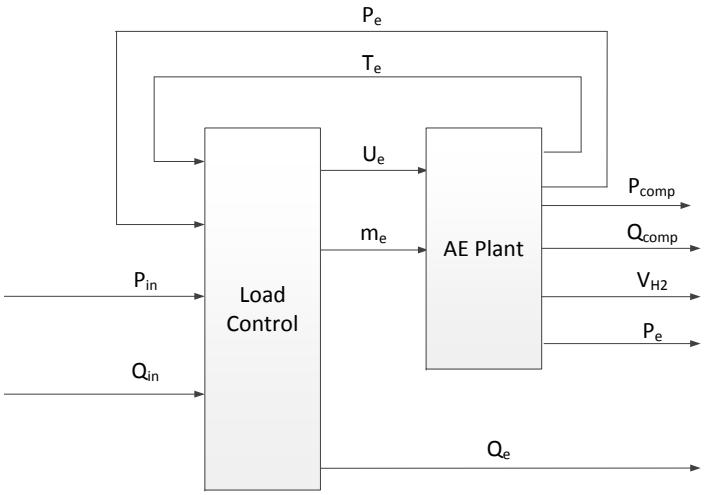

Figure 4.30: Composite frame of the alkaline electrolyzer module

The signals sent to the Load Control slot are the active and reactive power command for the set-point of the electrolyzer-converter module, (P_{in} and Q_{in}). These signals come from a higher control level which simultaneously controls the 15 electrolyzer modules, and the measurement of the reactive power provided by the converter, depicted in Figure 4.28. The Load Control output signals are the electrolyzer cell voltage (U_e) and the mass flow rate of the electrolyte ($\dot{m}_e$), which are inputted to the AE Plant, and the reactive power consumed by the electrolyzer (Q_e). This last slot determines the produced hydrogen ($\dot{V}_{H_2}$), the temperature of the electrolyte (T_e), the active power consumed by the electrolyzer unit (P_e) and the active and reactive power consumed by the compressor (P_{comp} and Q_{comp}).

In the following the Load Control and AE Plant slots are explained into more detail.

Load Control of the Alkaline Electrolyzer

In order to control the consumed active power (P_e) and temperature of the electrolyte (T_e), the voltage of the electrolyzer cell (U_e) and the electrolyte mass flow ($\dot{m}_e$) are used, respectively. In order to achieve this control a PI controller has been used in both cases, as explained in the model provided by [47]. In this way, the needed electrolyte mass flow to maintain the temperature

within limits is found, whereas the consumed power of the electrolyzer is controlled through the applied voltage at the electrolyzer.

Furthermore, the reactive power control (Q_{out}) that emulates the power converter interface has been added. The latter is controlled according to a direct reactive power command (Q_{in}) coming from a higher level control. The reactive power signal is limited by the nominal apparent power of the converter and the active power that it is delivering at each moment. This limitation is implemented in the Limiter block. The block diagram of the Load Control slot is shown in Figure 4.31.

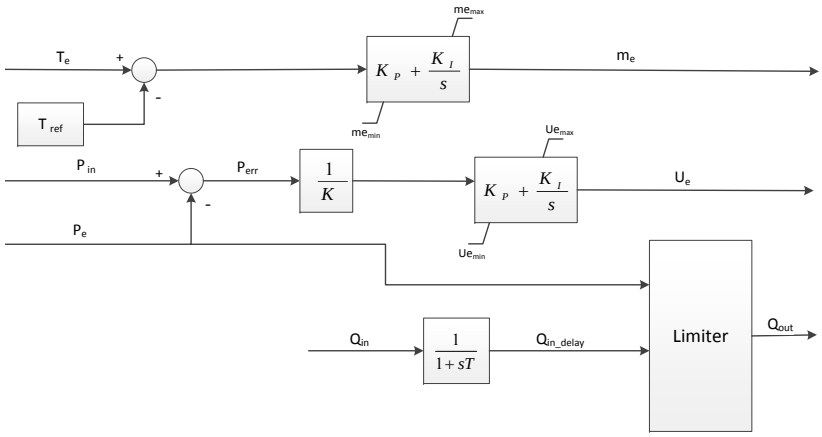

Figure 4.31: Block diagram of the load control slot of the alkaline electrolyzer

Alkaline Electrolyzer Plant Model

The model of the electrolyzer is divided in four submodels: the I-U characteristic, the thermal model, the hydrogen production and the hydrogen compressor. Figure 4.32 illustrates the block diagram of the AE.

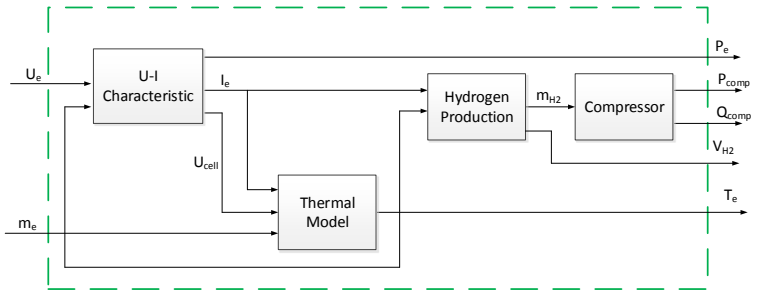

Figure 4.32: Block diagram of the alkaline electrolyzer

As previously explained, the input signals of this block diagram are the voltage of the electrolyzer cell (U_e) and the electrolyte mass flow ($\dot{m}_e$) and the output signals are the active power consumed by the electrolyzer unit (P_e), the temperature of the electrolyte (T_e) and the active and reactive power consumed by the compressor (P_{comp} and Q_{comp}). The internal variables are the current applied to the electrolyzer (I_e), the voltage of the electrolyzer cell (U_{cell}) and the flow rate of produced hydrogen ($\dot{m}_{H2}$). The four submodels are detailed in the following:

U-I characteristic: The voltage-current curves are used to define the kinetic behavior of the electrolyzer when a certain temperature is applied. An empirical U-I relationship was presented in [34], which defined the electrolyzer voltage depending on the number of cells, its resistance characteristics, the temperature of the electrolyte and the DC current drawn, among others. These

U-I curves have been produced for several temperatures, applying for this purpose the equations presented in [47], and later introduced as look-up tables in the I-U block in PowerFactory. The results of this can be observed in Figure 4.33.

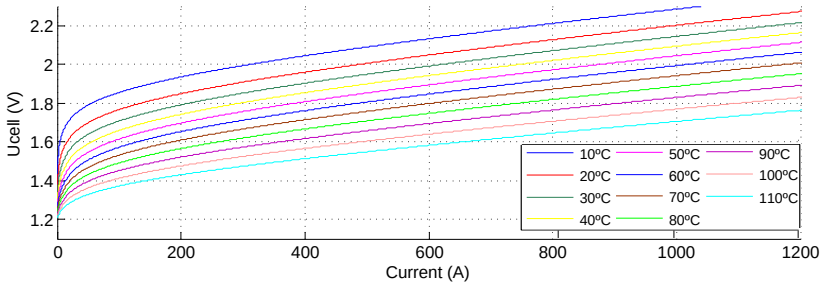

Figure 4.33: U-I characteristic curves for different temperatures of the alkaline electrolyzer

Thermal Model: This model is used to determine the temperature variation of the electrolyte, which is influenced by the electrolyte mass flow. It is derived through the following energy balance equation:

$$C_t \frac{dT_e}{dt} = Q_{gen} - Q_{loss} - Q_{cool} \tag{4.4}$$

Where C_t is the thermal capacitance of the electrolyzer. The term Q_{gen} represents the internal heat generation of the electrolyzer, Q_{loss} is the total heat loss and Q_{cool} is the cooling demand.

The internal heat generation of the electrolyzer depends on its consumed power and efficiency, the heat loss is calculated by the temperature difference of the electrolyzer and the ambient divided by the thermal resistance, and the energy needed for cooling depends on the circulation of the electrolyte through the heat exchanger and its temperature.

Hydrogen Production: The production rate of hydrogen ($\dot{n}_{H_2}$ in mol/s) is defined by Faraday's electrolysis law as it follows:

$$\dot{n}_{H_2} = \eta_F \frac{n_c I}{zF} \tag{4.5}$$

Where z is the number of electrons transferred in the reaction, in this case 2, and F is the Faraday constant, which is $96485C/mol$. The Faraday efficiency (η_F) is found as the difference between the produced hydrogen and the maximum in theory. In order to have the production of hydrogen ($\dot{m}_{H_2}$ in kg/s), the molar mass of the hydrogen ($M_H = 1.00794g/mol$) is used as it follows:

$$\dot{m}_{H_2} = \frac{\dot{n}_{H_2} \cdot M_H \cdot z}{1000} \tag{4.6}$$

In order to calculate the hydrogen volume flow rate, Eq. 3.11 is additionally implemented in this block.

Compressor: In this model, the active (P_{com}) and reactive power (Q_{com}) consumed by the compressor are determined. This unit compresses the hydrogen up to 150 bar in order facilitate its storage afterwards. The compression includes an intermediate cooling stage, therefore it is divided in two parts (W1 and W2):

$$P_{com} = \dot{m}_{H_2}(W_1 + W_2) \tag{4.7}$$

$$Q_{com} = P_{com} \cdot tan\Big(cos^{-1}(0.88)\Big) \tag{4.8}$$

4.5.3 Test of the Alkaline Electrolyzer Module Model

The described model has been tested by giving different active and reactive power set-points. Figure 4.34 shows the temperature of the device, whereas Figure 4.35 shows the given set-points for the active power and the actual active power consumption.

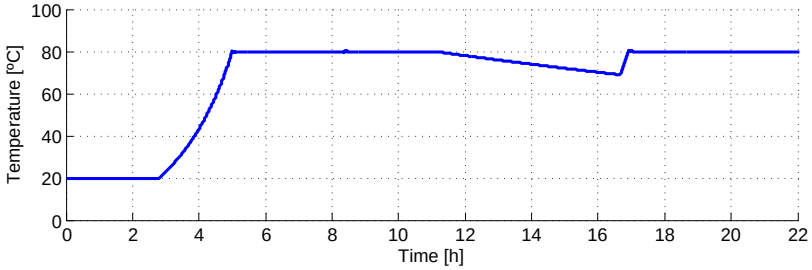

Figure 4.34: Operating temperature [$°C$] of the 355kW alkaline electrolyzer

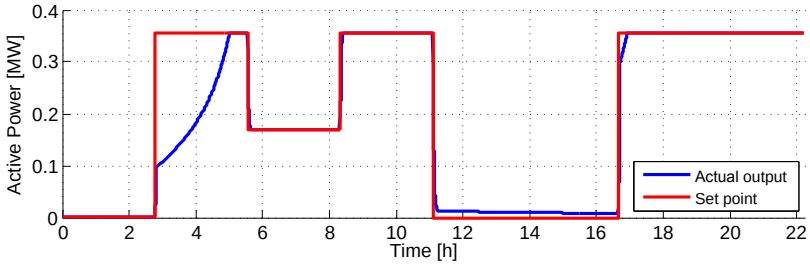

Figure 4.35: Active power set-points (red) and actual consumption (blue) [MW] of the 355kW alkaline electrolyzer

As stated in [47], the active power consumption of the electrolyzer is limited by its operating temperature. When the set-point is changed around $t = 2.7h$, the device takes around $2h$ to change its power output. As seen in the temperature plot, the slow thermal dynamics of the device are the responsible of the upper power limitation. However, a fast upwards or downwards response will occur as long as the temperature is kept close to the rated ($80°C$).

From approximately $t = 11h$ to $t = 16.5h$ the electrolyzer undergoes stand-by operation, leading to a temperature decrease. After the stand-by period the electrolyzer was requested to run at full power, reaching the set-point after $15min$, which was due to the temperature fall during stand-by operation. Therefore, effectively controlling the temperature of the device is crucial in order to provide fast regulation services (down-regulation or effective voltage support).

In the following, the reactive power controller is tested. Since it is provided by the converter, the reactive power capability will depend on its rated apparent power and on the measured active power output from the electrolyzer. As it can be appreciated in Figure 4.36, the reactive power set-point is set to the rated, i.e. $0.355Mvar$. It can be appreciated that the actual reactive power is below the set-point for most part of the hours, due to the relatively high active power output, observed above in Figure 4.35, and the limited converter rated power of $0.355MVA$.

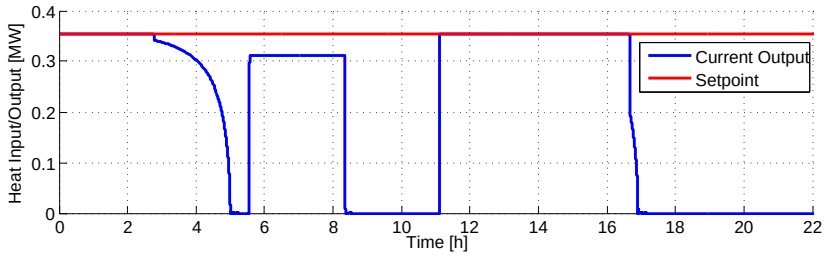

Figure 4.36: Reactive power set-points (red) and actual output (red) of the alkaline electrolyzer

Finally, Figure 4.37 shows the active and reactive power from the compressor. It can be appreciated that during full power its consumption is nearly 0.08 MW, which accounts for around 20% of the rated power of the electrolyzer.

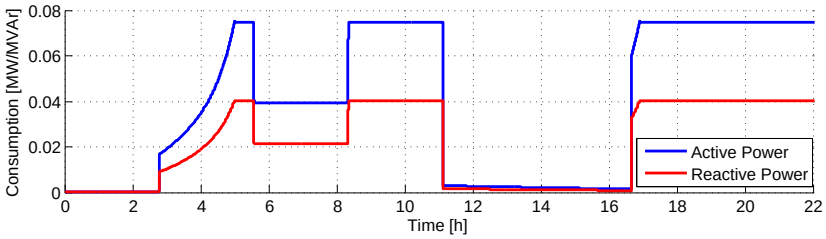

Figure 4.37: Active (blue) and reactive power (red) from the compressor

4.6 Modeling of the Hydrogen Storage

As presented in Section 3.1.3, the hydrogen produced in the electrolysis plant is injected in the gas pipes of the CHP plant. It is additionally stated that the size of the storage is assumed to be planned for a seasonal purpose; therefore, only the hydrogen variation will be presented. Figure 4.38 shows the applied composite frame in order to calculate the hydrogen variation.

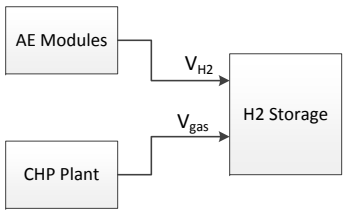

Figure 4.38: Composite frame of the hydrogen storage

The volume flow rates of the produced hydrogen ($\dot{V}_{H_2}$) and consumed gas ($\dot{V}_{gas}$) were calculated in the models of the AE and the CHP plant, respectively. Hence, the volume variation of hydrogen, in $[Nm^3]$, can be calculated integrating Eq. 4.9, assuming that a 10% of hydrogen concentration is constantly bled into the CHP's gas pipes. This equation is implemented in the H2 Storage block.

$$\frac{dV_{H2}}{dt} = \dot{V}_{H2} - 0.1 \cdot \dot{V}_{gas} \tag{4.9}$$

The test of this model will not be assessed since the results it presents depend on the operation strategy of the electrolyzer.

4.7 Conclusions

The most important finding of the implementation of the different dynamic models is presented in this section. This is the significant difference between the active power ramp rates of the wind farm and CHP units respect to the one of the electrolyzer. Figures 4.39, 4.40 and 4.41 show, respectively, the fast dynamics of the wind farm output, the quick start-up of the CHP gas turbine units and the slow start-up of the electrolyzer, assuming an ambient temperature as initial condition.

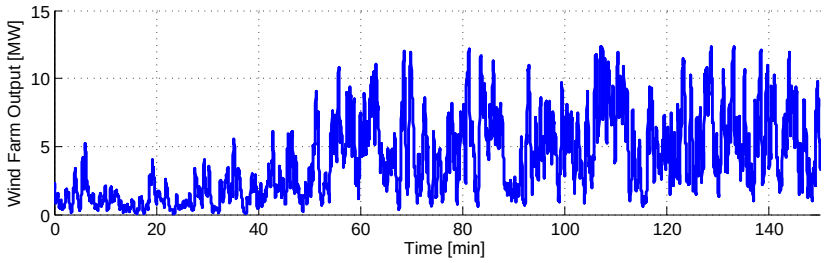

Figure 4.39: Wind farm active power output

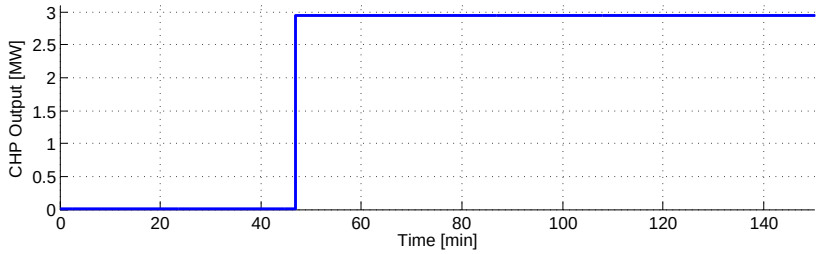

Figure 4.40: CHP unit 1 active power output

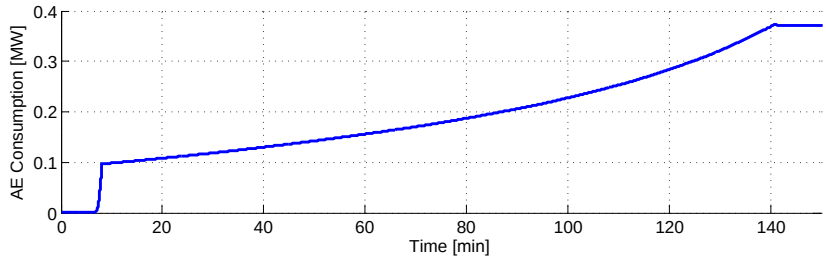

Figure 4.41: Electrolyzer's active power consumption

It has been measured that the electrolyzer takes 132 min to reach full power from cold start-up. When compared with the ramp rates of the wind turbines and CHP units, it is expected that the electrolyzer would not be able to adapt its active power consumption to the production of the distributed generation units, in order to provide effective voltage regulation.

Furthermore, when analyzing the participation in the different wholesale markets, namely Elspot, Elbas or regulation power, it is crucial to understand the capability limitation of the AE due to the temperature. If the device is not able to meet with the market schedule, this could bring economic consequences to the DSO. A solution for this issue will be presented in Chapter 6. Regarding the following chapter, the consequences of the active power capability limitation will be mitigated with reactive power.

5 Voltage Support from P2G Systems - Dynamic Analysis

In this chapter the effectiveness of the P2G implementation to provide voltage regulation is assessed. For this purpose, the results of simulating the case study grid incorporating the models mentioned in Chapter 4 are presented. These are presented as done in Chapter 3, starting with the base case and sequentially integrating the OLTC, reactive power control of wind turbines and CHPs, and finally the alkaline electrolyzer units. Each scenario is simulated during a winter and summer week, i.e. 168 hour. Furthermore, the hydrogen bleeding strategy proposed in Chapter 3 is tested in the scenario including the electrolyzers. It should be noted that, as Feeder 2 nor the loading of the components of Feeder 1 did not present issues, they are not taken into account in the simulations carried out in this chapter.

5.1 Base Case

In this scenario, the grid is analyzed without the influence of the OLTC, power factor control of the DG units and alkaline electrolyzer. The presented results are used to give an overview of the operation of the grid. These are the following: a) power flow of Feeder 1, b) DG production and c) voltage in the most critical buses. As presented in Chapter 3, the buses that present higher values of over and undervoltage are bus 1, 7 and 9, and therefore, the voltage results will be presented for these nodes. These results are presented in both winter and summer scenarios.

5.1.1 Winter Scenario

The dynamic behavior of the grid is analyzed using the winter profiles of the DG, i.e. wind turbines and CHP, and the loads. Figure 5.1 illustrates the obtained results regarding power flow of the external grid, production of the DG units and the voltage of the most critical buses during the winter week.

The power flow of Feeder 1, in plot a), reflects the situations where power is supplied to the MV grid (positive value), and when power is absorbed by the external grid (negative value). It is observed that the periods that the studied grid is supplied by local production account approximately for the same energy as the ones supplied by the external grid, as confirmed later in Table 5.1.

The high fluctuation of power of the wind farm can be observed in plot b), where the active power of the wind farm and the CHP units is plotted. The CHP power output follows an "ON/OFF" behavior as it was modeled to follow the behavior of a typical CHP plant, as explained in Section 4.3, and therefore its production ranges from 0 to 3 MW per CHP unit. Regarding the wind farm, its power output is dependent on the wind speed, and thus ranges from 0 to 12 MW.

Plot c) shows the voltage of the most critical buses, where the upper and lower voltage limits are highlighted in a red dashed line. It is observed that the voltage of buses 7 and 9 surpasses 1.05 p.u. whenever the wind turbines and CHP units produce simultaneously. The maximum voltage is 1.122 p.u. at bus 9. Similarly, when the CHPs and wind turbines have low production the voltage of buses 7 and 9 drops below 1 p.u., however, no undervoltage issues are observed, being the minimum 0.957 p.u. at bus 11.

Figure 5.2 shows a close-up of day 1, where the highest peak of voltage is observed in bus 9. In this graph the high voltage fluctuation due to the wind power can be appreciated, affecting the

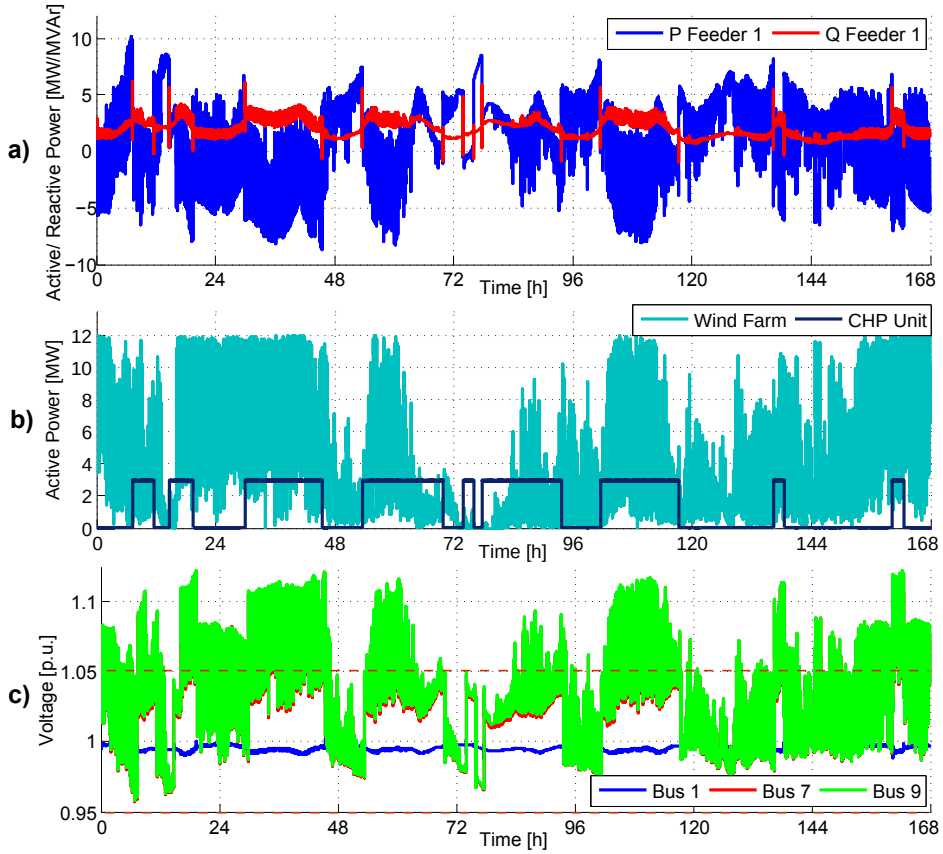

Figure 5.1: Results of the grid in base case, during a winter week

graphical representation of the voltage.

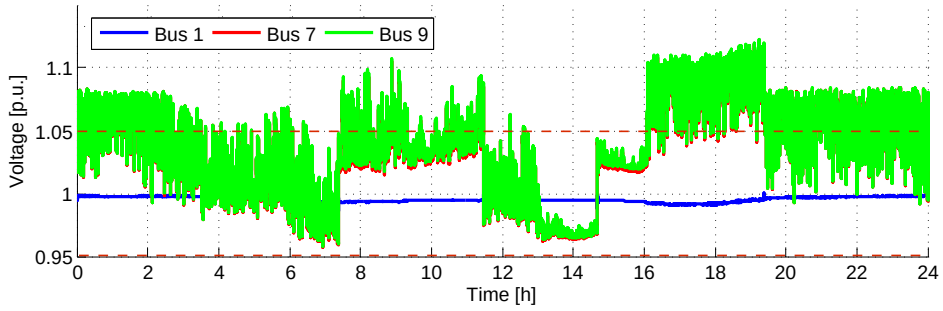

Figure 5.2: Results of the grid in base case, during day 1 of the winter week

Finally, Table 5.1 summarizes the values of generation, load, active and reactive power import from the external grid to Feeder 1 and the losses throughout the week. It is observed that the losses correspond to a 4.77 % of the loads.

Table 5.1: Total generation, load, external grid import and losses, during the winter week

Generation	Load	P Import	Q Import	Losses
1134.39 MWh	1249.35 MWh	174.60 MWh	339.2 Mvarh	59.63 MWh

5.1.2 Summer Scenario

In this section, the dynamic behavior of the grid is analyzed utilizing the summer profiles of wind turbines, CHP and loads. Figure 5.3 illustrates the obtained results regarding power flow of the

external grid, production of the DG units and the voltage of the most critical buses.

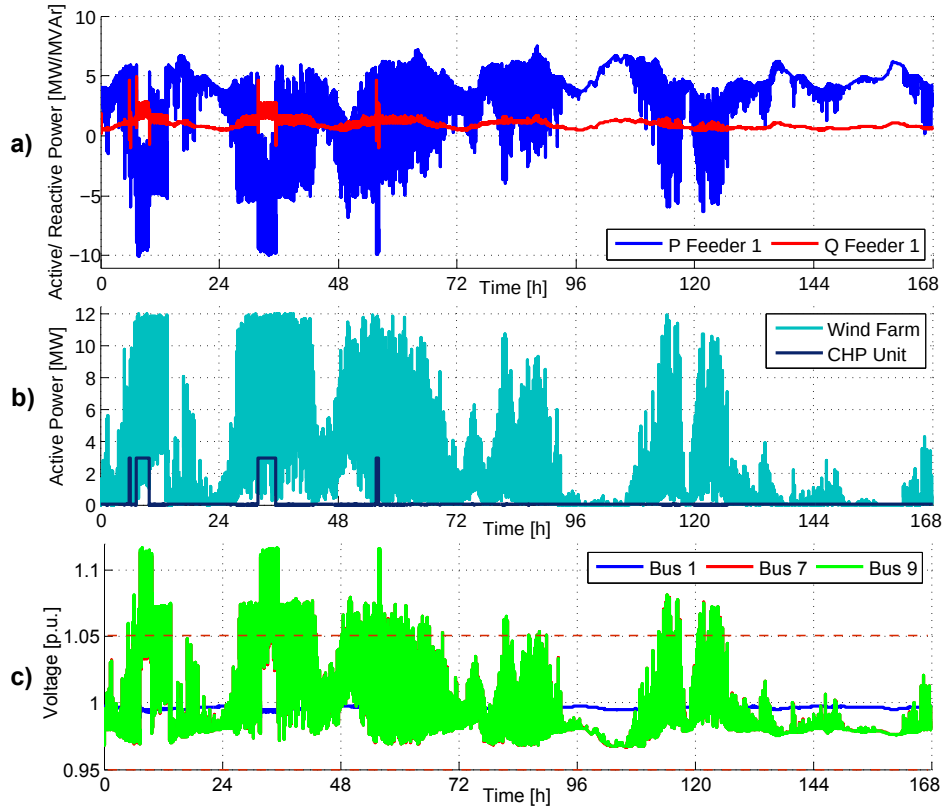

Figure 5.3: Results of the grid in base case, during a summer week

Plot a) shows the active and reactive power flow from Feeder 1. It can be observed that the peak value of active power is slightly lower than in the winter case, due to the reduced consumption of the loads.

Plot b) depicts the operation of the wind farm and CHP plants in summer. It can be noticed that they produce less than in the winter scenario, specially the CHP plants due to the lower heat demand, as explained in Section 4.3.

It can be seen in plot c) that the voltage of buses 7 and 9 presents overvoltage, however for a shorter period than in the winter scenario. The influence of the operation of the CHP can be easily spotted, as the voltage rises considerably. The highest value occurs at bus 9 with 1.117 p.u., as it can be observed in Figure 5.4, which illustrates a close-up on the first 24 hours. It can be observed that value of the voltage within a day ranges from below 1 p.u. to over 1.1 p.u..

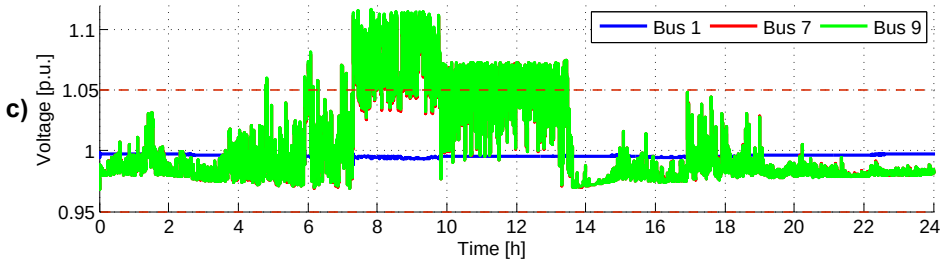

Figure 5.4: Results of the grid in base case, during day 1 of the summer week

The values of generation, loads, import from the external grid and losses are summarized in Table 5.2. All values have decreased respect to the winter scenario, except for the value for active power

import. This value has increased as the local generation has decreased considerably. On the other hand, the losses have decreased considerably, as they now account for 2.41 % of the load.

Table 5.2: Total generation, load, external grid import and losses, during the summer week

Generation	Load	P Import	Q Import	Losses
426.02 MWh	714.15 MWh	305.31 MWh	160 Mvarh	17.18 MWh

5.2 Voltage Support from OLTC

The aim of this section is to show the results of implementing the OLTC to the case study grid, previously analyzed in Section 5.1. This is done in order to assess the operation of the OLTC before the implementation of power factor control in the DGs and the alkaline electrolyzer. The presented parameters are the following: a) external grid power flow, b) DG production, c) tap changer positions and d) voltage in the most critical buses.

5.2.1 Winter Scenario

In this scenario, the grid is analyzed with the implementation of the OLTC utilizing the winter profiles of wind turbines, CHP and loads. Figure 5.5 gives an overview of the operation of the grid, presenting the most important results.

Compared to the scenario without the application of an OLTC, presented in Section 5.1.1, plots a) and b) present the same active power values, as the generation and consumption of the grid remains unchanged. However, the reactive power consumption and export of Feeder 1 has slightly increased.

Plot c) shows the behavior of the tap changer by showing its position. It can be observed that the tap changer operates most of the time at the negative half, thus correcting overvoltage by decreasing the voltage of bus 1. It is observed that the lower position of the tap changer is reached during several hours of the week. The total number of tap changes at the end of the week is 149. However, as mentioned in Section 4.4, the recommended number of taps per week is below 140. Therefore in this case it is surpassed, but still within an acceptable range.

As it can be seen in plot d), the voltage in buses 7 and 9 still presents overvoltage in several hours of the week, reaching a maximum of 1.111 p.u. in bus 9. However, compared to the previous scenario, the overvoltage issue has been improved as highlighted in the black dashed circle. This improvement has been achieved by decreasing the voltage of bus 1 to nearly 0.95 p.u.. The main disadvantage of the implementation of the OLTC is that its slow dynamics create over- and under-voltage issues, as highlighted in purple dashed circles. These spikes occur due to quick changes of power as can be seen in plots b) and c).

Figure 5.6 shows the behavior of the OLTC and the voltage in day 1. As it can be appreciated, the voltage of bus 1 follows the same behavior as the tap changer position and the voltages of buses 7 and 9 are regulated accordingly. The slow dynamics of the OLTC are appreciated in the highlighted purple areas. The first represents the undervoltage that occurs when the tap was at a low position and there is a sudden decrease of power generation. The second represents the oposite case, when the tap changer was at a high position, and a sudden increase of local power occurs.

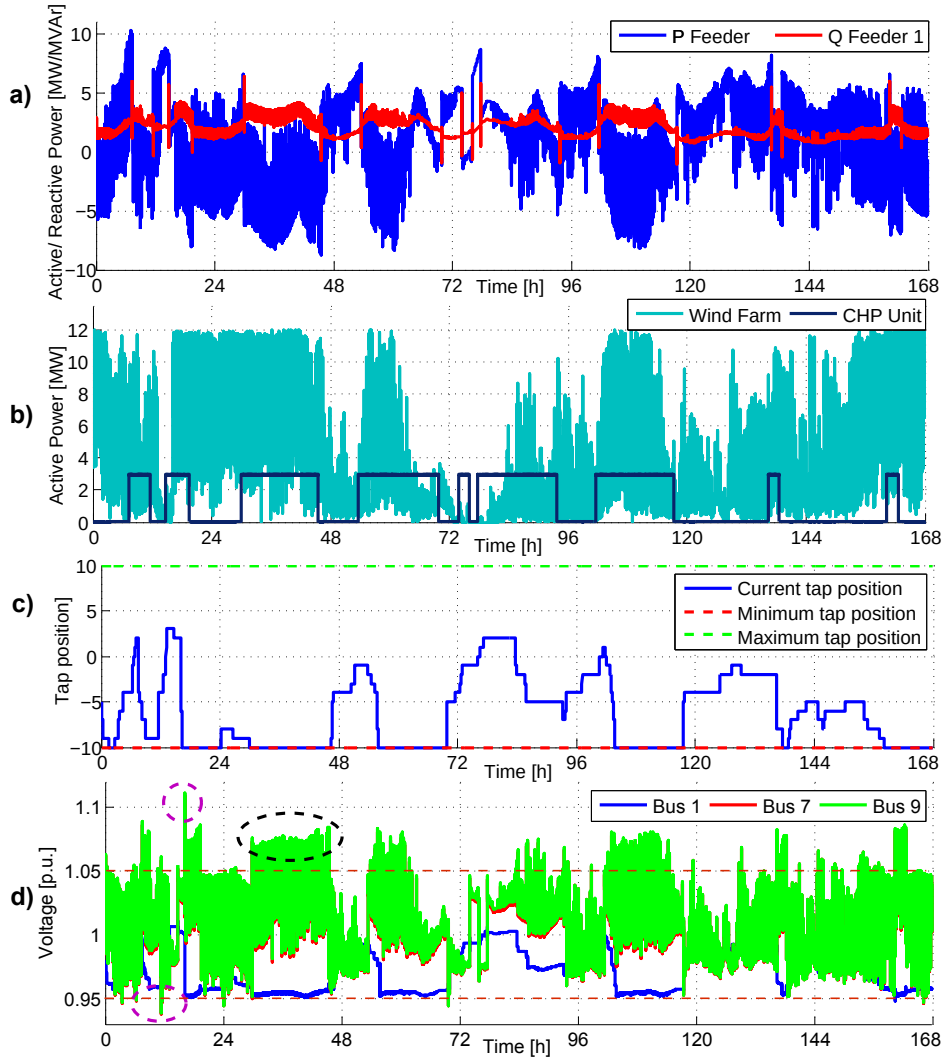

Figure 5.5: Results of the grid with OLTC implementation, during a winter week

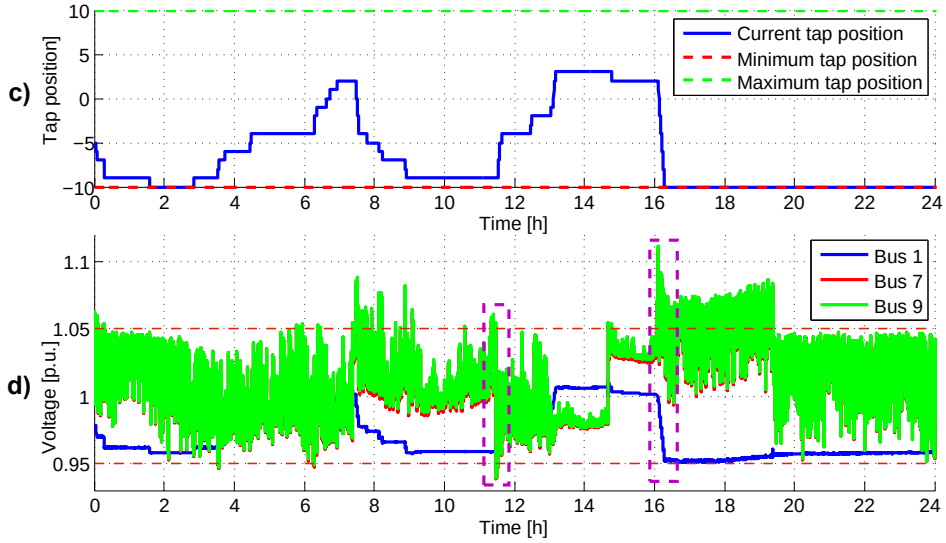

Figure 5.6: Results of the grid with OLTC implementation, during day 1 of the winter week

Table 5.3 summarizes the weekly values of generation, load, import from the external grid and losses. The value of generation remains as the previous scenario. In case of the load, its value

throughout the week has decreased due to the voltage decrease, since they are not modeled as constant power. Consequently, the active power import has decreased. On the other hand, the reactive power import presents an increase of 0.8 MWh. Finally, the losses have increased, which as mentioned in 3.2.2, it is due to the higher current through the lines as the voltage has decreased. They account for 5.09 % of the consumption of Feeder 1.

Table 5.3: Total generation, load, external grid import and losses, during the winter week

Generation	Load	P Import	Q Import	Losses
1134.39 MWh	1234.94 MWh	163.41 MWh	340.0 Mvarh	62.83 MWh

5.2.2 Summer Scenario

In this subsection, the influence of the implemented OLTC is analyzed during the summer week. Figure 5.7 shows the obtained results that illustrate the behavior of the grid and its components.

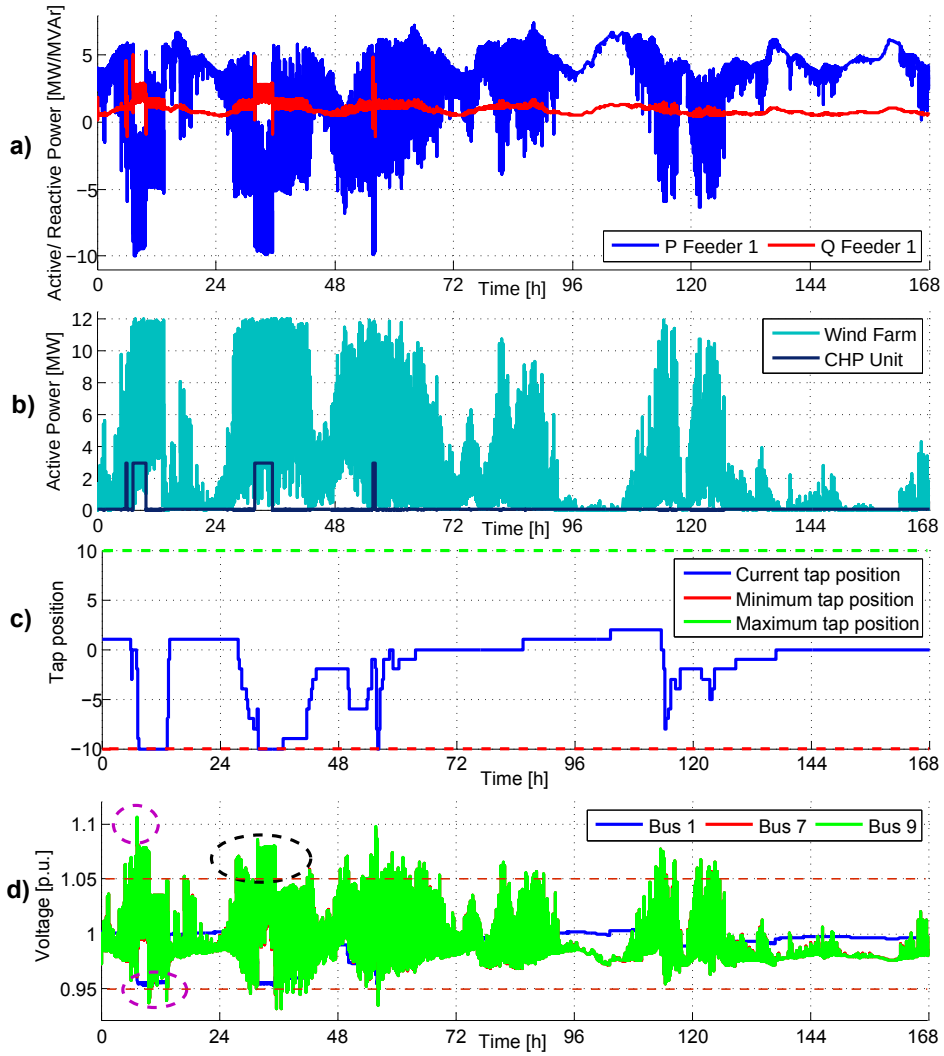

Figure 5.7: Results of the grid with OLTC implementation, during a summer week

Plot a) shows the power exchange of Feeder 1. The active power remains unchanged respect to Section 5.3, however the reactive power exchange has increased. Plot b) illustrates the DG production, which remains unchanged respect to the previous scenario.

Plot c) represents the tap position of the OLTC, where it can be observed that, as in the winter

case, it usually operates in the negative half and thus correcting overvoltage. The number of taps per week is 111, being below the recommended number of taps per week.

As shown in plot d) the implementation of the OLTC decreases the voltage of buses 7 and 9, as highlighted in the black circle. However, as previously explained, the slow response of the tap changer mechanism creates under- and over-voltage issues at certain occasions, such as the marked in purple circles. These occur when there are sudden changes of power from the local generation and the tap position change is slower. In this case the highest voltage occurs at bus 9 with 1.106 p.u. and the lowest at bus 7 with 0.931 p.u..

The mentioned under and overvoltage issues caused by the OLTC are shown into more detail in Figure 5.8, highlighted in purple. The first marked area represents the overvoltage issue, happening when there is a sudden increase of power, in this case both from CHP units and wind farm. The second highlighted area occurs due to a drop of wind power. The slow dynamics of the OLTC can be appreciated in both cases. As in the winter case, it can be seen that the behavior of bus 1 is determined by the tap position.

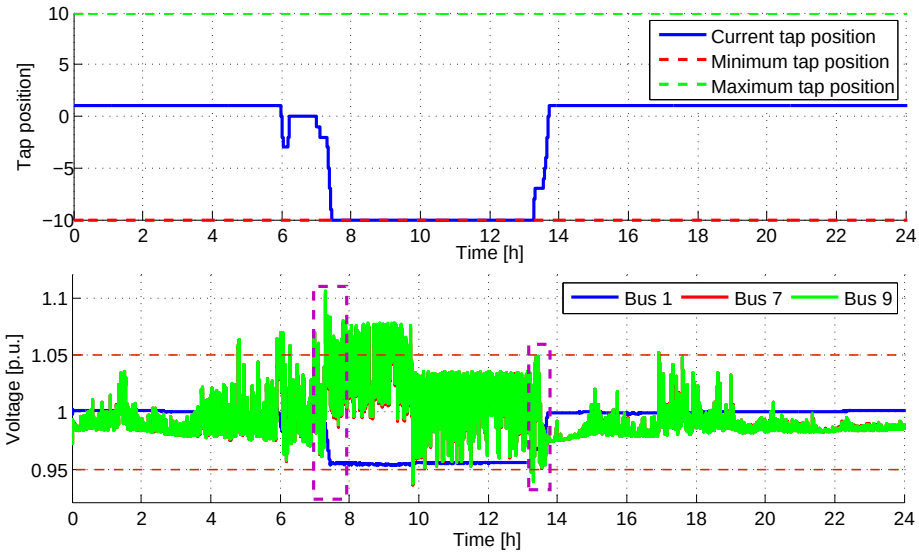

Figure 5.8: Results of the grid with OLTC implementation, during day 1 of the summer week

The weekly values of generation, consumption, import from the external grid and losses for the summer week are summarized in Table 5.4. It is observed that all values are very similar to the previous scenario, without the implementation of OLTC. The losses in this case account for 2.52 % of the total consumption.

Table 5.4: Total generation, load, external grid import and losses, during the summer week

Generation	Load	P Import	Q Import	Losses
426.15 MWh	712.83 MWh	304.80 MWh	160.50 Mvarh	17.98 MWh

5.2.3 Summary

As observed in both winter and summer scenarios, the implementation of the OLTC presents a noticeable improvement in the voltage of the grid. This is due to the capability to increase or decrease the voltage of bus 1, and consequently the rest of the buses of the grid. In the winter case the number of tap changes surpassed the recommended number of 140 changes per

week, however in the summer scenario it remained within limits with only 111 changes. It has been observed that the OLTC has slow dynamics and triggers under- and over-voltage when a sudden change of power occurs. Finally, it has been noted that the losses through the lines and transformer have increased in both winter and summer cases.

5.3 Voltage Support from Reactive Power Dispatch

In this section the utilization of reactive power dispatch from wind turbines and CHP plants is analyzed, additionally to the tap changer. As mentioned in Section 3.2.3, the DSO is able to demand these units to absorb or supply reactive power. According to the technical regulations provided by Energinet.dk, wind turbines should be able to operate within 0.975 lagging and 0.975 leading power factor [63], whereas the CHP should be capable to operate within $-0.20 \leq tan\phi \leq 0.40$ [65]. This reactive power capability is implicit in the V-PF droops and the assets coordination presented in Section 3.2.3, which are to be tested in this Section.

5.3.1 Winter Scenario

In this subsection, the combination of OLTC and reactive power dispatch from the DGs is analyzed during a winter week. The obtained results are summarized in Figure 5.9.

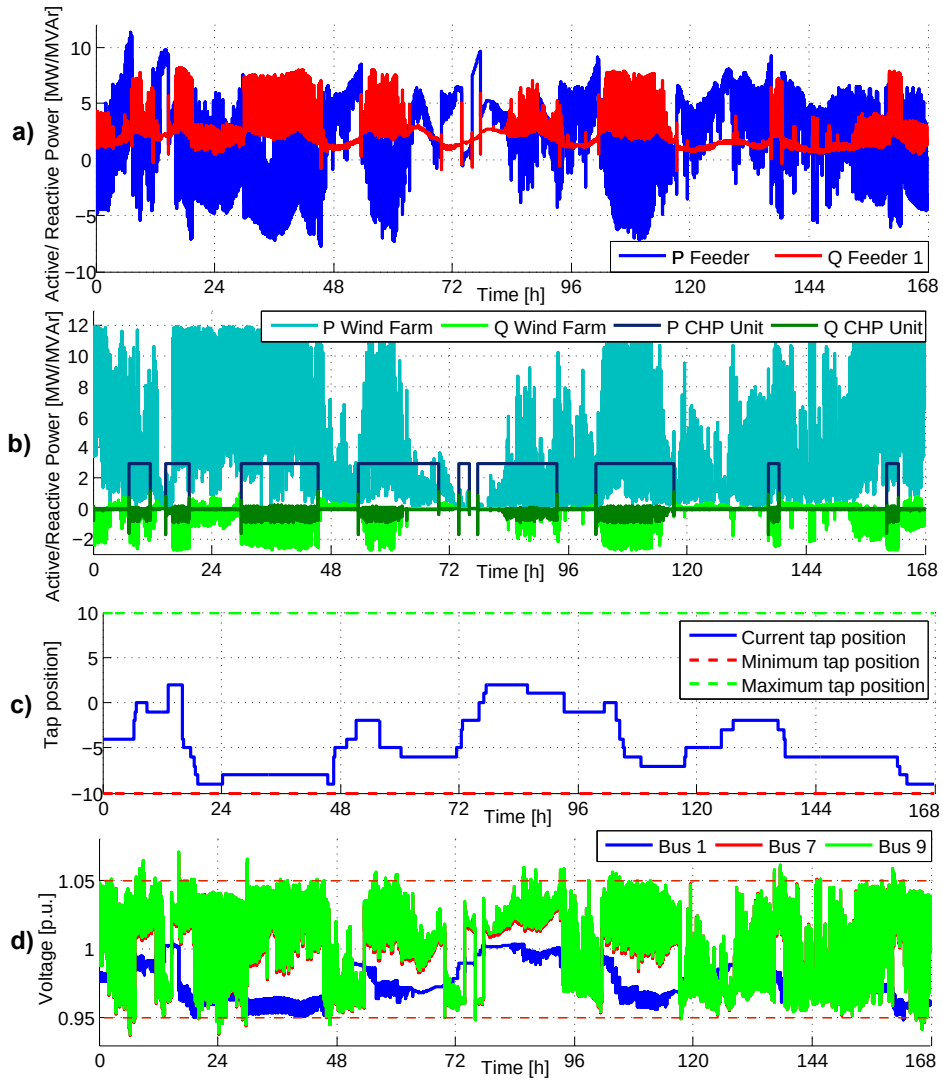

Figure 5.9: Results of the grid with reactive power dispatch, during a winter week

Plot a) illustrates the active and reactive power flow from Feeder 1. It can be noticed that the reactive power supply has increased compared to the previous case. This increase is due to the ability of the DGs to absorb reactive power in order to decrease the voltage.

Plot b) shows the behavior of the wind farm and the CHP units. As it can be appreciated, the implemented control of the reactive power dispatch, previously explained in Section 3.2.3, gives a set-point to these units to consume reactive power, depending on the needs of the grid. However, reactive power absorption or consumption is only available when the units are operating. For what concerns active power, it remains unchanged respect to the previous scenarios.

As shown in plot c), the tap changer covers a bigger position range than in the previous scenario, operating from position 5 to -10. It can be observed that the reactive power dispatch has relieved the tap changer, as it does not reach the minimum position. The number of tap changes per week has also decreased, being 63.

Finally, the voltage of buses 1, 7 and 9 can be seen in plot d). The combination of OLTC and power factor control of the DG units has decreased the voltage, as the upper limit is only surpassed in limited moments. The highest voltage has also been decreased, from 1.111 p.u to 1.078 p.u.. This significant improvement is due to the fast response of the DG units to absorb reactive power. The voltage is decreased by increasing the apparent power through the lines and thus increasing the voltage drop. However, the consequence of reducing overvoltage using reactive power is the creation of undervoltage in buses 1, 7 and 9.

Figure 5.10 provides a zoom in the first 24 hours of the simulation, showing the behavior of the DG units, the position of the OLTC and the voltage at the most critical buses.

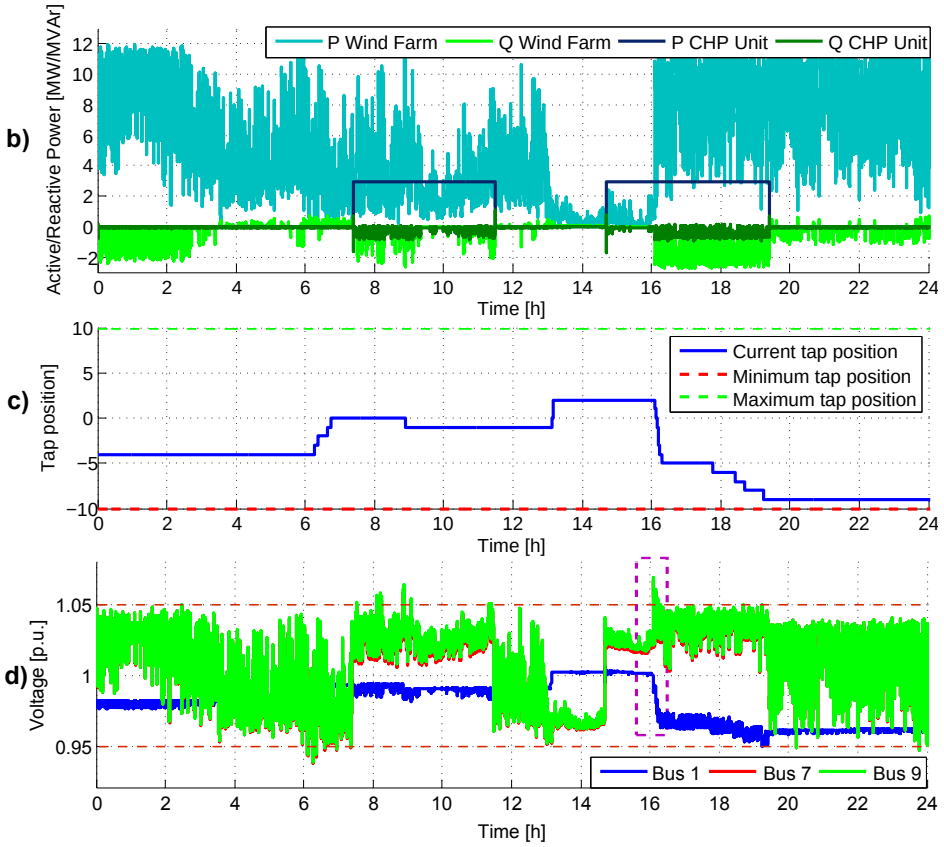

Figure 5.10: Results of the grid with reactive power dispatch, during day 1 of the winter week

It can be seen that reactive power absorption only occurs when the units are operating and voltage

support is required. The issue regarding the slow response of the OLTC is still visible at hour 16, as marked in purple. However, compared to the previous scenario shown at Figure 5.6, the overvoltage peak has decreased.

Table 5.5 presents the total results of generation, load, active and reactive power import from the external grid to Feeder 1 and the losses of this feeder. It can be observed that the reactive power import increased by 64.5 MVArh, as the DGs have the capability to absorb reactive power to provide voltage support. Consequently, the losses have increased accounting for a 5.32% of the load.

Table 5.5: Total generation, load, external grid import and losses, during the winter week

Generation	Load	P Import	Q Import	Losses
1134.39 MWh	1236.30 MWh	167.78 MWh	404.50 Mvarh	65.85 MWh

5.3.2 Summer Scenario

In this subsection, the combination of OLTC and reactive power dispatch from the DGs is analyzed during the summer week. The obtained results are summarized in Figure 5.11.

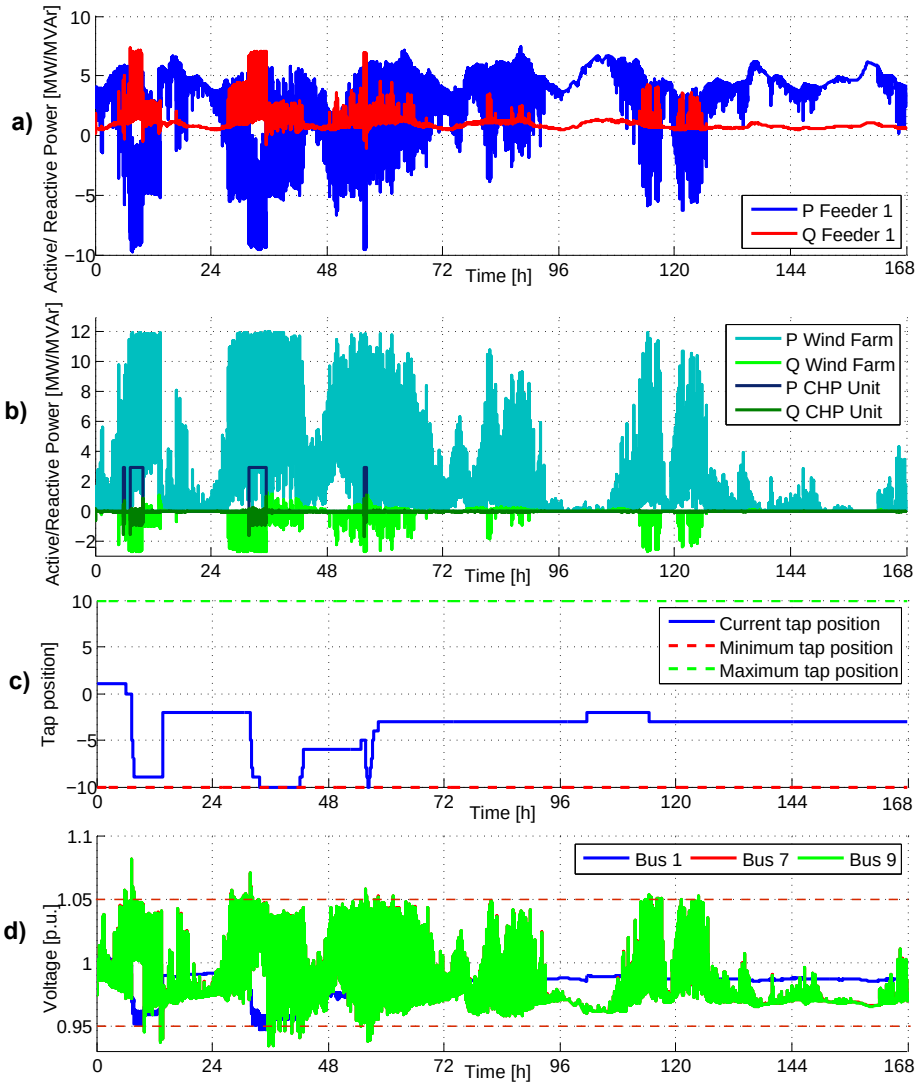

Figure 5.11: Results of the grid with reactive power dispatch, during a summer week

Plot a) shows the active and reactive power supplied or absorbed from the external grid. The supply of reactive power increases as the DG units consume it to provide voltage regulation, while the active power remains unchanged.

Plot b) represents the behavior of the wind farm and the CHP units. The consumption of reactive power occurs whenever the units are producing power, in order to contribute to decrease the voltage. However, as the operation of the DG units is lower in the summer scenario, the capability of using reactive power dispatch is also lower.

The behavior of the tap changer is depicted in plot c), where it can be seen that its position mostly remains in the negative half, thus contributing to decrease the overvoltage. Regarding the number of tap changes per week, it also presents a considerable decrease, being only 44.

The result of the implementation of reactive power dispatch can be seen in the voltage, shown in plot d). The overall voltage has decreased, however some peaks still remain due to the slow response of the tap changer. The highest voltage, occurring at bus 9 has decreased from 1.106 p.u. to a value of 1.073 p.u.. As mentioned in the winter scenario, it is observed that the implementation of reactive power dispatch has decreased the voltage of the grid, producing undervoltage.

Figure 5.12 provides a zoom into the first day of the simulation, where the previously mentioned issues can be observed into more detail. The decrease in voltage due to the slow dynamics of the OLTC are still visible, since the voltage of buses 7 and 9 present undervoltage, as highlighted in purple.

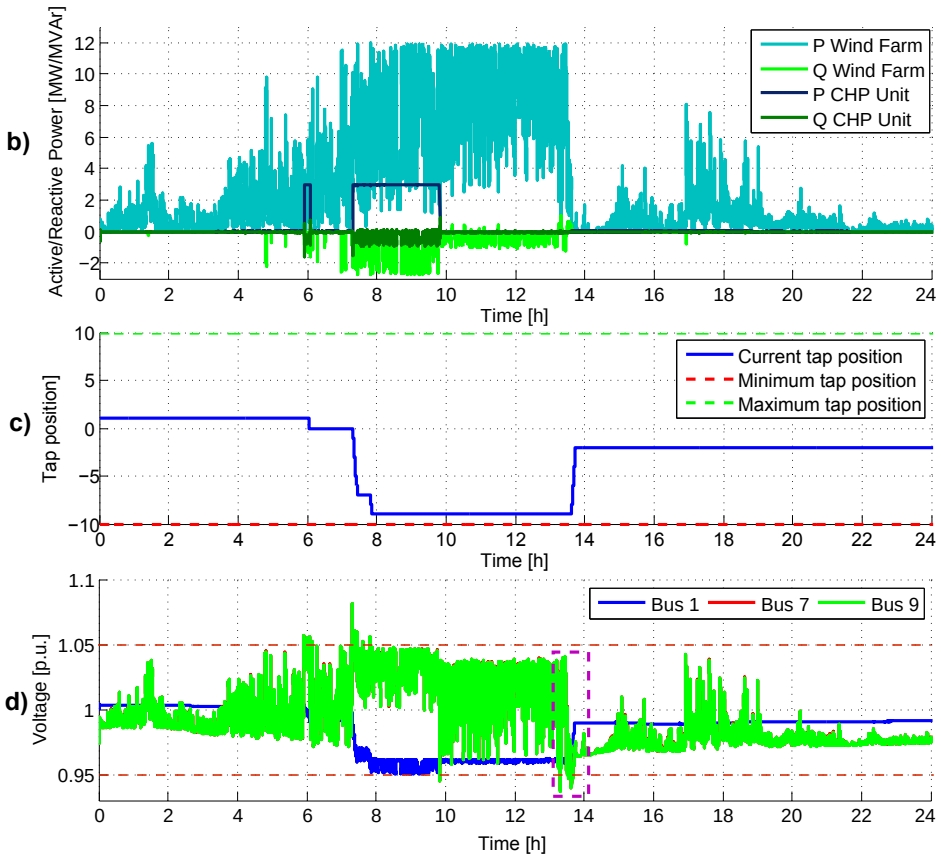

Figure 5.12: Results of the grid with reactive power dispatch, during day 1 of the summer week

Table 5.6 shows the values of generation, consumption, active and reactive power import and

grid losses at the end of the week. In this case, the import of reactive power does not present a big increase as in the winter case. This is due to the reduced time of operation of the DG units compared to the winter case. The losses account for a 2.62% of the load, a higher value than in the previous scenario.

Table 5.6: Total generation, load, external grid import and losses, during the summer week

Generation	Load	P Import	Q Import	Losses
426.15 MWh	712.80 MWh	305.44 MWh	178.70 Mvarh	18.66 MWh

5.3.3 Summary

In this section, the integration of reactive power compensation together with the OLTC has been analyzed. As seen in both winter and summer scenarios, the overvoltage issue presented in Section 5.2 has been improved. Overvoltage is now limited to extreme cases of sudden power increase, partly due to the issue presented by the slow dynamics of the OLTC. On the other hand, the implementation of reactive power compensation is not ideal as it creates undervoltage in bus 1. As specified in Figure 5.12, the OLTC decreased the voltage to nearly 0.95 p.u. by changing its position, and the reactive power flow aggravates it further. Therefore, it should only be utilized in extreme conditions

As summarized in Tables 5.5 and 5.6, the reactive power import to the grid increased, as the CHP units and wind turbines utilize reactive power to create a voltage decrease. Consequently, the losses increased, with values of 5.32% and 2.62% of the total consumption in winter and summer cases respectively.

5.4 Voltage Support from Alkaline Electrolyzers

As it has been previously analyzed in sections 5.2 and 5.3, the implementation of an OLTC and reactive power dispatch from wind turbines and CHP units is not enough to correct the overvoltage that the grid presented initially, as explained in Section 5.1. Therefore, the aim of this scenario is to evaluate the efficacy of implementing a Power to Gas System in order to provide voltage regulation to the studied distribution grid. A first steady state analysis was carried out in Section 3.2.4, where its location was determined to be in bus 9, and have a size of 6.525 MW. Furthermore, the coordination of the the OLTC, DGs' reactive power and alkaline electrolyzer, presented in the mentioned Section, is now tested.

As done in the previous scenarios, the presented results for the winter and summer cases include the active and reactive power flow from Feeder 1, the production of the DG, operation of OLTC and the voltage profile during the week. Additionally, the basic parameters of the electrolyzer units are presented, such as active and reactive power consumption, operating temperature and hydrogen production.

5.4.1 Winter Scenario

Figure 5.13 illustrates the results of the implementation of P2G in the distribution grid during winter scenario. It can be seen in plot a) that the power exported to the external grid is considerably lower, as part of the locally produced power is now utilized by the electrolyzer units. This result demonstrates the capability of the installed electrolyzers to provide energy management and, at the same time provide voltage support.

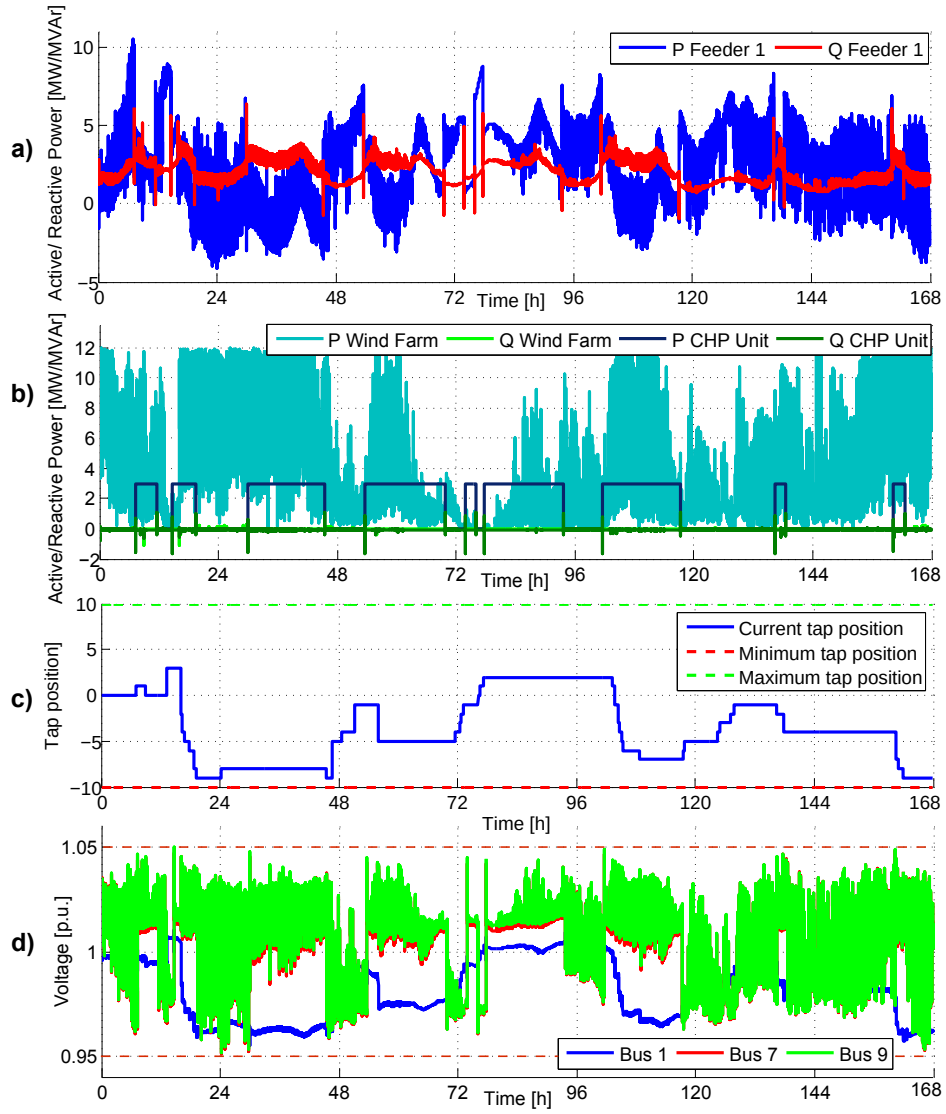

Figure 5.13: Results of the grid with P2G implementation, during a winter week

It can be seen in plot b) that the active power production of the DGs remains unchanged. However, it can be observed that the reactive power from the wind turbines and CHP units is only utilized at the moment of start-up of the CHPs in order to decrease the overvoltage, as a sudden increase of active power occurs.

Plot c) shows the position of the OLTC, where a reduced number of tap changes is observed throughout the week, being 61 in total. Its operation has been reduced by half since it starts operating when the voltage deviation is higher than $\pm 3\%$. In this scenario the electrolyzer units have priority in terms of voltage regulation as explained in Section 3.2.4.

The voltage profile of buses 1, 7 and 9 is shown in plot d). The improvement in the voltage profile due to the integration of alkaline electrolyzers is visible, as the allowed limits are not surpassed. The highest voltage corresponds to bus 9 with a value of 1.0499 p.u. and the lowest occurs in bus 7 with a value of 0.9513 p.u..

Figure 5.14 provides a zoom of the first 24 hours of the simulation, presenting the previous plots b, c and d. As previously mentioned, the voltage remains within the limits. As highlighted in the black rectangle, the voltage of buses 7 and 9 presents a sudden increase from 0.975 p.u. to 1.0499 p.u., due to the start-up of the CHPs. As the peak lasts 10 seconds, the OLTC does not

sense it, and its position remains unchanged.

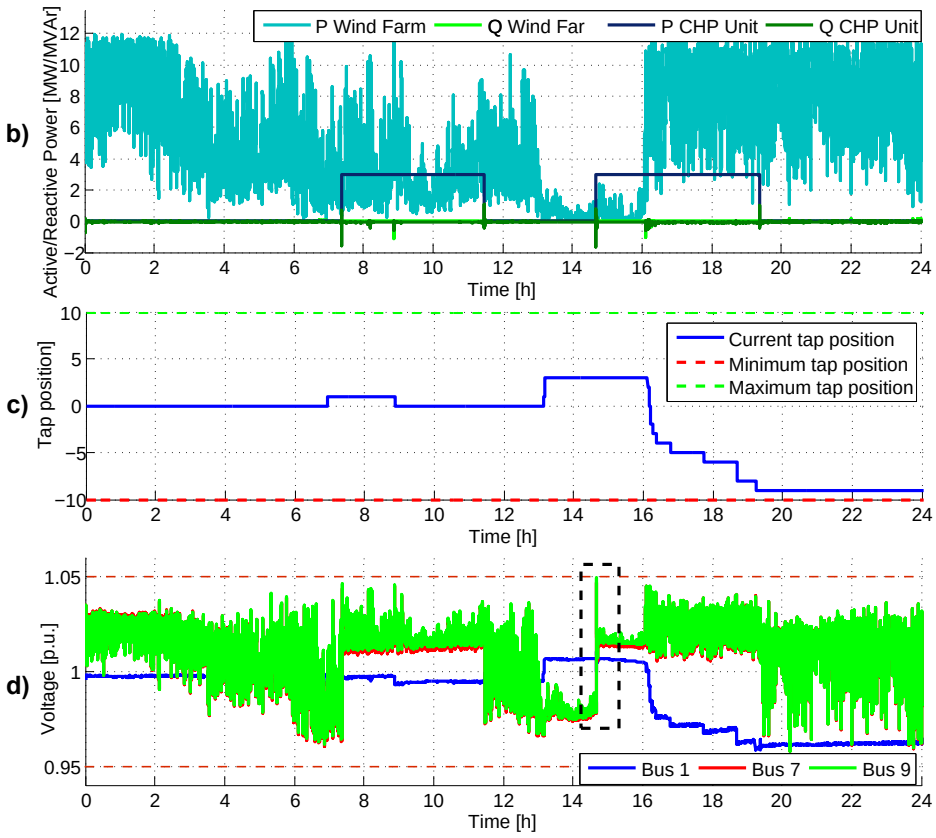

Figure 5.14: Results of the grid with P2G implementation, during day 1 of the winter week

Figure 5.15 represents the most important parameters in the operation of an alkaline electrolyzer unit. The active power set-point and the actual output are shown in plot e), where it is observed that the AE is able to reach the demanded power most of the times. Nevertheless, it is important to mention that between hours 120-144 the temperature fell below 60 °C and the set-point was not reached.

It is observed that the minimum consumption of the AE is 4.6 kW. This is due to the I-U characteristic of the electrolyzer cell when its operation temperature is near 80 °C. The minimum voltage of the AE module's active power PI controller is selected to be 257.4 V, parameter obtained from [47]. When dividing by the number of cells in parallel, i.e. 180, the resultant voltage per cell is 1.43 V. When checking with 1.43 V and 80°C in the look up table presented in Figure 4.33, the obtained current is not zero; hence, the power consumption remains slightly positive.

Plot f) shows the reactive power output of one AE unit. It is observed that the current output follows the set-point, with negligible deviation. Reactive power is consumed whenever the active power cannot reach its set-point, and provided when it is required to correct undervoltage.

The capability of reaching the set-point is determined by the temperature of the electrolyzer, which is illustrated in g). The rated temperature at which the electrolyzer can flexibly adapt to its set-point is 80 °C, as explained in Section 4.5.3. Therefore, it can be appreciated that the active power set-point was reached when the operating temperature was 80 °C. As previously explained, when the temperature fell below 60 °C, the electrolyzer could not reach the active power set-point. It should be noticed that this mismatch was compensated, in terms of voltage, with the reactive power absorption coming from the electrolyzer's converter.

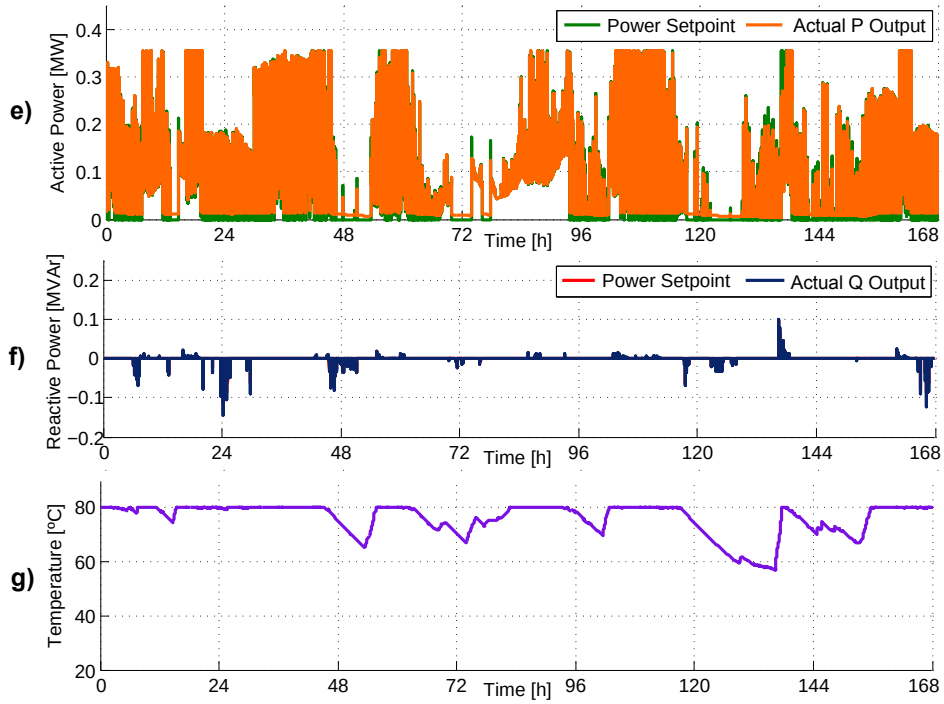

Figure 5.15: Alkaline Electrolyzers parameters, during a winter week

Figure 5.16 provides a zoom in day 6 of the winter week simulation. The set-point and actual active power, plot e), and the temperature of the alkaline electrolyzer, in plot g), are shown in order to observe in detail the dependance on the temperature, as previously mentioned.

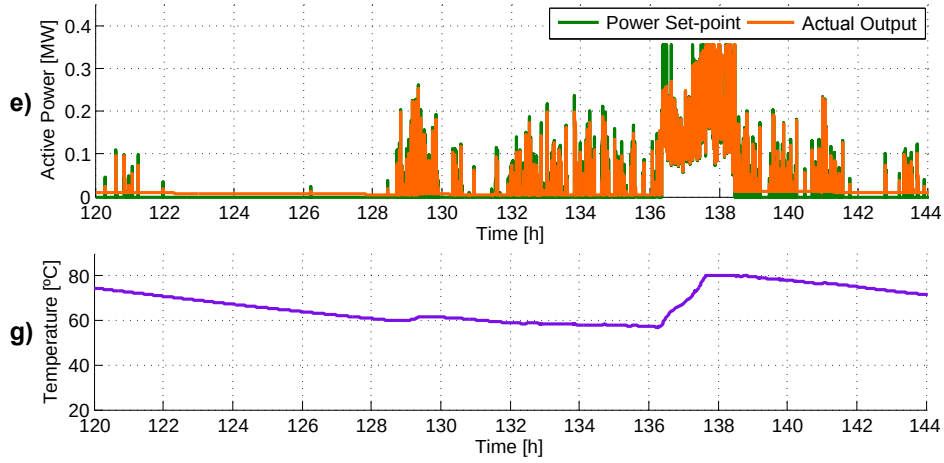

Figure 5.16: Alkaline Electrolyzers parameters, during day 5 of the winter week

The values of generation, consumption, power flow from Feeder 1 and the grid losses are summarized in Table 5.7. It can be observed that compared to the previous scenario, which included reactive power compensation from the DGs and OLTC regulation, the final value of the active power consumption and active power import have increased due to the implementation of 15 electrolyzer units. The reactive power import has decreased, as the regulation utilizing the reactive power capacity of the DGs is limited to voltage variations higher than 1.04 p.u.. On the other hand, the utilization of the P2G system contributes to reduce the losses of the grid, as the excess power of the DG units is consumed locally, being a 2.18 % of the consumption, while in the previous scenario it was 5.32 %.

Table 5.7: Total generation, load, external grid import and losses, during the winter week

Generation	Load	P Import	Q Import	Losses
1134.37 MWh	1521.65 MWh	420.45 MWh	343.40 Mvarh	33.17 MWh

Additionally, the hydrogen production, injection and storage variation should be analyzed, as depicted in Figure 5.17. Plot h) shows the AE's hydrogen production and plot i) depicts the injected hydrogen into the CHP's gas pipes, both in $[Nm^3/h]$. The resulting volume variation in the storage can be observed in plot j).

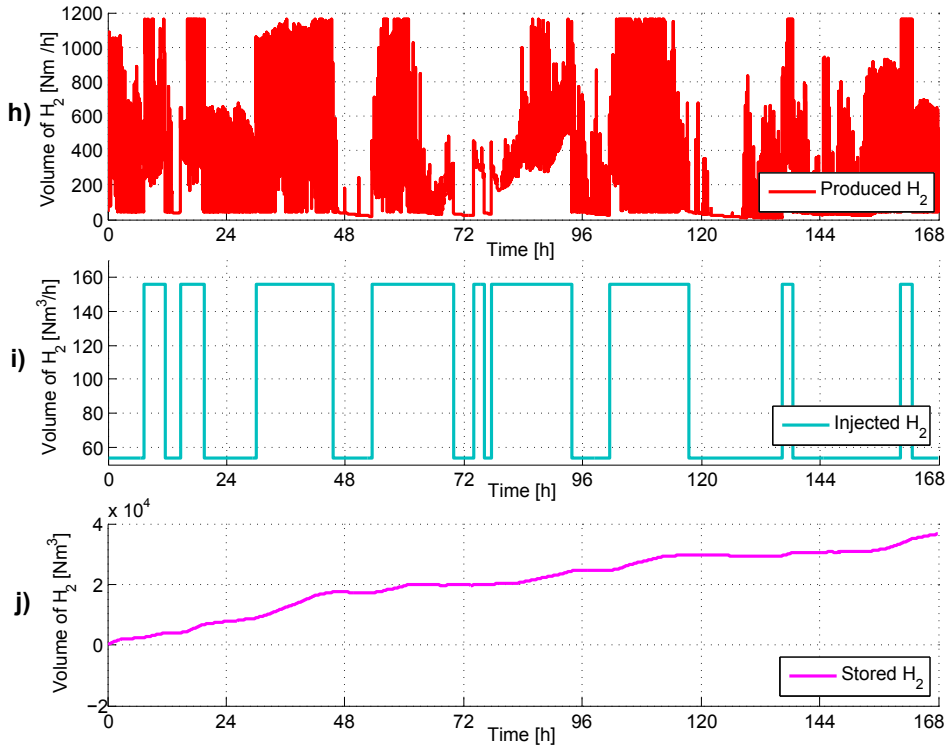

Figure 5.17: Hydrogen storage relevant variables, during a winter week

The limitation of hydrogen injection is observed, as the value of produced hydrogen is around 7 times higher than the injected one. The analyzed week is a particularly cold winter week, where the CHP plant has to produce more heat than in any other period of the year; hence, the gas consumption should be proportionally high. The fact that the hydrogen storage variation is highly positive under the mentioned circumstances shows that relying only on the hydrogen injection in order to supply the produced hydrogen is infeasible. Therefore the excess hydrogen has to be somehow utilized. The possible solutions in order to consume the produced hydrogen could be the following: direct connection to the gas transmission network, local hydrogen loads such as hydrogen mobility and providing to local SNG (Synthetic Natural Gas) plant or hydrogen fired CHP units. However, the analysis of these solutions is beyond the scope of the present work.

5.4.2 Summer Scenario

In this subsection, the testing of the implementation of the Power to Gas system is carried out in the summer week. Figure 5.18 shows the results obtained for this simulation.

The active and reactive power flow through Feeder 1 is represented in plot a), where it can be seen that the active power export to the external grid is lower due to the additional load of the alkaline electrolyzers.

Plot b) represents the active and reactive power from the wind farm and CHP units. The active power production remains unchanged, while the reactive power is now only used in extreme situations such as start-up of the CHPs or a sudden change of power from the wind farm. It can also be seen that reactive power is only utilized when the voltage is higher than 1.04 p.u., as explained in Section 3.2.4.

The operation of the OLTC is illustrated in plot c), where it can be seen that its operation has been highly reduced, as it starts regulating from a deviation of $\pm 3\%$ of the voltage. Therefore, the total number of tap changes per week is 44.

The voltage results are presented in plot d), where the improvement respect to Section 5.3 can be observed. It should be noticed that the voltage surpasses the upper limit in two occasions, as the electrolyzer is not able to reach its set-point, where the highest peak is 1.06 p.u. at bus 9.

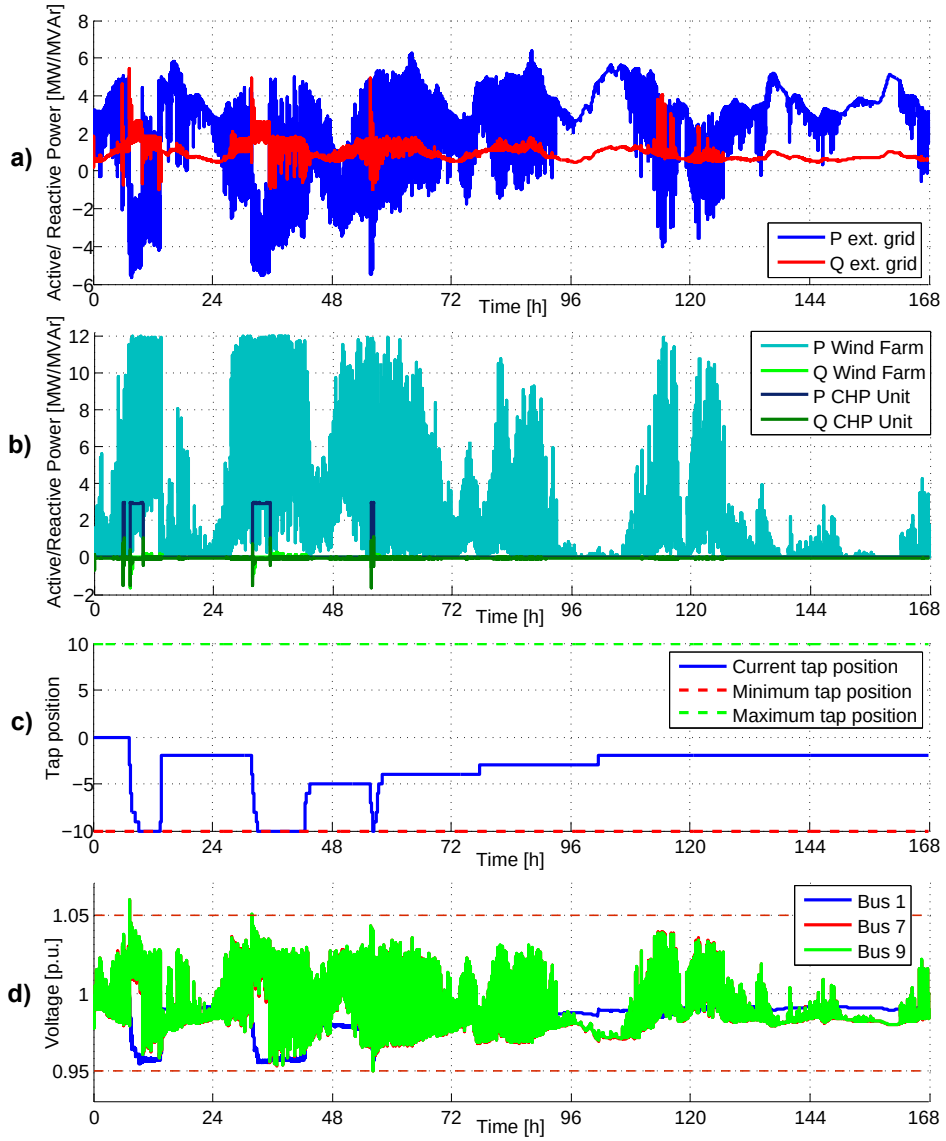

Figure 5.18: Results of the grid with P2G implementation, during a summer week

Figure 5.19 provides a zoom in the first 24 hours of the simulation, showing the previous plots b c and d. The highest overvoltage peak can be observed in plot d) highlighted in black, between hours 7 and 8. It can be seen that it occurs when the CHP starts operating. At the same time, the tap changer was set at position 0, and due to its delay, it takes time to reach a lower position.

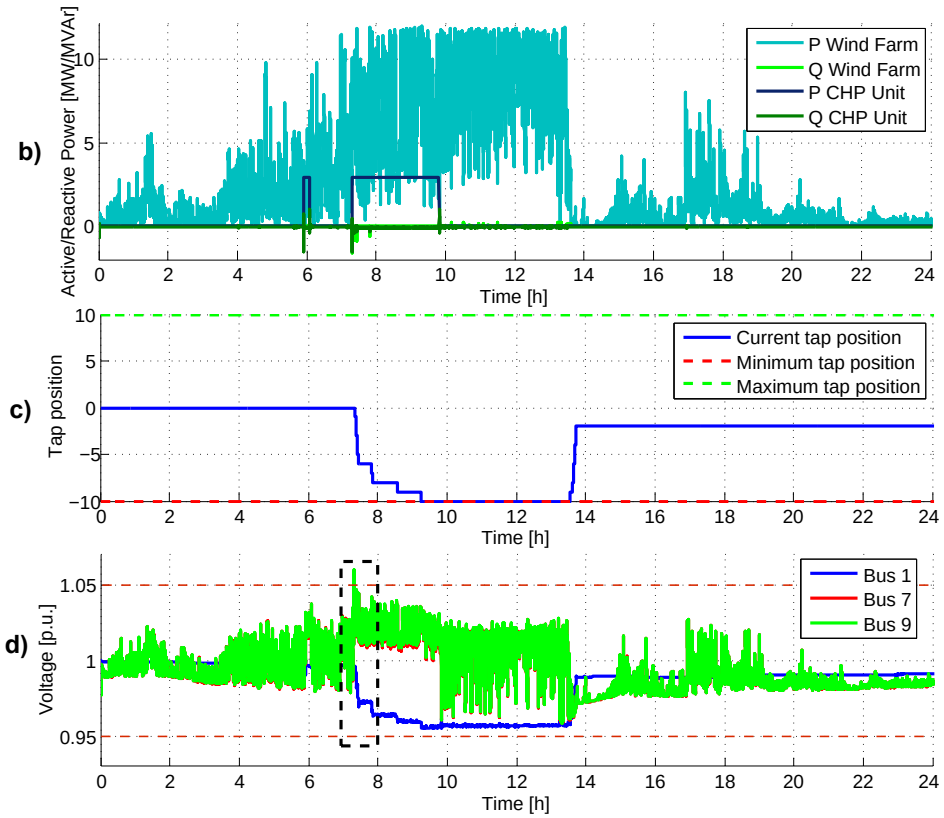

Figure 5.19: Results of the grid with P2G implementation, during day 1 of the summer week

The most relevant parameters of one electrolyzer unit are represented in Figure 5.20. The active power consumed by one unit is shown in plot e), where it can be seen that its operation is decreased in the summer scenario. As a consequence of low operation, it can be seen that the active power set-point is not met after a period of standby, as for example in the fifth day of simulation. Plot f) shows the reactive power that is consumed and supplied by the converter of the electrolyzer. As in the winter case, the set-point is reached during all week.

The temperature of the electrolyzer is shown in plot g), where the decrease due to standby is observed. The temperature drops from 80 °C to 27.7 °C at hour 113. It can be appreciated that, during that period the electrolyzer is less capable to meet the given set-point. Finally, plot h) presents the produced hydrogen, which is directly dependent on the consumed power shown in plot e).

Figure 5.21 provides a zoom in the fifth day of the simulation, in order to see in detail the period where the temperature has reached the lowest value and the electrolyzers are required to provide voltage regulation. It can be seen in plots e) and h) that the capability to reach the set-point is totally dependent on the temperature, as the consumed active power is closer to the set-point when the temperature is closer to 80 °C.

Table 5.8 summarizes the obtained results for the generation, load, active and reactive power import from Feeder 1 and its losses. As in the winter case, the values of load and active power import have increased due to the implementation of the electrolyzers. Regarding the value of reactive power import, it has decreased to the value obtained in Section 5.2.2. Additionally, the value of the losses in the grid has also decreased from 2.62 % of the consumption in the previous scenario to 1.35 % with the P2G system.

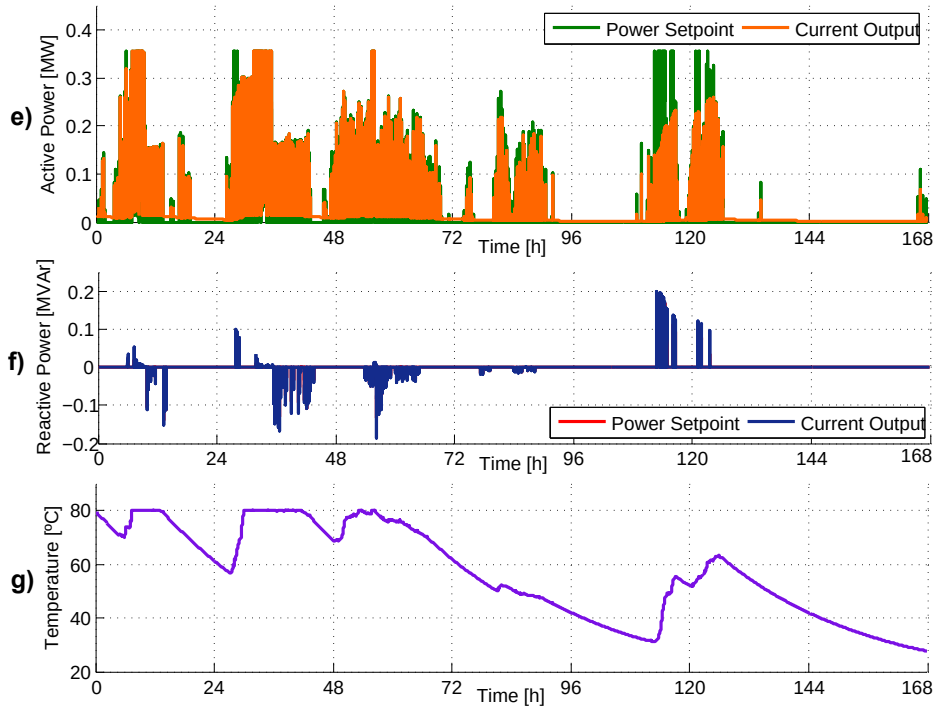

Figure 5.20: Alkaline Electrolyzers parameters, during a summer week

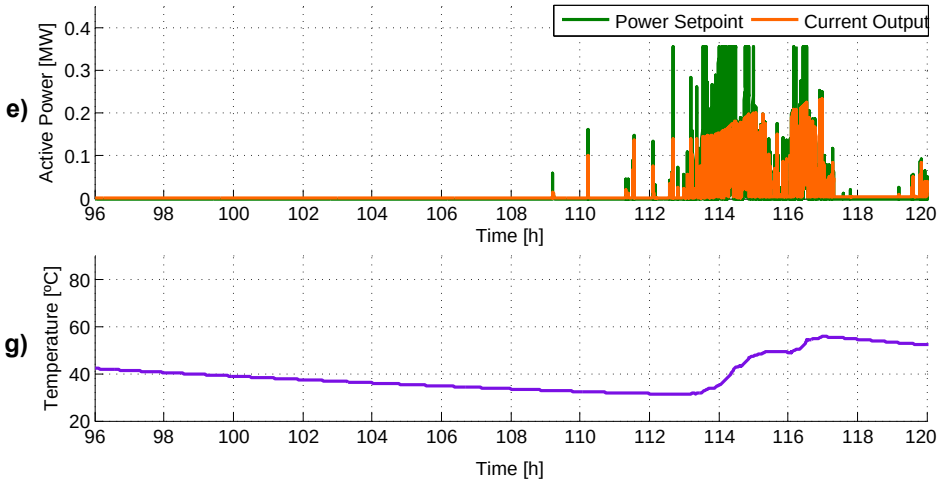

Figure 5.21: Alkaline Electrolyzers parameters, during day 5 of the summer week

Table 5.8: Total generation, load, external grid import and losses, during the summer week

Generation	Load	P Import	Q Import	Losses
426.15 MWh	793.89 MWh	378.63 MWh	160.5 Mvarh	10.75 MWh

As in the winter scenario, the hydrogen production, injection and storage variation are analyzed. Plot h) shows the hydrogen production of the AE unit and plot i) depicts the injected hydrogen into the CHP's gas pipes, both in $[Nm^3/h]$. The resulting volume variation in the storage can be observed in plot j).

It can be observed that the hydrogen increment in the storage is still positive, although smaller than in the winter week (15000 vs. 40000 Nm^3). This is due to the less frequent operation of the electrolyzer, as the average voltage is not as high as in the winter case. This result also confirms the need of an additional hydrogen demand.

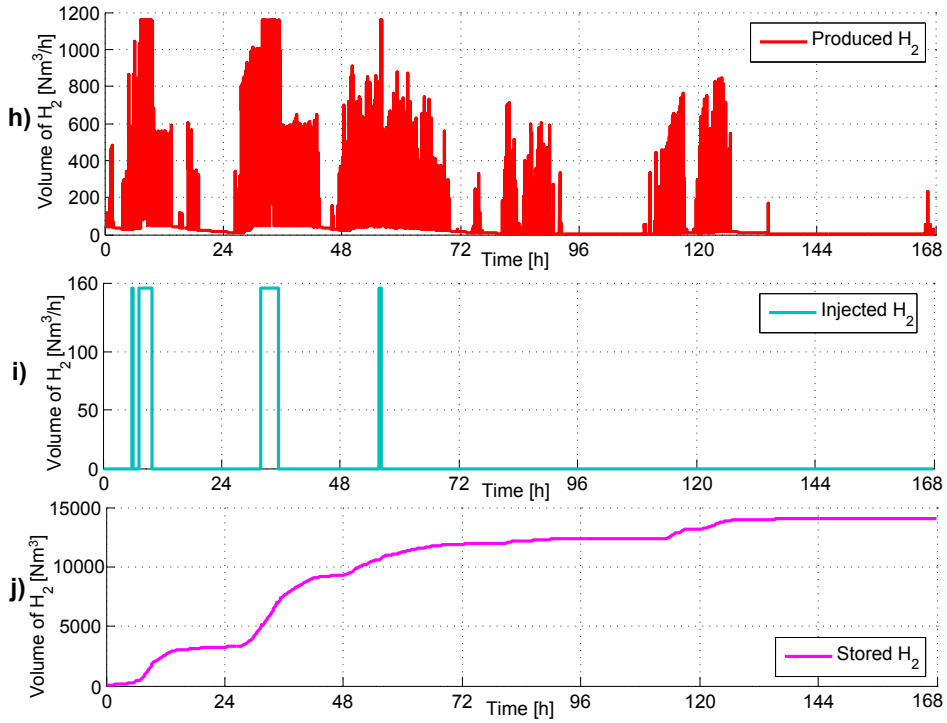

Figure 5.22: Hydrogen storage relevant variables, during a summer week

5.4.3 Summary

As observed in both winter and summer cases, the voltage of buses 1, 7 and 9 are within the limits, except for a very short period of time in the summer week. Another important improvement was found regarding grid losses, which were reduced by half in both cases. Therefore, it has been found that the integration of of alkaline electrolyzers in the case study grid results to be efficient in voltage support and energy management.

5.5 Conclusions

In the present chapter three different voltage regulation strategies have been tested, besides the base case which did not have any voltage regulation. Table 5.9 shows relevant values concerning the voltage quality, grid losses, reactive power import and number of tap changes. The voltage quality parameters include the average deviation from 1 p.u. ($\overline{\Delta V}$) and the time the voltage surpasses the allowed limits ($T_{|\Delta V|>0.05}$).

Table 5.9: Voltage quality, grid losses, reactive power import and number of tap changes during the analyzed cases

	Base Case		OLTC		OLTC & DGs		OLTC, DGs & AE	
	Winter	Summer	Winter	Summer	Winter	Summer	Winter	Summer
$\overline{\Delta V}[p.u.]$	0.040	0.023	0.024	0.018	0.019	0.016	0.017	0.015
$T_{\|\Delta V\|>0.05}$	56.0 h	14.3 h	16.5 h	4.3 h	35 min	27 min	0 s	7 s
Losses [MWh]	59.6	17.2	62.8	18.0	65.8	18.7	33.2	10.8
Q Import [Mvarh]	339.2	160.0	340.0	160.5	404.5	178.7	343.4	160.5
nº Tap Changes	-	-	149	111	63	44	61	44

The base case presents a voltage profile which would not allow the case study grid to operate under normal conditions. The first improvement can be appreciated with the introduction of the

OLTC, with a significant flattering of the voltage profile. However, the voltage profile is out of the allowed range during a significant period of time and the amount of tap changes during the winter week surpass the recommended limit, leading to a decreased life time of the mechanism.

The introduction of the reactive power of the DGs drastically improves the voltage profile and reduces significantly the stress of the OLTC. The amount of time the voltage surpasses the grid codes' limits is in the range of minutes during the week. Nevertheless, Figures 5.9 and 5.11 (in Section 5.3) show short term voltage overshoots due to the slow dynamics of the tap changer controller. The same applies for the OLTC case, aggravated by the fact that there is no extra voltage support. Continuing with the DG's case, the big amount of reactive power required for the voltage regulation increases significantly the reactive power import and the losses. As stated in Section 3.2.3, this is not beneficial neither for the TSO nor the DSO.

Finally, with the implementation of the the alkaline electrolyzer the voltage profile is further improved. The time where the voltage is beyond the limits, due to transients, becomes insignificant and within the recommendations stated in [76]. It should be reminded that first order delays were added to the voltage measurement for both wind turbines and AE, in order to facilitate the convergence of the simulation. These delays do not represent the real behavior of the controllers and are the main responsible of the mentioned transient overvoltages. Regarding losses, they are reduced more than in any other scenario due to the local consumption of the generation. The reactive power import, since its usage was limited when the voltage was above $1 \pm 0.04 p.u.$, is reduced to a similar magnitude as in the base and OLTC cases, whereas the OLTC is barely stressed. The results in terms of voltage quality, losses, reactive power import and tap changes make this strategy the most reasonable technical solution, although some aspects need to be improved. These are, operational temperature below the rated that lead to a capability limitation and the lack of dependence on market prices. If these are not taken into account, the consequences for the DSO would be not consuming power it purchased in the markets and purchasing unnecessary energy during high prices, respectively.

Operating the AE reduced the reverse active power flow through TR1; however, the fact of providing energy management services is not explicitly analyzed. For this purpose, the following questions have to be addressed in order to improve the existing AE's voltage regulation strategy, which include the previously presented issues:

- Regarding the energy management strategy, what is the price the DSO would be willing to pay in order to reduce the reverse power flow through TR1?
- Taking into account the capabilities/limitations of the AE based on its operating temperature, is it feasible to participate in the main wholesale markets?

These questions will be addressed in the next chapter, with the aim of creating an energy management strategy which complements with the existing voltage regulation including all OLTC, DGs' reactive power and AE.

6 Energy Management from P2G Systems - Market Strategy and Dynamic Analysis

In this chapter an improvement of the voltage regulation strategy provided in Section 5.4 is presented. As stated in Chapter 5, the active power absorbed by the electrolyzer did not take into consideration the electricity market prices. Moreover, providing energy management services, i.e. minimizing the active power export through TR1, was not explicitly analyzed. Therefore, the aim of this chapter is to develop a market strategy that copes with both the voltage regulation and energy management requirements. Nevertheless, the market strategy will need to deal with two different issues:

- The capability of the AE is limited by its operation temperature, which might bring economical consequences when participating in the electricity markets
- Energy management and voltage regulation are services which have a benefit for the DSO, although the associated economical benefit of these services cannot be easily established in this specific work

Regarding the dynamic analysis, the AE control models depicted in Figure 4.28 and Figure 4.29, in Section 4.5, will be modified in order to incorporate the active power set-points of the presented strategy. Additionally, a new coordination of the OLTC, reactive power of the DG and active and reactive power of the AE will be presented in order to keep a balance among different constraints:

- Maintaining the voltage within the allowed limits, as in the results obtained in Section 5.4
- Daily number of tap changes below 20
- Reduce as much as possible the active power deviations from the schedule
- Keep the reactive power import as low as possible

In the following section, the market strategy is explained and the steady state hourly results are presented, both technical and economical. Furthermore, the economical results are compared to the average values obtained in Section 5.4, in order to determine the achieved improvement.

6.1 Market Strategy - Steady State Analysis

6.1.1 Introduction

The purpose of this section is to provide an overview of the developed market strategy. Firstly, the approach taken in the strategy is explained, where the different markets, the market players and the process to determine the schedule of the AE, are introduced. Secondly, a detailed scheme of the strategy is presented, where the differentiated parts in which the bid is calculated, are explained. This explanation includes the data exchange between the differentiated parts and the flowchart with the logical sequence of the market strategy.

Approach: markets, players and scheduling process

The target of the implemented market strategy is to schedule the hourly operation of the AE according to the technical requirements of the grid and the market prices. For this purpose, the different markets in which the AE takes part and the different players involved in the bidding process are introduced. In the following, the most important characteristics of the analyzed markets are presented, in order to know the different time windows in which the bids have to be made. The analyzed markets are: the spot market (Elspot), the intraday market (Elbas) and the regulation power market. The presented information has been taken from Appendix A, where more detailed information about the electricity markets can be found. As explained in Section 2.3, a new market for flexibility is still to be introduced, where the grid companies can avoid congestion by participating in it. Therefore, the implemented strategy only takes into account the currently existing markets.

- Elspot: This market closes at 12:00 am the day before delivery and bids are made for a 24 hour period corresponding to a natural day.
- Elbas: Bids can be forwarded from the closing of the Elspot market until 1h prior operation. The bidding period is assumed to be one hour. When deciding the volume of the bid, the already purchased power in the spot market has to be taken into account.
- Regulation Power Market: Bids have to be forwarded before 17:00 the day prior operation; nevertheless, they can be modified up to 1 hour before. The minimum size of the bids is 10 MW and the bidding period is 1 hour. The regulation power has the peculiarity that it is activated only when the TSO requires it. Furthermore, activation time should not take longer than 15 minutes. It should be noticed that the electrolyzer might not be able to fulfill this condition if its temperature is not high enough. Since the AE is a load, only down regulation is considered.

In the following, the market players, i.e. DSOs and BRPs, are presented.

- DSOs: Normally they do not participate in the electricity markets. However, as study grid DSO requires active power for the electrolyzer, it will purchase electricity directly in the wholesale markets. For this purpose, it has to have an agreement with a BRP in order to balance the schedule. In this context, the DSO forwards the bid to the BRP, who is responsible for placing the bid in the market. As stated in Section 2.2, DSOs are expected to be customers of the upcoming flexibility market. However, this flexibility market is not completely developed nowadays and DSOs have to obtain the flexibility by scheduling the electrolyzer in an intelligent way. In other words, instead of aggregators and BRPs offering products to the DSOs in the flexibility market, these have to create the flexibility on their own.
- BRPs: They possess agreements with different producers, traders and big consumers, which includes the DSOs. They receive the bid forwarded by the DSO, aggregates it with the bids forwarded by the rest of the BRP's customers and places the aggregated bid in the market. This is relevant when analyzing the participation of the DSOs in the regulating power market as the rated power of the AE is 6.525 MW but the minimum bid is 10 MW. Thus, it is assumed that the BRP possesses more regulation capacity that allows the bid to reach 10 MW.

Once the markets are known, the scheduling process can be summarized as depicted in Figure 6.1, this includes the data exchange between the different assets and players. First, the DSO forwards the bid to the BRP according to: the previously purchased power in the closed markets and a load flow forecast that includes this purchased power. The latter aggregates the bid with the ones coming from other customers and places it in the market. Once the prices are revealed, the power that the AE purchases in that market is known and added to the purchased in the already closed markets.

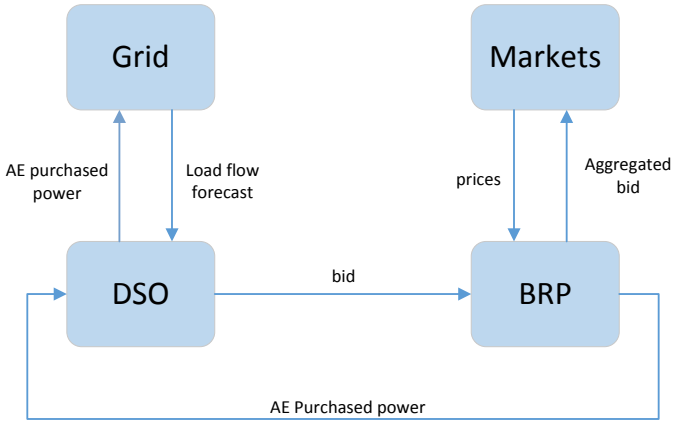

Figure 6.1: Basic scheme of the scheduling process

It should be noticed that the DSO is assumed to possess the ability of forecasting the grid state, which might not be a realistic for many DSOs. Therefore, this assumption implies a limitation of the proposed market strategy. Furthermore, it is evident that the grid forecast that determines the bid for a specific market has to be done before the closing of the market. Therefore, a day-ahead forecast is suggested for the spot market, a 4 hour-ahead forecast for the intraday market and an hour-ahead for the regulation power market. It should be noted that in the approach taken in this project, the forecasts are not done as such but simplified with load flow estimations, which implies another limitation of the proposed strategy. A further analysis of the load flow estimations is presented later on in Section 6.1.2.

In the following, the process of the DSO to formulate a bid according to the grid state forecast are specified. As an introduction, a basic scheme of the parts included in the process and the data exchange between each of them are presented in Figure 6.2. These are the load flow estimations, active power requirements functions and decision making.

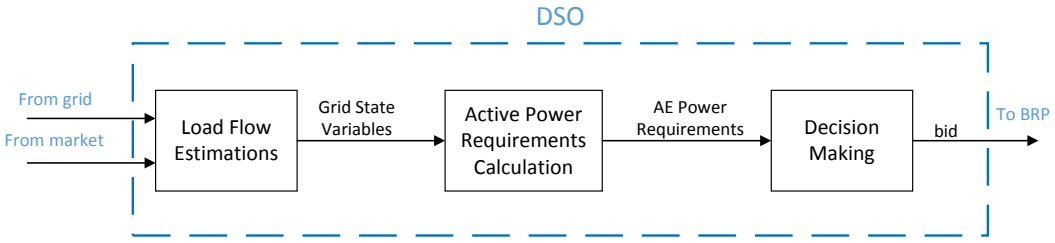

Figure 6.2: Basic scheme of the bidding process

Firstly, the detailed bidding process the DSO follows is explained. This includes more detailed description of the different blocks presented in Figure 6.2. Nevertheless, these three parts will be explained in detailed in Sections 6.1.2, 6.1.3 and 6.1.4, since they conform the core of the market strategy.

Detailed bidding process

As previously explained, the bidding process incorporates three differentiated parts. These are load flow estimations for each market; calculation of the active power requirements according to the estimations; and the decision making, where a bid is forwarded to the market. A brief explanation of each is presented as follows:

- Load flow estimations: as presented before, they emulate the load flow forecast that the DSO is assumed to realize.
- Active power requirements: calculation of the active power that the AE has to absorb in order to bring the voltage within limits (voltage regulation requirement), cancel the active power export from Feeder 1 (energy management requirement) or the maximum power it can absorb in order not to cause undervoltage (maximum power requirement).
- Decision making: fuzzy logic decision maker which, with the obtained active power requirements and different constraints, calculates the bid.

Figure 6.3 shows a detailed scheme of the implemented strategy for participating in each market. The sequence of the strategy is implemented as follows: first, a load flow estimation is done for each hour of the bidding period, taking into account the schedule of the AE in the markets that have already closed. Then, the voltage in bus 9 (V_9), V-P sensitivity in bus 9 (dV_9/dP_9) and power export from Feeder 1 (P_{exp}) are used in order to implement functions that calculate the voltage regulation (VR), energy management (EM) and maximum power (MP) requirements. Afterwards, the decision making is determined according to the results obtained from the mentioned functions and a bid is forwarded to the BRP that the DSO is associated with. The bid is limited by the available capacity (6.525 MW) minus the power purchased in market(s) that already closed. Finally, the market prices are revealed; hence, the power that the AE absorbs in that market is known. The total is used in order to calculate the load flow estimation for the next market.

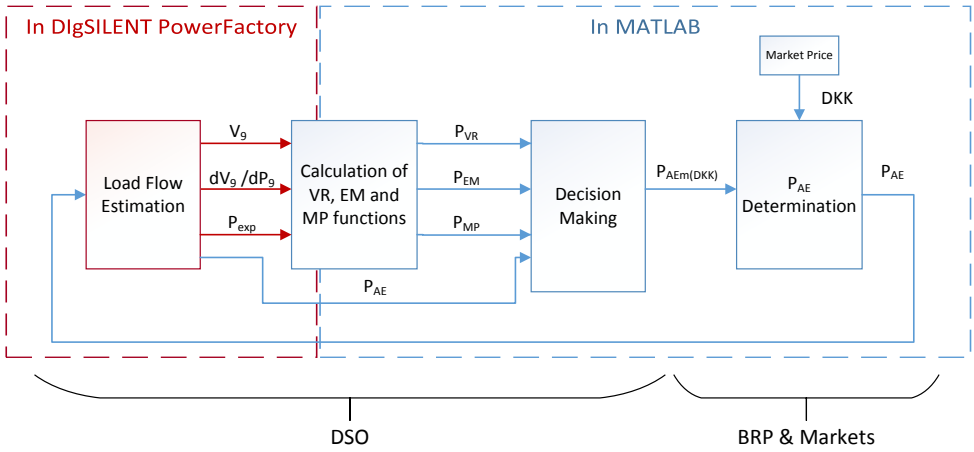

Figure 6.3: Detailed scheme of the market strategy

The logical flowchart of the developed market strategy is shown in Figure 6.4. As it can be seen, it begins in the hour $h = 1$, which is the first hour of the week. Then, the voltage regulation (VR), energy management (EM) and maximum power (MP) requirements are calculated for that hour, according to the load flow estimations implemented for the market m_n. Finally, the bid is made according to the mentioned requirements. The same is repeated during each hour until the last hour of the week is reached ($h = 168$). After the market closes, the market prices are revealed by

Nord Pool; hence, the active power the AE is scheduled to consume during the bidding period, P_{AE}, is known. This flowchart is applied for each of the markets where the AE participates in, starting with the market that closes more in advance (spot market), continuing with the intraday market and finishing with the one that closes the nearest to the hour of operation (regulation market).

It should be noticed that the algorithm does not follow the natural timing of the bidding process in each market, which would be as follows. The day before operation, a day ahead load flow estimation is done for the 24 hour period of the next day; accordingly, a bid is made for this period. For each of the 24 hours of the period, a new estimation is made when the current time is 4 hours prior to the hour of operation; accordingly a bid is forwarded to the intraday market. If some energy is traded in this market, between 1-4 hours before operation, the same load flow estimation is updated and a bid for the same single hour is forwarded to the regulation market. In this algorithm, the bidding periods last 168 hours for the three markets, since the load flow estimations are already known. This fact responds to a simplification purpose, but it emulates in a feasible way the real timing of the bidding process.

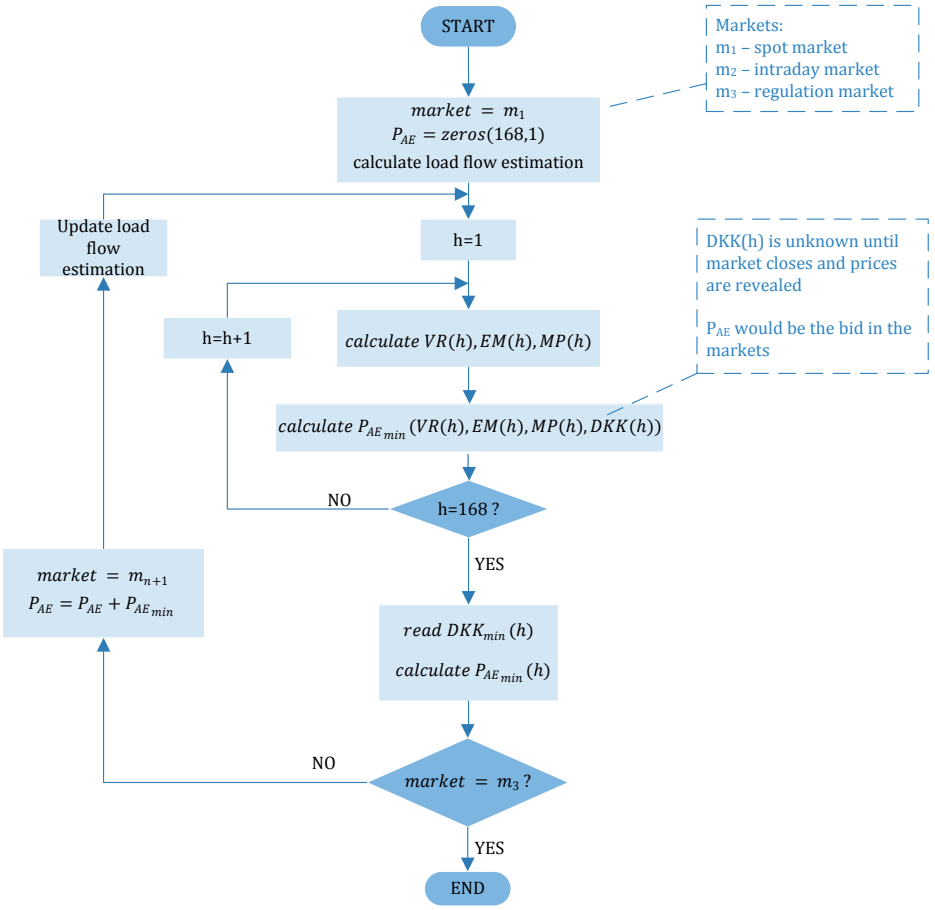

Figure 6.4: Overall flowchart of the market strategy

In the following sections, the load flow estimations, the active power requirements and the decision making method, i.e. determining the bid, are presented. They conform the core of the market strategy; thus, they are explained into detail.

6.1.2 Load Flow Estimations

As previously explained, a load flow estimation is made for the generation and the consumption; a day-ahead estimation is made for the spot market; and an hour-ahead for the intraday and regulation markets. The purpose of these estimations is to emulate the error in the forecasting method that the DSO implements. In both estimations it is assumed that the generation of the CHP plant and the consumption of the loads are known. However, it should be remarked that this is not completely certain for the CHP plant. As stated in Section 4.3, the CHP participates in both spot and up regulation markets. However, only accurate predictions can be made for the spot market in both day-ahead and hour-ahead estimations. Additionally, predictions in the up regulation market could not be made accurately, since activation signals are sent a maximum of 15 minutes before the actual activation. Hence, assuming that the CHP's market behavior is known, implies a limitation in the estimation method; even though the power that the CHP purchases in the regulating power market is significantly lower than in the spot market

Regarding the estimation errors of the wind power, normal distribution parameters have been taken from [77]. Parameters for day-ahead estimation have been taken for the Danish power system, whereas the hour-ahead ones have been approximated by taking them for the German power system, since the reference did not provide hour-ahead errors for the Danish one. With the obtained normal distribution parameters, i.e. average (μ) and typical deviation (σ), an hourly time series of power errors (P_{forec}) has been calculated and added to the actual wind power (P_{actual}), which has been obtained by calculating an hourly average of the power output presented in Section 4.2. Eq. 6.1 shows the applied calculation for each hour of the week:

$$P_{forec}(h)[MW] = P_{actual}(h)[MW] + 12[MW] \cdot normrnd(\mu_{forec}, \sigma_{forec}) \tag{6.1}$$

Where 12 MW is the installed wind power in the case study and $normrnd(\mu_{forec}, \sigma_{forec})$ is a Matlab function that creates random values that belong to a normal distribution characterized by μ and σ. Figure 6.5 shows the hourly average of the actual wind power compared to the day ahead and hour ahead estimations.

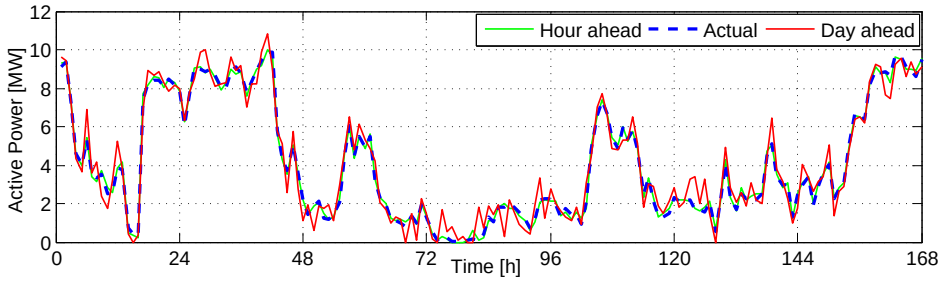

Figure 6.5: Actual hourly wind power vs. hour and day ahead estimations

Once the estimations of generation and consumption are known, power characteristics are created for the 168 hours of the analyzed weeks in order to input these values to PowerFactory. It should be noticed that the load characteristics are already created since they were used in Chapter 3. A modified time sweep in DIgSilent Programming Language (DPL) is run for the 168 hours in order to write into a file the following variables: voltage in bus 9 (V_9), active power export though TR1 (P_{exp}), voltage sensitivity in bus 9 respect to the injected active power in bus 9 (dV_9/dP_9) and AE active power consumption (P_{AE}). It is important to remark that the OLTC has been left in the tap position $tap = 0$ during the time sweep.

6.1.3 Active power requirements

As previously introduced, the active power requirements can be defined as the active power that the AE has to absorb in three different situations, which will determine the AE's bid in the market after the decision making:

- The minimum active power to bring the voltage below an upper boundary (P_{VR}), calculated in the voltage regulation (VR) algorithm.
- The necessary active power to cancel the active power export from Feeder 1 to the external grid (P_{EM}), calculated in the energy management (EM) algorithm.
- The maximum active power the AE can absorb, maintaining the voltage above a lower boundary (P_{MP}), calculated in the maximum power (MP) algorithm.

In order to implement these algorithms, the three variables obtained from the load flow estimation time sweep are sent to a Matlab script, namely: the voltage in bus 9 (V_9), the voltage sensitivity in bus 9 respect to the active power injection in bus 9 (dV_9/dP_9) and the active power export from Feeder 1 (P_{exp}). It should be noticed that the parameters of the algorithms do not vary depending on the analyzed market, but the outputs might do. This is due to different inputs from the load flow estimation according to each market, which will lead to different outputs. In Figure 6.4 it can be seen that when the market changes the load flow forecast is updated, which changes the inputs for the VR, EM and MP functions. In the following, the algorithms for obtaining the voltage regulation, energy management and maximum power requirements are presented.

Voltage regulation function

The active power requirement for voltage regulation (P_{VR}) is defined as the minimum active power that the AE has to absorb in order to bring V_9 down to 1.033 p.u.. This is taking into account that the OLTC also contributes in voltage regulation by varying its tap position down to $tap = -5$. It should be noticed that 1.033 p.u. has been chosen instead of 1.05 p.u., which is the upper limit. This responds to two reasons: the presence of big voltage fluctuations in the dynamic simulation, which require a voltage margin in order not to surpass the upper limit, and the fact that the deadband of the OLTC is exactly ± 0.033 p.u.. Furthermore, limiting the tap position down to $tap = -5$, when the OLTC's capacity goes down to $tap = -10$, intends not to stress the OLTC with excessive tap changes. As explained in Chapter 5, the reactive power capability of the DGs is not included in the schedule. The reason for it is that its absorption is not desirable since it increases losses at the distribution level and the need of reactive power compensation at the transmission level. The flowchart of the voltage regulation algorithm is presented in Figure 6.6.

The term $\Delta V_9/\Delta tap$ is the voltage sensibility in bus 9 to a tap change in TR1. As stated in In Section 3.2.2, each tap change varies the voltage in bus 1 by $\pm 0.4\% p.u.$. According to Eq. 3.3, a simplification can be made and also assume that V_9 varies $\pm 0.4\% p.u.$ with each tap change in TR1. The logical sequence of the flowchart is explained as follows:

- For each of the hours of the week, V_9 and dV_9/dP_9 are read from the load flow estimation.
- V_9 is compared to 1.033 p.u.. If it is equal or smaller there is no need to absorb power and $P_{VR} = 0$. If it is bigger, the OLTC will try to lower the voltage until the tap position $tap = -5$ is reached or V_9 is smaller than its deadband, 1.033 p.u..

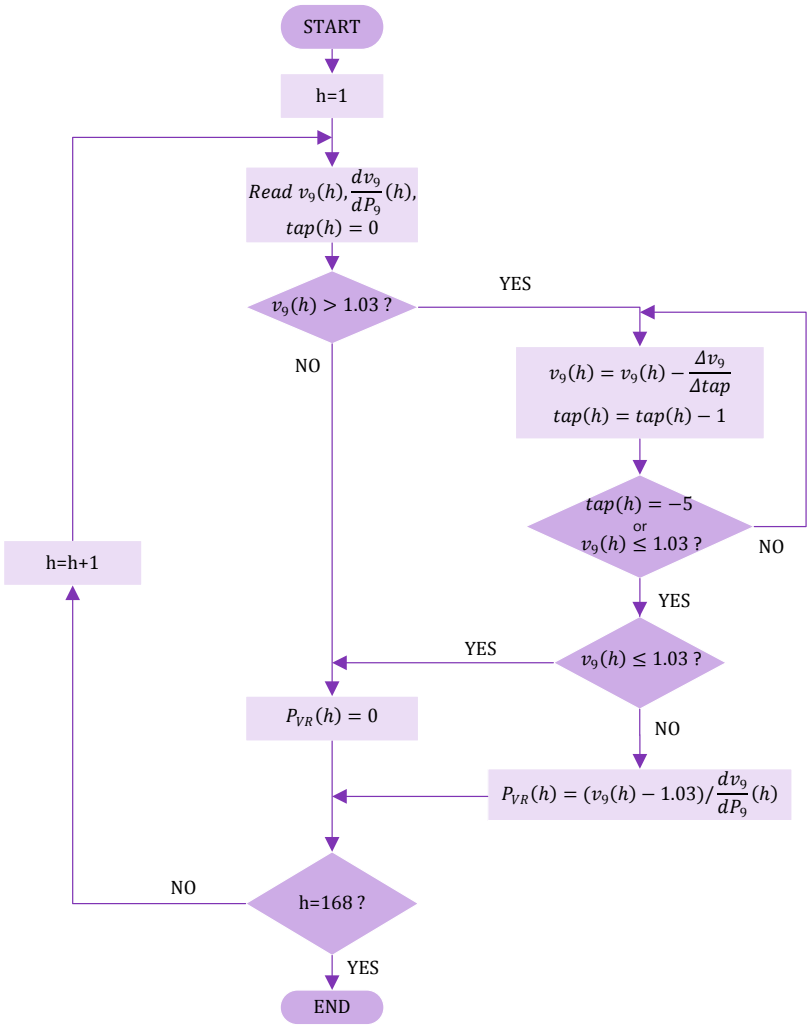

Figure 6.6: Flowchart of the voltage regulation algorithm

- After the OLTC corrects the voltage, V_9 is again compared to 1.033 p.u.. If it is equal or smaller there is no need to absorb power and $P_{VR} = 0$. If it is bigger, the AE will absorb the necessary active power in order to lower the voltage down to 1.033 p.u., according to V_9 and dV_9/dP_9.

Energy management function

Moving forward to the energy management power requirement (P_{EM}), the function is defined as the necessary power the AE has to absorb in order to decrease to zero a positive active power export through TR1, maintaining the voltage in bus 9 below 1.033 p.u. at the same time. Hence, this function includes the voltage regulation plus the energy management functions.

In order to understand the effect that the energy management has on the voltage of bus 9, load flow simulations have been carried out representing the hour with highest and lowest demand, i.e. hours 105 and 121, as presented in Section 3.2, both in maximum generation scenario. Additionally, the tap changer position of TRF1 was selected to be $tap = -5$. In each case, the active power of the AE was selected to be the necessary to reduce the active power export to zero.

The results of these load flows showed that for the biggest load hour the active power absorbed by the AE was 6.7 MW and the voltage in bus 9 was 1.01 p.u.. On the other hand, in the case of the

lowest load, the absorbed active power was 13.4 MW and the voltage of bus 9 1.04 p.u.. It should be noticed that, in both cases, the active power consumed by the AE is higher than its rated power; nevertheless, the purpose of this example is just didactic since the maximum generation scenario is quite improbable. The most important conclusion that can be inferred from this is that, depending on the loads state, the energy management power might satisfy the voltage regulation condition, i.e. $V_9 \leq 1.033$, or not. Hence, the energy management algorithm will chose the maximum AE power between the required for energy management (EM) and voltage regulation(VR), in order to fulfill both targets. Figure 6.7 shows the flowchart of the energy management algorithm:

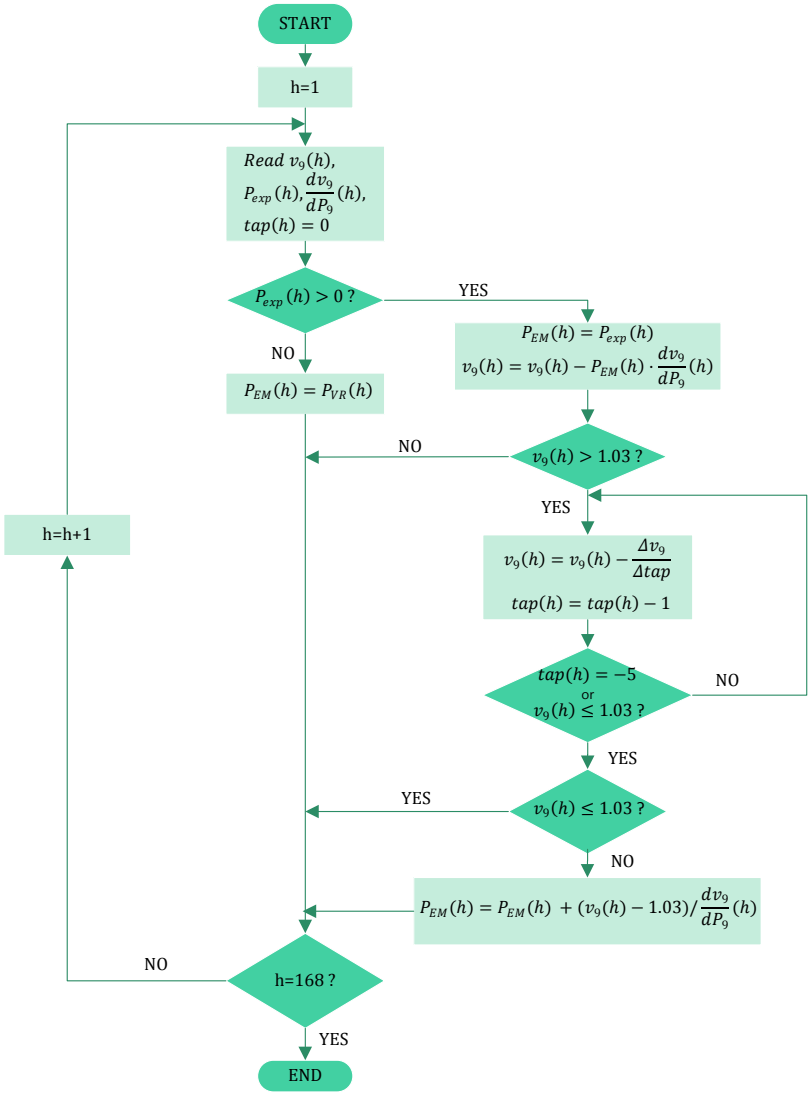

Figure 6.7: Flowchart of the energy management algorithm

The logical sequence of the energy management algorithm is now explained:

- For each hour of the week, V_9, dV_9/dP_9 and P_{exp} are read from the load flow estimation.
- P_{exp} is compared to zero. If it is smaller it means that there is active power import and there is no requirement for the AE to absorb power. In this case, the power absorbed by the AE should be the minimum necessary to bring the voltage below 1.033 p.u., therefore $P_{EM} = P_{VR}$. If it is bigger than zero, there is active power export and P_{EM} is selected

to be P_{exp} in order to cancel it. Consequently, the voltage V_9 is estimated to be reduced according to P_{exp} and dV_9/dP_9.

- In case of selecting $P_{EM} = P_{exp}$, V_9 is compared again to 1.033 p.u.. If it is equal or smaller there is no need to regulate the voltage and P_{EM} does not change. If it is bigger, the OLTC will try to lower the voltage until the tap position $tap = -5$ is reached or V_9 is smaller than its deadband, 1.033 p.u..
- After the OLTC actuates, V_9 is compared once again to 1.033 p.u.. If it is equal or smaller there is no need to regulate the voltage and P_{EM} does not change. If it is bigger, the AE absorbs the necessary extra power, in addition to P_{exp}, in order to bring V_9 down to 1.033 p.u.., according to V_9 and dV_9/dP_9.

The following remarks should be made regarding this algorithm. First, the power that the AE absorbs in order to cancel the power export is approximated to the actual export. Actually, an export will remain when selecting this power for the AE, since the losses are expected to decrease. Second, if the voltage remains higher than 1.033 p.u. after the AE absorbs the energy management power, the OLTC will use its capacity to bring down the voltage in order to avoid purchasing extra power for voltage regulation. Finally, the possibility of incurring in an undervoltage when absorbing energy management power is null, as showed in the didactic example provided above.

Maximum power function

Finally, the maximum power function (P_{MP}) is presented. As explained later in Section 6.1.4, there might be periods of low prices where running the AE at full power is beneficial for the DSO. Nevertheless, this option could lead to undervoltage and therefore it will not always be possible. Provided this, the maximum power function is defined as the maximum power that the AE can absorb in order to maintain the voltage above 0.967 p.u., while utilizing the tap changer up to the position $tap = 5$. As it can be appreciated, it is the opposite function of the voltage regulation algorithm. Figure 6.8 shows the flowchart of the developed algorithm:

The logical sequence of the maximum power algorithm is explained in the following:

- For each hour of the week, V_9 and dV_9/dP_9 are read from the load flow estimation.
- The AE's power is selected to be the rated, which implies $P_{MP} = 6.525$. V_9 updated accordingly to that power consumption increase.
- V_9 is compared with 0.967 p.u.. If it is equal or bigger there is no need to vary P_{MP}. If it is smaller, the OLTC will try to rise the voltage until the tap position $tap = 5$ is reached or V_9 is bigger than its deadband, 0.967 p.u..
- After the OLTC corrects the voltage, V_9 is compared again with 0.967 p.u.. If it is equal or bigger there is no need to vary P_{MP}. If it is smaller, the AE will decrease its active power consumption in the necessary amount in order to rise the voltage up to 0.967 p.u., according to V_9 and dV_9/dP_9.

Concluding the present subsection, it should be stated that, during each hour of the week, the following condition is always fulfilled, provided the definition of the three mentioned functions:

$$P_{VR}(h) \leq P_{EM}(h) \leq P_{MP}(h) \tag{6.2}$$

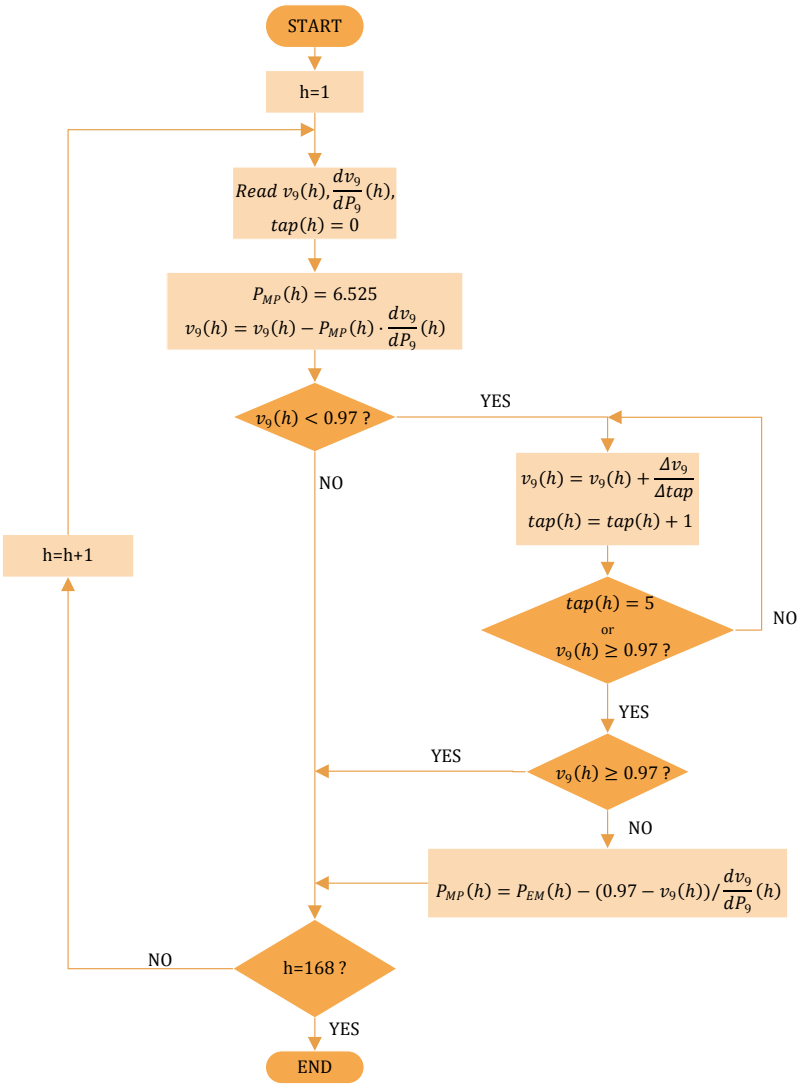

Figure 6.8: Flowchart of the maximum power algorithm

This fact will be decisive in order to understand the decision making rules presented in the following subsection.

6.1.4 Decision making

As stated in the introduction of the present section, the decision making determines the AE's power bid forwarded to the BRP, who aggregates bids from different players in the markets. The bid is a function of P_{VR}, P_{EM} and P_{MP}. An optimal bid could be done by means of solving a linear programming method, where the objective function would include maximizing the benefit of the DSO, having as constraints the voltage limits and the maximum and minimum power that the AE can absorb. This benefit can be described as the revenue from the produced hydrogen minus the investment in the electricity markets. Nevertheless, the DSO's benefit of obtaining energy management services cannot be explicitly calculated. For this reason, the bid is determined by means of implementing fuzzy logic decision, as further explained in the following.

Short introduction to fuzzy logic

A fuzzy logic system consists of nonlinear mapping of an input data vector into a scalar output, having the peculiarity of handling simultaneously numerical and linguistic data. Therefore, it has

a great potential for solving problems that are inherently complex to model [78]. In every fuzzy logic system, numerical inputs that belong to linguistic variables are assigned to linguistic terms in a certain degree of truth, normally within the range of [0,1]. For example, a spot price of 245 DKK/MWh can defined as 0.5 medium price and 0.5 high price. In this case, the price is the linguistic variable, high and medium are the linguistic terms and 0.5 is the membership μ_i. Membership functions are the responsible to convert the numerical prices into fuzzy ones, in the process known as fuzzification. The next step is converting the fuzzy inputs to numerical output by means of IF-ELSE rules. Continuing with the spot price example, the fuzzy rules could be stated as:

"If the spot price is high, then the purchased power is 1MW"

"If the spot price is medium, then the purchased power is 2MW"

In order to obtain a numerical output, a defuzzification is to be made. Normally, it is done by using the center of gravity method, shown in Eq. 6.3.

$$U = \frac{\sum_{n=1}^{i} \mu(u_i) \cdot u_i}{\sum_{n=1}^{i} \mu(u_i)} \tag{6.3}$$

Where u is the output and $\mu(u_i)$ is the membership of each variable u_i. Therefore, for the previous example, the purchased power (P) would be calculated as described in Eq. 6.4.

$$P = \frac{0.5 \cdot 1 + 0.5 \cdot 2}{1} = 1.5MW \tag{6.4}$$

It should be noticed that the fuzzy rules normally assign fuzzy outputs to the fuzzy inputs, instead of numerical outputs as it is stated in the example. Nevertheless, choosing directly the numerical output turns out to be a shortcut in the method and it fits better with the determination of the AE's power bid. The structure of a typical fuzzy logic system can be observed in Figure 6.9.

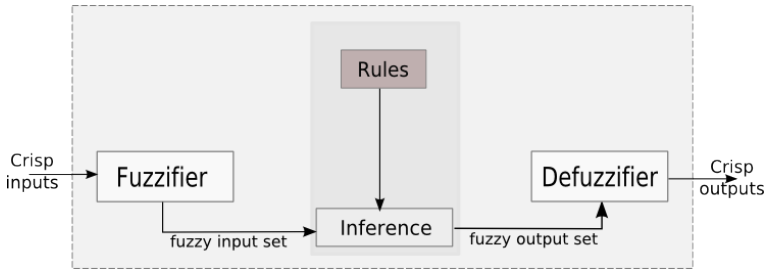

Figure 6.9: Typical structure of a fuzzy logic system [79]

The explained fuzzy logic theory has been obtained from [79] and [78], which the reader is suggested to check for further information. In the following the fuzzy logic system is presented for the case study purpose.

Fuzzy logic decision making

The numerical input values for the studied fuzzy logic system are the market prices. The different fuzzy terms assigned to the market price are low, medium and high. The membership functions

of the fuzzy terms are chosen to be triangular; as represented in figure 6.10. The equations of the membership functions can be found in Appendix D.

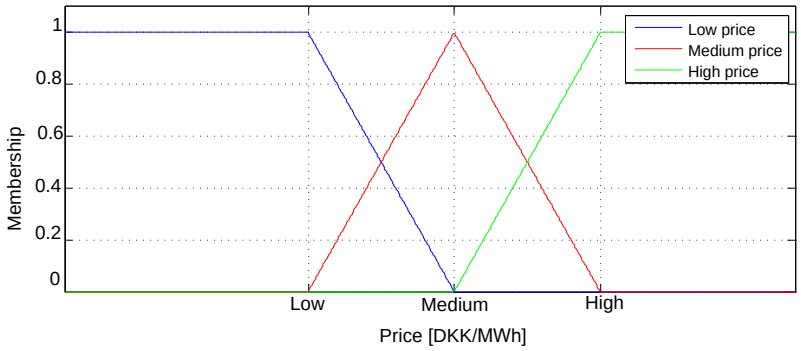

Figure 6.10: Membership functions for the market prices

A spot price analysis has been done for the DK1 area during year 2014. After statistically analysing the data, it was found that the average price was 228 DKK/MWh. Besides, approximately 50% of the spot prices during that year stayed within the range [200,260] DKK/MWh. Hence, 230 DKK/MWh was selected to be the medium price, 200 DKK/MWh the low price and 260 DKK/MWh the high price. It should be remarked that it has been assumed that the DSO can predict tendencies in the electricity prices and that the same price boundaries apply for the intraday and regulation markets. The flexibility of this method relies on the possibility that the DSO has to change the price boundaries according to its predictions.

The applied fuzzy rules are presented in Table 6.1, where the active power to purchase is associated to a fuzzy term, i.e. market prices. It should be recalled that, for a certain hour, it is always true that $P_{VR}(h) \leq P_{EM}(h) \leq P_{MP}(h)$, which helps to understand the applied rules.

Table 6.1: Fuzzy rules for the decision making

Low price	Medium price	High price
$P_{MP}(h)$	$P_{EM}(h)$	$P_{VR}(h)$

It is understandable that when the price is high the purchased power is the minimum and viceversa. It should be noted that the study case presents a big wind power penetration and the spot prices are correlated to the wind power, as shown in Figure 6.11.

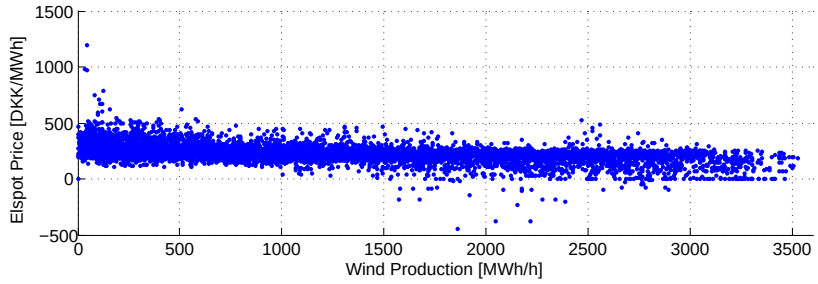

Figure 6.11: Correlation between spot price and wind power generation in DK1 area during 2014

It can be observed that a slight linear correlation exists between the elspot price and the wind production, since a low wind power production leads to higher prices and viceversa. This means that, if a big wind power generation leads to a drop of the spot price, the full capacity of the AE will be purchased in the market. If the opposite occurs, and an absence of wind produces an

increase of the spot price, the purchased power will be zero since the absence of wind will not produce overvoltage. Nevertheless, the method is prepared to withstand no correlation between wind power and market price since the OLTC provides flexibility in the voltage regulation.

For the defuzzification process, the center of gravity method is applied and the power bid is defined as in Eq. 6.5. It should be noticed that the memberships μ_{Low}, μ_{Med} and μ_{High} vary with the price according to Figure 6.10. In the following the constraints applied to the output of the fuzzy logic decision maker are presented.

$$P_{AE}(h) = \mu_{Low} \cdot P_{MP}(h) + \mu_{Med} \cdot P_{EM}(h) + \mu_{High} \cdot P_{VR}(h) \tag{6.5}$$

AE's power constraints

In the following, the power constraints imposed to the AE's power consumption are presented. Firstly, the temperature constraint is analyzed and subsequently, the constraints are applied to the results obtained in the fuzzy logic decision maker.

As stated in the conclusions of Chapter 4, the electrolyzer requires approximately 132 minutes to reach full power from cold start. This limitation might compromise the participation of the electrolyzer in the different markets, not reaching the scheduled active power set-point. In order to avoid this, three different solutions are proposed:

- Estimate the evolution of the temperature and limit the purchase of power for the operation hour $n+1$ according to the temperature of the device at the end of the hour n.
- Use additional sources of heat in order to maintain the temperature at the rated value, i.e. $80°C$.
- Operate the electrolyzer at the minimum power so its temperature does not go below $80°C$.

The first proposed solution has a complex execution, whereas the second does not appear in the literature and might present technical issues in its implementation; therefore, the last proposed solution is implemented in the present work.

It was found out that giving the electrolyzer module a set-point above 0.053 MW (0.067 MW including compression power), the temperature remained constant at $80°C$. Hence, a minimum of 1.005 MW, accounting for the 15 units, will be purchased in the spot market in order to keep the temperature at the rated and assure full regulation capability. However, it should be noticed that there is a minimum load requirement in order to produce hydrogen without compromising its purity. In [47] this minimum stated to be within the range 15-20%. The calculated minimum for the temperature limitation is of 14.9%; hence, it is assumed that the produced hydrogen will not possess any quality issue.

Once the fuzzy logic decision maker calculates the active power for each of the markets, upper and lower limitations have to be applied to the obtained values:

- For the spot market, the upper limitation is the rated capacity of the AE (6.525 MW) whereas the lower is the minimum power in order to maintain the AE's temperature at $80°C$ (1.005 MW).
- For the intraday market, the upper limitation is the difference between the rated capacity and the power traded in the spot market, whereas the lower capacity is zero.

- For the regulation market, the upper limitation is the difference between the rated capacity and the power traded in the spot and intraday markets, whereas the lower capacity is zero.

Figure 6.12 shows an example of a bid forwarded to the spot market for hour 27 during the winter week. The lower power limit, at 1.005 MW, is the result of the voltage regulation algorithm after adding the minimum power limitation, which is associated to the highest prices. The upper power limit, at 6.525 MW, is the result of the maximum power algorithm after adding the upper limitation, associated to the lowest prices. In between, around 2.7 MW, the result of the energy management algorithm can be appreciated, for a price of 230 DKK/MWh. The bid varies linearly between the highest and medium power and the medium and the lowest power.

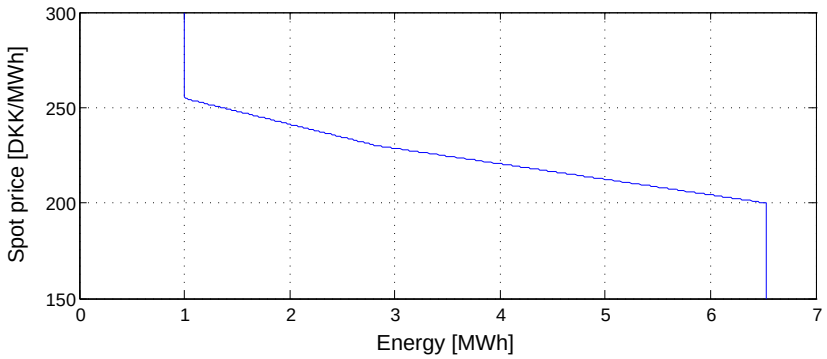

Figure 6.12: Bid in the spot market for hour 27, winter week

In the next subsection, the steady state results obtained with this scheduling method are presented.

6.1.5 Hourly results

As a conclusion of the market strategy, the steady state results are presented in order to give the reader an idea of the implications of the scheduling. Only the winter week will be taken into account, since the wind power generation is bigger and leads to more technical issues, as determined in Section 5.4. For carrying out the time sweeps, the OLTC has been switched to voltage remote control of bus 9 in order to emulate its dynamic behavior; however, the actual deadband cannot be emulated and the behavior is just an approximation. The analyzed technical results include the following: voltage in bus 9 [p.u.], active power export through TR1 [MW] and active power consumption of the AE [MW]. Figures 6.13, 6.14 and 6.15 show, respectively, the named variables.

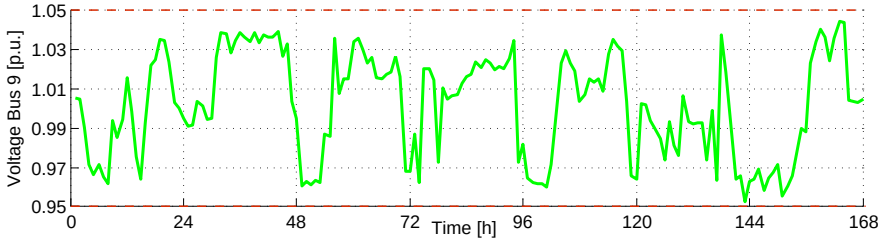

Figure 6.13: Voltage in bus 9 in the market case, winter week

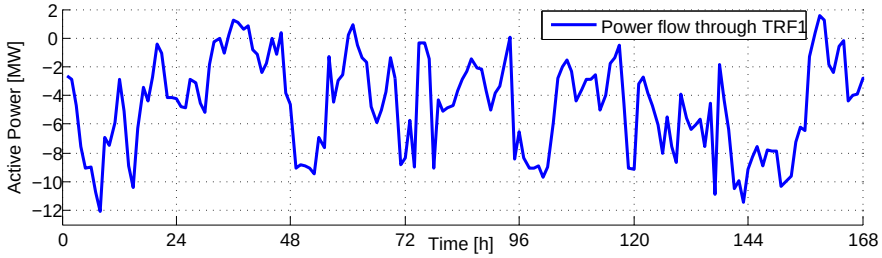

Figure 6.14: Active power export through TR1 in the market case, winter week

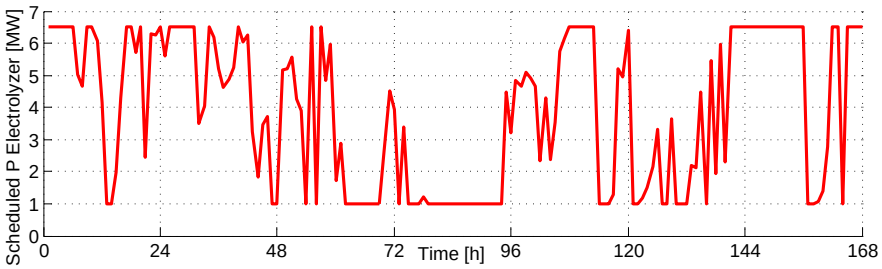

Figure 6.15: Alkaline electrolyzer's active power consumption in the market case, winter week

It can be observed that the voltage in bus 9 is kept within limits. However, during some hours it is out of the range [0.967,1.033] p.u., which was the target of the algorithm. Most part of the voltage values that are out of this range are close to it, as a result of the inaccuracy of the load flow estimation. Additionally, it should be noticed that the actual value of wind power generation was applied in the time sweep. Despite the estimation inaccuracies, the power export is just positive during a few amount of hours, in which the AE is not operated at full power. This fact is due to high prices in the market.

Regarding economical aspects, Table 6.2 shows the traded energy, the total price and the average price per MWh for both cases, throughout the winter week. As a reference, the results are compared with the ones obtained in Section 5.4. In order to distinguish the two cases, the first will be referred as the market case, whereas the second will be referred as the voltage regulation case. For the obtained results in the voltage regulation case, the AE is only expected to participate in the spot market. Furthermore, it should be noticed that the variables plotted in Figures 6.13, 6.14 and 6.15 have not been showed for the voltage regulation case. This decision responds to the different nature of the data, which comes from the dynamic simulation and includes other variables not considered as the dynamics of the tap changer and the DGs' reactive power.

Table 6.2: Economical comparison between the market and the voltage regulation cases

	Market Case	**Voltage Regulation Case**
Traded energy [MWh]	656.3	278.9
Total price [DKK]	148970	81083
Avg. price [DKK/MWh]	227.0	290.7

It can be observed that in the market case the electrolyzer purchases more energy, probably due to favorable prices and requirement for implementing energy management. Furthermore, selecting 1.005 MW as minimum power also contributes to increase the purchased energy. Due to the previous facts, the electricity bill is accordingly higher. On the other hand, the intelligent way of selecting the power according to the price leads to a significant decrease in the average price of the purchased electricity, even though the method is penalized by the minimum power

to purchase. The same market strategy was performed without including the minimum power constraint, giving the following results: the same energy was purchased (656.3 MWh) for a lower price, both absolute (125164 DKK) and average (190.7 DKK/MWh).

Concluding this section, the market strategy maintains the steady state voltage within the limits that were chosen for the algorithm during most part of the hours. Furthermore, it leads to an insignificant active power export through TR1 and the average price of the purchased MWh is reduced respect to the voltage regulation case. Nevertheless, these results have to be further tested in the dynamic simulation, where the voltage undergoes severe fluctuations and the tap changer tends to operate over the recommended limit. The dynamic analysis is presented in the following section; in which the obtained results are expected to be the final finding in the present master thesis.

6.2 Dynamic Analysis

In the present section, the AE scheduling method that was presented in Section 6.1 is tested in a dynamic simulation; the results are presented and compared to the ones obtained in Section 5.4. For this purpose, the AE control models have to be adapted to incorporate the scheduling; moreover, and a new coordination of the OLTC, DGs' reactive power and AE is discussed. In the following, the modification of the AE models is presented.

6.2.1 Adaptation of the AE control models

In the beginning of Section 4.5, the composite model of the control of the AE and the block diagram, where the active and reactive set-points are determined, were shown in Figures 4.28 and 4.29, respectively. When giving a schedule to the AE, the set-points should not be directly calculated from the voltage deviation with a V-P droop, but from a file containing the schedule. This will emulate the set-point signals sent by the DSO to the AE according to the schedule. Figure 6.16 shows the new composite frame which contains, in the Pe setpoint slot, a measurement file with the schedule. It should be noticed that the active power signal of the AE module (P_e) is not fed-back to the AE Dispatch slot anymore.

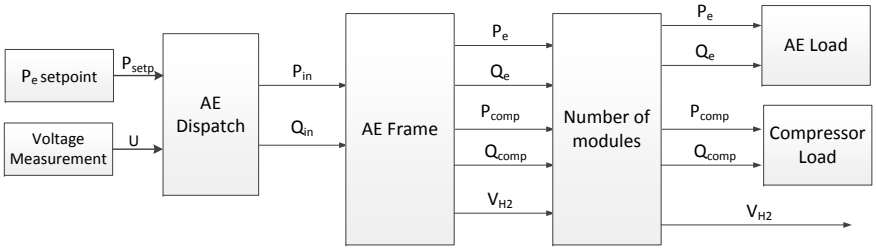

Figure 6.16: Modified AE's control composite frame for the market case

It might be noticed that the modifications are almost insignificant; however, the calculation of the set-points is completely different from the presented in Figure 4.29. Regarding the active power, it is achieved in a similar way as the primary control in a prime mover's governor: the set-point is fixed and slight power variations are added according to the frequency fluctuations, with a f-P droop. For the present case, the voltage is the equivalent to the frequency. For what concerns the reactive power control, the V-Q droop presented in Section 4.5 is maintained. The difference is that now it does not depend on the active power mismatch, hence the absence of the P_e signal feed back. This is due to the minimum active power that assures that the temperature will never go below $80°C$, leading to a quick response. Furthermore, the reactive power will "regain" an important role in the coordination, as explained in the next subsection. Additionally, the settings of the presented droops will be presented in the mentioned. Figure 6.17 shows the new set-point

calculation block diagram.

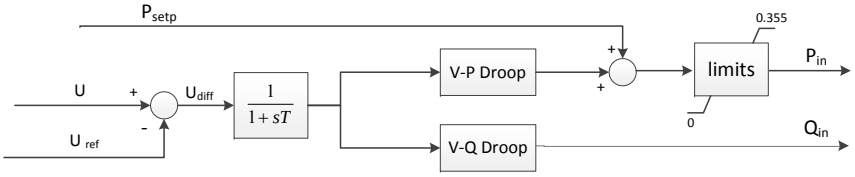

Figure 6.17: Modified AE's set-point calculation block for the market case

Discussion

It is interesting to mention that other control alternatives have been analyzed. The first alternative was simply giving the AE the schedule set-point, not allowing the reference to vary due to high voltage fluctuations. The result is a decreased voltage regulation capability, which leads to an excessive tap changing and to surpass the upper and lower voltage limits during a significant number of times.

The second alternative was adding a PI controller instead of the droop, so the power variations added to the schedule try to keep the voltage in the reference. The reference voltage is the obtained in the hour-ahead load flow estimation after adding the schedule of the AE. It would need to be added to the DSL block, represented in Figure 6.17, with an additional measurement file. The obtained voltage results are very promising, since the AE manages perfectly to follow the reference. However, the AE deviates excessively from the schedule and the reason is not only due to the wind power estimation inaccuracy. The fast dynamics of the AE normally keep the voltage within the range [0.967-1.033] p.u., as it is the purpose of the scheduling method, which is within the deadband range of the OLTC. Due to this fact, the OLTC does not have time to act provided its slow dynamics and the deadband range. Therefore, the AE is correcting more voltage than it was scheduled; specifically, the voltage it had scheduled plus the voltage that the OLTC was expected to correct plus the voltage variation due to the wind power estimation inaccuracy. It should be reminded that according to the different algorithms, the OLTC was expected to vary its tap position by ± 5 taps. Concluding, it should be added that this method would be really interesting if the OLTC was provided with communications that allowed a tap position set-point. Theoretically, the AE would be capable of correcting the power mismatch of the wind farm in the electricity market by increasing its own, achieving a really good voltage quality.

6.2.2 Coordination of the OLTC, DGs' reactive power and AE

As explained in the previous discussion, the OLTC undergoes an excessive tap changing when the dynamic voltage regulation capability of the electrolyzer is not available. This strategy was applied with the same coordination presented in Section 5.4, where the reactive power was only used to avoid over/under-voltages. The OLTC, as shown through Chapters 3-5, is a really useful device for providing voltage regulation; however, it possesses slow dynamics and the tap frequency changing is limited due to reliability issues. Therefore, it is not able to smooth the voltage fluctuations introduced by the wind power.

The question arising at this point is the following: how can the voltage be kept within admissible limits in the dynamic simulation, without incurring in excessive tap changing, big deviations from the schedule of the AE or reactive power import? Since all the voltage regulations assets appeared to be somehow constrained, the approach taken in this project is dismissing the constraint that appears to have less economical consequences for the DSO, which is not limiting the reactive power import.

In the coordination of the OLTC, reactive power of the DGs and active and reactive power of the AE, the reactive power will be activated the first, just when the voltage surpasses $1 \pm 0.023 p.u.$. The reactive power control strategy for the DGs, as explained in Section 3.2.3, follows a V-pf droop, whereas for the AE, it was previously explained that it follows a V-Q droop. In the case of a positive voltage deviation, approximately 50% of the reactive power capacity of all components is used when the voltage reaches 1.033 p.u.. On the other hand, in the case of a negative voltage deviation, all the regulating capacity is released when the voltage reaches 0.967 p.u.. The reason why only half of the reactive power capacity is used in case of positive voltage responds to the bigger capability that it has, as the reactive power output depends on the current active power output. Hence, during low voltage periods, the absence of DG generation leads to lack of reactive power to bring up the voltage. During high voltage periods, the reactive power capability is considerably higher; therefore, in order to limit its usage, the capability is limited. Regarding the operation of the OLTC, it starts acting when the voltage surpasses the $\pm 0.033 p.u.$ boundary. Finally, the AE's active power is varied just before a voltage issue arises, its deadband is set at $\pm 0.04 p.u.$ and it will act at full power when the voltage surpasses the allowed range. It should be noticed that in the AE's droop, the power output is a variation from schedule (ΔP_{AE}) and not an absolute value (P_{AE}). Figure 6.18 illustrates the explained coordination:

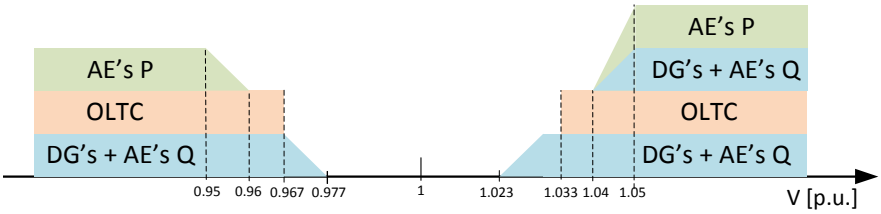

Figure 6.18: Modified coordination of the voltage regulation assets for the market case

It should be noticed that in the margin between the ranges [0.96-0.967]p.u. and [1.033-1.04]p.u. there is no power variations coming from the voltage regulation assets; this is done in order to allow the OLTC to act without influence. The reactive power that acts prior to the OLTC has the purpose of avoiding excessive tap changing, whereas the AE's active power and rest of reactive power that is deployed after $\pm 0.04 p.u.$ has the purpose of avoiding the consequences of the OLTC's slow dynamics. In the next subsection, the dynamic simulation results are analyzed. The simulation includes the schedule, the AE's model adaptations and the presented coordination.

6.2.3 Results

In this section the technical and economical results of the market strategy are presented. In the following, the technical results of this implementation are compared to the results obtained in Section 5.4. The results regarding the behavior of the grid are presented in Figure 6.19.

Plot a) shows the active and reactive power flow through Feeder 1. As in Chapter 5, positive values represent power transfer from the external grid to Feeder 1, whereas negative values represent power transfer from Feeder 1 to the external grid. Therefore, it can be observed that in this case the import of active power is significantly higher. This is due to the constant operation of the electrolyzers, as their priority is to follow the market prices. Furthermore, it has been calculated that the active power exports have been reduced from 38.1 MWh in the voltage regulation case to 23.3 MWh in the market case. This means that the implemented market strategy leads to an increased use of the local generation; i.e. a more effective energy management strategy. Regarding the reactive power, it can be appreciated that its consumption is higher, resembling the results obtained in Section 5.3. This a result of the important role that the reactive power has in order to maintain the voltage.

Plot b) presents the active and reactive power production and consumption from the CHP units and wind farm. The active power production remains unchanged, whereas the reactive power absorption from the DGs is higher, as it is used to correct undervoltage.

A significant change is seen in the behavior of the tap changer, shown in plot c). In this case the function of the OLTC is to correct undervoltage, as its position remains in the upper half, thus increasing the voltage of the secondary of TRF1. This is caused by the constant operation of the electrolyzer and the lower reactive power generation of the DGs. In Section 5.4 the OLTC operation was mainly restricted to overvoltage situations. Therefore the number of tap changes per week has increased, being 89.

Finally, plot d) illustrates the obtained voltage profiles of buses 1, 7 and 9. The voltage of all buses is within limits, except the two overvoltage peaks at hours 9 and 161, accounting for a total of 30 seconds. Even though the voltage during the voltage regulation case did not surpass the limits at any point, only 30 seconds of overvoltage during a whole week is admissible for a normal operation of the grid as showed in the recommendations presented in [76]. The overvoltages are caused by the sudden start-up of the CHPs and wind farm, while the position of the OLTC is above 0. The voltage average deviation $\overline{\Delta V}$ increases from 0.017 p.u to 0.020 p.u., which shows a bigger oscillation in the voltage for the market case.

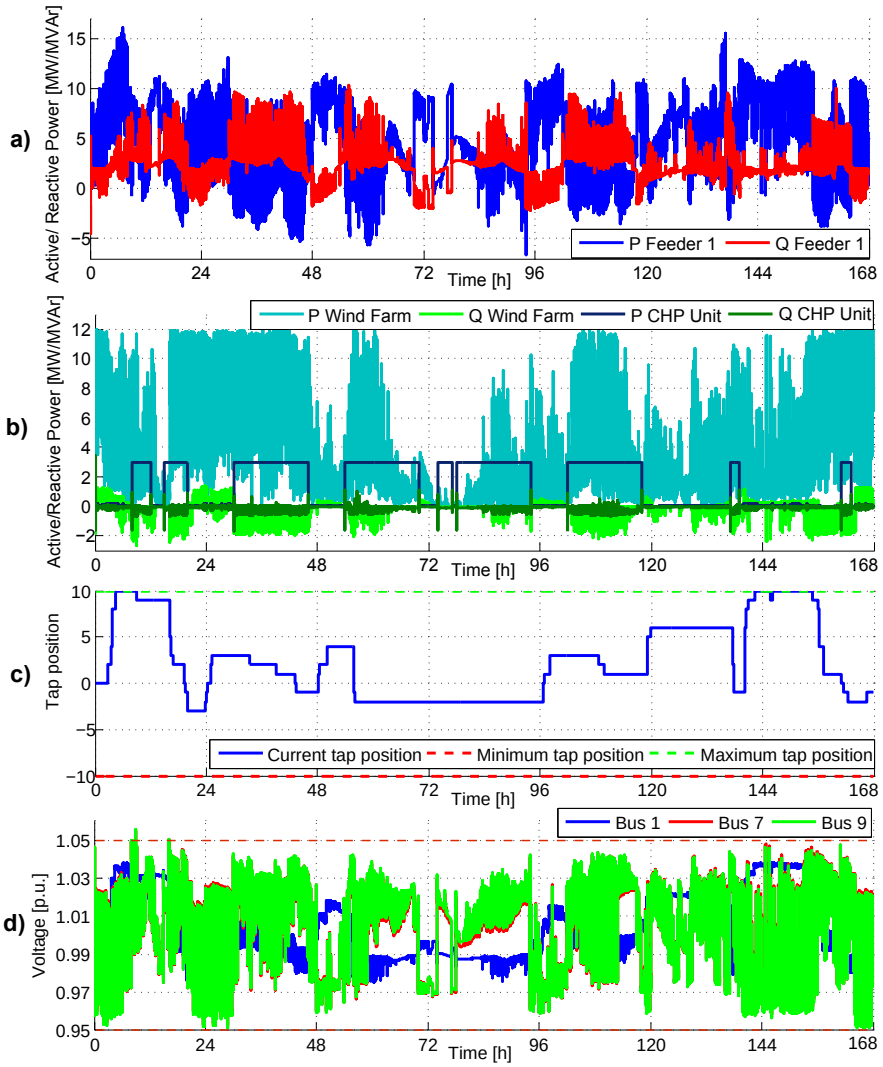

Figure 6.19: Results of the grid implementing the market strategy, during the winter week

The operation of one alkaline electrolyzer unit is specified in Figure 6.20. Plot e) shows the active power setpoint and the actual output. It can be seen that the active power setpoint of the electrolyzer is more steady, as its priority is to follow the predefined market, whereas the results presented in chapter 5 included a highly fluctuating setpoint in order to compensate voltage imbalances. A remarkable difference is seen in the actual active power output, since it is able to follow the setpoint. This improvement is due to the constant temperature of 80 °C, shown in plot g).

The reactive power setpoint and actual output are shown in plot f), where it is seen that its actual consumption and production range from 0.2 to -0.2 Mvar, rarely reaching the defined setpoint. This occurs as the regulation of the reactive power is limited by the converter capacity. Thus, it is observed that the reactive power is only used when the active power output is not maximum.

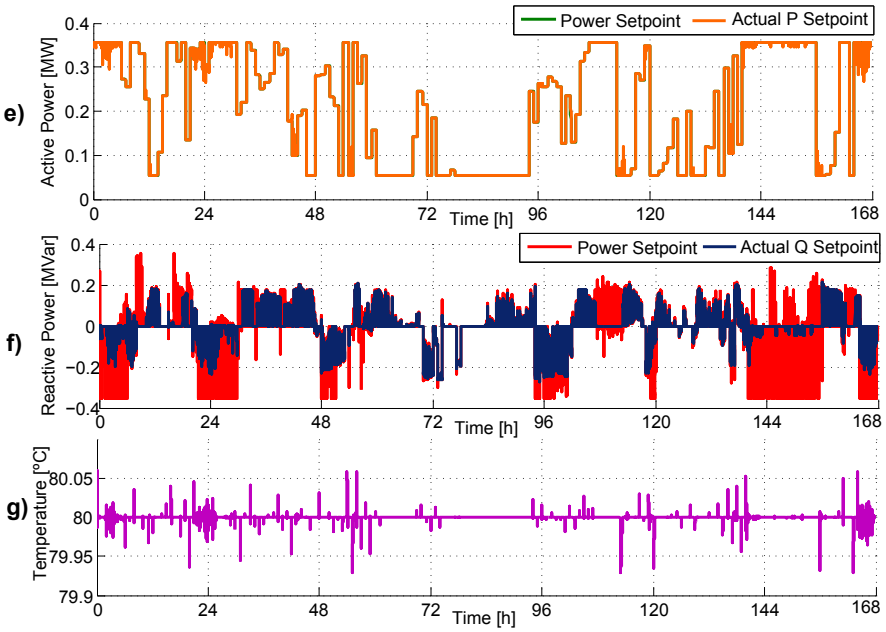

Figure 6.20: Alkaline Electrolizer parameters, during the winter week

Finally, the results of the produced hydrogen, hydrogen injected in the CHP's gas pipes, and volume variation in the storage, are presented in plots h), i) and j). The fact that the AE consumes more energy in the market case than in the voltage regulation case leads to a higher hydrogen surplus in the storage.

Table 6.3 summarizes the obtained results for the generation, load, active and reactive power import from Feeder 1 and its losses. For the market case, the values of load and active power import have increased due to the bigger energy consumption of the electrolyzers in the mentioned case. Regarding the value of reactive power import, it has increased respect to the voltage regulation case since it is the first to be activated in the coordination. Consequently, the value of the losses in the grid has increased in absolute terms; although, in relative comparison with the load it has decreased from 2.2% to 1.9%.

In the following, the economical results are presented, which include: the price of the purchased power of AE in the electricity market(s), the hydrogen produced and the average price of that hydrogen. It is interesting for the DSO to know the associated cost/benefit of running the electrolyzer. It should be noticed that in the economical results presented in Section 6.1, the electricity purchased for the AE was shown, but not the hydrogen. It should be recalled that the hydrogen production is only modeled for the dynamic simulation.

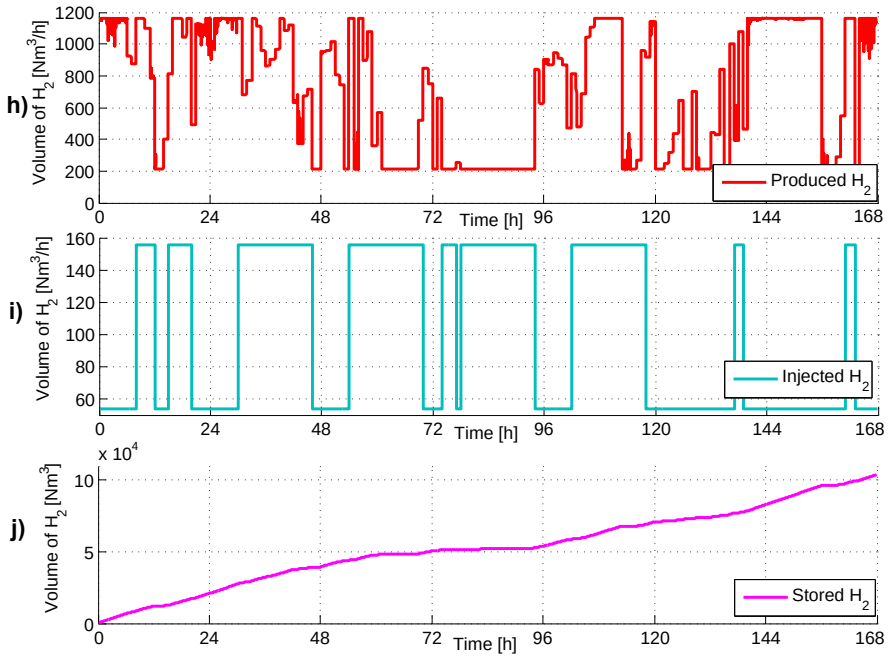

Figure 6.21: Hydrogen storage relevant variables, during the winter week

Table 6.3: Total generation, load, external grid import and losses comparison between the market and voltage regulation cases, winter week

	Market Case	**Voltage Regulation Case**
Generation [MWh]	1134.4	1134.4
Load [MWh]	1899.1	1521.7
P Import [MWh]	799.8	420.5
Q Import [Mvar]	437.6	343.4
Losses [MWh]	35.1	31.2

In order to determine the electricity bill in the market case, the consumption over the schedule has to be determined for each hour and purchased in the balancing market, as explained in appendix A. Prices for balancing power for consumption have been acquired for the studied period. The market penalization has to be added to the electricity bill resulting for the trade, which was been presented in Table 6.2. For the voltage regulation case the electricity bill is already calculated in the previously mentioned table; it is assumed that the device only participates in the spot market and does not have to purchase any balancing power.

Analyzing the power deviation from schedule of the AE throughout the week, it was calculated that the device had periods with an over consumption, accounting for 0.21 MWh, which cost an extra of 63 DKK in the balancing market. It is interesting to show that the periods of under consumption account for 0.37 MWh. It should be noted that the DSO purchased this energy in the markets but did not make benefit out of it. Table 6.4 shows the total price, produced hydrogen and average price of the hydrogen for the analyzed week. As it could be expected from the first results provided in 6.1, the price and energy in the market case are much bigger whereas the price of the produced hydrogen has been significantly reduced from 2.19 to 1.43 DKK/Nm^3.

6.3 Conclusions

In this final chapter a market strategy has been presented and evaluated, comparing the obtained technical and economical results with the ones from Section 5.4, known as voltage regulation case.

Table 6.4: Economical comparison between the market and the voltage regulation cases

	Market Case	**Voltage Regulation Case**
Total price [DKK]	149033	81083
Produced H2 $[10^3 Nm^3]$	104	37
Price H2 $[DKK/Nm^3]$	1.43	2.19

The main purpose of the market strategy is to reduce the price of the produced hydrogen and the positive power export through Feeder 1, while respecting the constraints of the grid. These have been accorded to be: voltage within limits, tap changes limitation and maintaining the reactive power import as low as possible. Table 6.5 shows a summary of the dynamic simulation results of both the market and the voltage regulation case. Where $\overline{\Delta V}$ represents the average voltage deviation, and $T_{|\Delta V|>0.05}$ represents the amount of time that the voltage limits were surpassed.

Table 6.5: Dynamic simulation results' summary for both market and voltage regulation cases, winter week

	Market Case	**Voltage Regulation Case**
$\overline{\Delta V}[p.u.]$	0.020	0.017
$T_{\|\Delta V\|>0.05}$ [s]	30	0
nº Tap Changes	89	61
Q Import [Mvar]	437.6	343.4
Losses [MWh]	35.1	31.2
P Export [MWh]	23.3	38.1
Produced H2 $[10^3 Nm^3]$	104	37
Total price [DKK]	149033	81083
Price H2 $[DKK/Nm^3]$	1.43	2.19

The results clearly show the advantages and the disadvantages of the market strategy. The hydrogen price and the active power export are clearly reduced, as these are the main purposes of the implemented strategy. On the other hand, some technical variables are compromised in the process. These are, mainly, the reactive power import and, in less magnitude, the tap changes and the losses. However, voltage quality remains almost unchanged, as the voltage limits are only surpassed for a few seconds. The increase of the reactive power import responds to the way the voltage regulation resources are coordinated; it should be reminded that the mentioned is activated the first. The reactive power import increase is the main responsible of the losses increment. Regarding the behavior of the OLTC, it undergoes more stress although within the reliability limits. Despite the reactive power releases the OLTC from been further stressed, the market strategy requires an increased use of its capability in order to allow a flexible operation of the AE, so the voltage regulation and market participation become more decoupled.

7 Conclusions and Future Work

7.1 Conclusion

The aim of this project was to analyze the capability of a Power to Gas system to provide energy management and voltage regulation services to distribution grids with high wind power penetration. The focus has been placed on the arising issues that the Distribution System Operator might encounter with the upcoming increase of renewable energy systems in medium voltage grids. For this purpose, a benchmark 20 kV distribution grid was modeled and analyzed in the DIgSILENT PowerFactory simulation software. The grid consists of two feeders, which include several buses with aggregated loads, a wind farm and a CHP plant. In addition to the electrical distribution grid, simplifications of the district heating and gas networks are introduced in order to evaluate their interactions with the electricity network. The district heating network represents the aggregated heat demand that the CHP plant has to provide, whereas the gas grid represents a hydrogen storage and the natural gas flow towards the CHP. The hydrogen is assumed to be injected to the CHP pipes with a volume limitation rate of 10%.

Firstly, the steady state behavior of the grid was analyzed taking into consideration two worst cases. These are (1): when the local generation, i.e. wind farm and CHP, are producing maximum power output and the loads are at their minimum, and (2): when there is no local production and the value of the demand is maximum. The results of the base case analysis, without any voltage regulation of grid assets, revealed that the most affected buses are 7 and 9 by overvoltage and undervoltage, respectively. It was found that the overvoltage in the first case surpassed the allowed voltage limits, determined by the grid codes. Further analysis in conducted with the application of an On-Load Tap Changer and reactive power compensation from the wind turbines and CHPs, as they are commonly used by system operators. However, their regulating capacity was not enough to rectify the high voltage deviation of the grid. Finally, the implementation of electrolyzers to bus 9 was assessed, as it is the most affected node regarding overvoltage. The size of the P2G system was determined to be the minimum in order to bring the voltage within allowed limits. Thus, 15 alkaline electrolyzer modules, accounting for a load of 6.525 MW, were implemented to the OLTC scenario. The reactive power capability of the CHP and wind turbines was not taken into account in the sizing. However, it was included in the coordination with the OLTC and electrolyzer, with the purpose of being activated during the dynamic simulations just before the voltage surpasses the allowed limits.

In order to incorporate the time-varying behavior of the assets in the grid, the dynamic models of its elements have been presented. As the CHP plant and the wind farm are assumed to be owned by private entities different from the DSO, they have been modeled as passive generators. Thus, the DSO can only regulate the power factor within the limits specified in the grid codes. More focus has been placed in those components where the DSO possesses full control for voltage regulation, i.e. OLTC and alkaline electrolyzer. Therefore, the most important implementations are the active and reactive control of the alkaline electrolyzer, the Line Drop Compensation model of the OLTC and the power factor control of the CHP plant and wind turbines. Within the models of the mentioned elements, decentralized voltage regulation coordination is implemented by adjusting the deadbands of the different voltage droops and OLTC controller. Furthermore, the heat and hydrogen production from both CHP and electrolyzer were modeled in order to represent long-term dynamic models of the district heating and gas network respectively.

The dynamic behavior of the case study grid was analyzed by assessing the coordinated voltage regulation strategy of the previously mentioned elements. Regarding the voltage profile, the

obtained results corroborated the findings in the steady state analysis. The OLTC, both on its own and together with the reactive power capability, is not able to bring the voltage within admissible limits. Furthermore, the excessive reactive power import when using the DG's reactive power capability leads to a significant increase of the grid losses. The voltage issues are corrected with the implementation of the P2G system which, at the same time, reduces the grid losses by almost 50% and demands negligible reactive power absorption for the DGs. Nevertheless, it was found that the regulating capacity of the alkaline electrolyzer was restricted by a low operating temperature which has resulted from stand-by periods. Furthermore, providing energy management services with the electrolyzer is not explicitly analyzed; the electrolyzer responds only to voltage signals and not to market prices. These issues are intended to be addressed by means of implementing an intelligent market strategy for the P2G system. Regarding the hydrogen, it was observed that the bleeding strategy cannot handle all the hydrogen that is produced during the process.

As the final contribution of this Master Thesis, a market strategy that copes with energy management and voltage regulation has been developed. Additionally, it was intended to respect the technical constraints faced during the dynamic analysis of the case study, namely: voltage limits, daily tap changes below the maximum recommended bounds and reactive power absorption. For this purpose, an algorithm that estimates the different power absorption requirements of the electrolyzer has been developed. Additionally, a fuzzy logic decision system that determines the bid in the market has been implemented and new control models and voltage regulation coordination have been proposed. The results from the dynamic simulation showed an increased consumption of the locally generated energy and a significant reduction in the cost of the produced energy, from $2.19 DKK/Nm^3$ to $1.43 DKK/Nm^3$. These benefits have been obtained by providing flexibility from the alkaline electrolyzer in the voltage regulation. However, the consequences are that the voltage is closer to the limits, the reactive power absorption increases significantly and the grid losses and tap changes present a slight increase. Nevertheless, the voltage remains within the recommended limits and the tap changes do not surpass the reliability constraint, which shows the feasibility of the proposed market strategy and validates the economical improvement it can provide. However, a cost benefit analysis has to be done to confirm the economical improvement of the presented strategy.

As the final conclusion of the present project, it can be stated that P2G is a very promising technology that might have an important role in the future integrated Danish energy system, which is expected to interconnect in a flexible way the electrical, district heating and gas networks to integrate more wind power. The scope of this work has been focused on the electrical behavior of the alkaline electrolyzer, which has been satisfactory tested to provide voltage regulation and energy management services under electricity market conditions. For this purpose, its operation has been coordinated with other typical voltage regulation elements of a distribution system, namely OLTC and reactive power. The findings of this project reveal that the DSO can decide the price to pay for using the local generation to produce hydrogen, while maintaining the voltage within the admissible limits. This fact gains importance when placed in the context of the future interconnection of the three energy sectors, where the decision of transforming electricity to gas/hydrogen will not only depend on the availability of the electricity but also on its price, which are not always correlated. Nevertheless, in order to implement the technology in a profitable way, a cost/benefit analysis must be done. At present, there is a just a limited amount of ongoing P2G projects, since the technology is expensive and still in research status. With a reduction of the capital, maintenance and operation costs in the near future, a P2G operation strategy, as the presented in this Master Thesis, could become economically feasible and open the possibility to new business opportunities.

7.2 Future Work

In this final section, the relevant tasks that could be interesting to explore as future work are presented.

- Operating the grid in meshed configuration: in the analyzed case study, the operation of the switches was disregarded and the topology of the grid was permanently radial. Nevertheless, the DSO might close the switches in order to optimize the load flow or improve reliability under contingency situations.
- Dynamic modeling of the wind turbines: their dynamic model, including the wind power curve, rotor blade angle control and shaft, could be presented in order to increase the accuracy of the active power generation.
- Grid state forecasting: in order to develop the market strategy, a load flow estimation was applied in order to represent the errors arising from a real forecast. Implementing a real grid state forecast method would help to assess, in a more realistic way, the technical and economical impacts of implementing the proposed market strategy.
- Forward hourly direct signals to the OLTC with the desired tap position: in Section 6.2 a PI controller was proposed in order to keep the voltage according to an hourly set-point. It was observed that the voltage profile is kept almost perfectly at the set-point and the AE could absorb the wind farm's deviations from schedule. In order to achieve this, an hourly tap position signal has to be forwarded to the OLTC.
- Dynamic modeling of the district heating and gas networks: the dynamic simulations have been carried out without incorporating the possible delays associated to the water and gas flow dynamics, which might have lead to further operational constraints.
- Additional hydrogen consumption: the proposed hydrogen injection strategy was not able to utilize all the production from the alkaline electrolyzers, hence, additional consumption is required. Possible solutions for its use include: direct connection of the AE to the transmission gas network, transforming the hydrogen into synthetic natural gas, include hydrogen mobility in the public transport of the area and including hydrogen-fired CHP plants.
- Intelligent temperature control method to allow complete disconnection of the electrolyzer: as shown in section 6.1, the electricity bill from participating in the electricity markets would be further reduced if the lower power constraint is not respected. This method would require predicting the temperature of the device and timing the start-up, which can take up to 132 minutes.

Appendices

A Electricity and Gas Market

In this chapter additional information about the electricity and gas market is presented.

A.1 Electricity Market

A.1.1 Roles

At present, these are the players in the electricity market and their role [15]:

- Producers: they generate electricity and offer it in Nord Pool or directly to the trader through a bilateral agreement.
- Traders: they purchase electricity in Nord Pool or directly from a producer and resell it to the end customers in the retail market.
- Balance Responsible Parties (BRPs): these players are committed with the TSO to balance their production and/or consumption according to the schedule. Every producer and trader needs to have an agreement with a BRP or be one by themselves.
- End users: they purchase electricity from the traders in the retail market. Since 2003 the retail market is deregulated and each end user can chose his own supplier.
- TSO: as mentioned in 2.1.1, Energinet.dk is the Danish TSO. It is mainly responsible of assuring the security of supply and balancing of the system.
- Grid companies: they operate the distribution grids and control the metering data of the BRPs, which they have to provide to the TSO.
- Companies with supply obligation: those who supply end users that have not exercised their right to choose another supplier.
- Nord Pool: common wholesale market for Denmark, Norway, Sweden and Finland.

A.1.2 Wholesale Markets

As stated previously in A.1.1, most part of the agreements take place via Nord Pool, where the offers from producers and traders meet through a bidding system that assures balance for each hour. In Nord Pool the day ahead (Elspot) and the intraday (Elbas) submarkets take place, which are coordinated in order to assure balance between production and consumption at every hour. In order to support these markets in real time, regulating power is purchased and sold in the Nordic Regulation Power Market.

A.1.2.1 Elspot Market

Before 12:00 noon the day before operation, producers and traders submit their bids to Nord Pool. These bids represent how much a player is willing to buy/purchase at a certain price. Figure A.1 represents the forwarded bid from a player in charge of both production and consumption parts, for a certain hour:

This means, for instance, that the player will buy 50 MWh if the price is 1.5 EUR cents/kWh or lower, sell according to the ramp if the price is between 2.25 and 2.5 EUR cents/kWh or produce

Figure A.1: Forwarded bid from a Norwegian player [17]

exactly his own demand if the price is between 2 and 2.25 cents/kWh [17]. In Nord Pool all the forwarded bids, as the previously mentioned, are placed together forming an aggregated curve, for both production and demand. Regarding the Danish production aggregated curve, local CHP production and wind power (P0 production) have low marginal cost due to feed-in tariffs [15]. This fact, together with their extended implementation in Denmark, leads to a drop in the spot price, when the P0 production is high, and to price volatility. An example of production and demand aggregated curves is presented in Figure A.2:

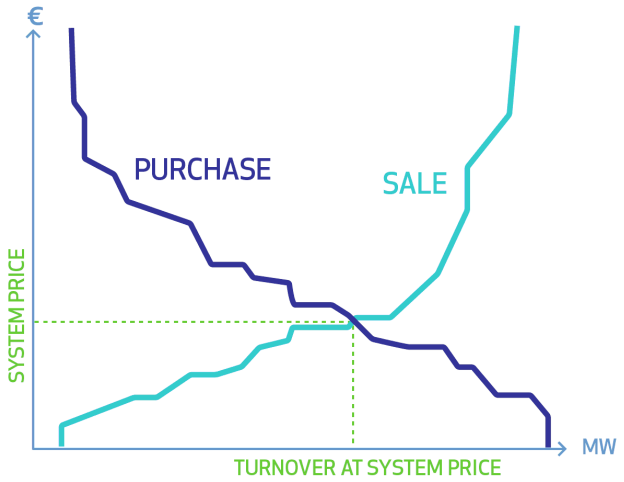

Figure A.2: Aggregated curves and formation of spot price [16]

It can be appreciated that both curves intersect in one point, which will determine the turnover and the system price (spot price) at which the system will be balanced. This date is published at 13:00 pm the day before operation. The spot price represents the marginal cost of the most expensive production bid activated and the marginal cost of the cheapest demand bid activated. This price will apply for the activated bids in all areas participating in Nord Pool. However, the interconnections or transmission lines within a country might be congested. In this case, the market is split in different pricing areas where the ones with overproduction become low price areas, due to the inability to balance with demand bids over the spot price. The opposite applies for the underproduction case. Denmark has two pricing areas, DK1 (West Denmark) and DK2 (East Denmark), connected by the Great Belt HVDC transmission line [16] [15].

Not all the agreements are settled directly via Nord Pool. There are also some bilateral agreements, like the future contracts, in which producers and traders agree to exchange a certain amount of power at a certain price, during a selected period. Both place the agreed amount of exchanged energy in Nord Pool but they have to compensate each other for the difference between the agreed

price and the spot price. Therefore, these agreements are also called financial contracts [17].

A.1.2.2 Elbas Market

After the closing of the spot market and prior to the hour of operation changes in production or consumption might occur. An improved wind forecast or an unexpected outage in a power plant can alter the programmed balance of the system. Therefore, a market in order to correct imbalances in the spot market is required. This is the main function of the intraday or Elbas market, which closes one hour before operation. These agreements can also be done bilaterally between players within the same pricing area [15].

A.1.2.3 Reserves and Regulating Power Market

Further imbalances, after the hour before and during the hour of operation, might occur. These are caused by the BRPs' forecasting imprecision or due to some outage, as explained previously. These imbalances are corrected by the TSO, Energinet.dk, buying upwards or downwards regulating power. There are different kinds of regulating power, namely: primary regulation, secondary regulation and tertiary regulation or manual reserves. Figure A.3 shows the amount and time of the activated power for the three types of regulation:

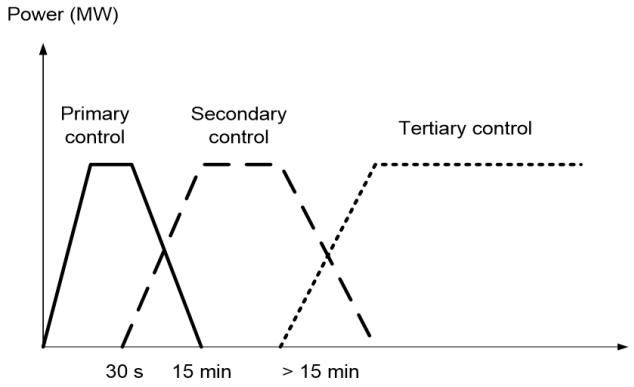

Figure A.3: Activated power and time of activation for primary, secondary and tertiary regulation [80]

Primary regulation comprises a frequency dependent control, which activates when frequency goes beyond 49.9-50.1 Hz (normal regulation) and 49.5-50.5 Hz (disturbance regulation). Secondary regulation has longer activation times. This reserves can be activated manually, in the most part of the cases in the Nordic countries, or automatically, with the Load Frequency Control (LFC). Primary and secondary regulation are not traded in the regulation market. Tertiary regulation is always activated manually and it involves the activation of more amount of power compared to the primary and secondary regulation. The main requisite is that the power is activated before 15 minutes after request. For this purpose Denmark has an automatic system for offer entry and offer activation, while other countries activate their reserves via telephone call. Tertiary reserves are, at the moment, the only ones present in the Nordic Regulation Power Market [18].

Tertiary regulation services are offered by the Balance Service Providers (BSPs), which are normally BRPs. Their offers have to enter the market not later than 17:00 pm the day before operation, but they are susceptible to be modified until one hour before delivery. Minimum and maximum amount of power offered is 10 and 50 MW, respectively. Energinet.dk purchases these offers from the BSPs via the regulation power market or via bilateral agreements (i.e. future contracts). Activation of bids goes from the cheapest to the most expensive, provided that there are no bottlenecks that prevent power transfer. The price for all activated bids will be the price of the most expensive activated bid. If there are bottlenecks the market will be split in different

pricing areas, as in the case of the spot market. In order to ensure security of supply, Energinet.dk needs to have available enough reserves for balancing the system in case of failure of the bigger production unit. For this purpose, it signs future contract with the BRPs. The reserve market is where the TSO and the BRPs meet for closing these kind of contracts [19].

As previously stated in A.1.1, imbalances are produced by the BRPs. This means that their actual production or consumption, measured during the hour of operation, differs from the schedule. Therefore, if they have a negative imbalance this energy has to be bought from the Energinet.dk. If the imbalance is positive Energinet.dk will buy the surplus. This energy is bough in the so called balancing market and it is closely related to the regulation power market. Whereas the regulating power is used in order to correct the systems' imbalance the balancing power is purchased or sold in order to correct the BRPs' individual imbalance. The price to pay by the BRPs for the balancing power depends on the direction of the system's imbalance: if the system has a surplus, the BRPs that incur in a negative imbalance (correcting the system's surplus) buy this energy at spot price. If they have a surplus (further increasing the system's imbalance) Energinet.dk buys this energy at the upwards regulating power price. The opposite applies in case of a power deficit in the system. P0 producers are exempt to pay for balancing power. Through the PSO tariff Energinet.dk covers the cost of the P0 producers' imbalances, as well as the feed-in tariffs that apply for them as explained in A.1.2.1 [19] [18].

A.2 Gas Market

The Danish gas market is liberalized since 2004, which means that every customer is free to choose its supplier. Nowadays there are three available capacity trading facilities [81]:

A.2.1 GasPoint Nordic

GasPoint Nordic is the wholesale market of natural gas. It was previously known as NordPool Gas, however, since 2012 it is owned by Energinet.dk and thus the name was changed. The gas exchange is offered in several time ranges: for the next day, the next month, within a day, within a weekend, within a month and finally physical delivery in Denmark and Germany. It is an anonymous and real-time electronic system where traders can place purchase and bids on sales all the time.

A.2.2 Gas Transfer Facility (GTF)

GTF is a virtual trading facility operated by Energinet.dk. It enables intra-day gas trading among shippers before and during a day. GTF is only the mean of communication between the shippers and it is a free service.

A.2.3 PRISMA

PRISMA is the facility that enables trading gas capacity across European borders. The shippers can participate in four different auctions: day-ahead, per month, per quarter of a year or per year. There are three entry-exit points in Denmark: Nybro, the entry point of the gas from the North Sea; Ellund, in the border with Germany; and Dragør, in the border with Sweden.

B Data of the Elements of the Grid

In this appendix all the data used to model the elements of the grid is summarized. This includes data for the grid elements, such as lines, transformers, loads and generation units; followed by the data used for the alkaline electrolyzer model; the adaptation of the CHP model; and finally the gas storage in the grid.

B.1 Network Elements Data

The elements of the grid such as lines, transformers and loads are specified in the following tables.

In table B.1 the positive sequence parameters are defined respectively for the two types of lines used in this project.

Table B.1: Positive sequence parameters of the two different types of lines

Type of line	**R [Ω/km]**	**X [Ω/km]**	**B [$\mu S/km$]**	I_{nom} **[A]**
Overhead Line (OHL)	0.510	0.366	3.17	500
Underground Cable (UC)	0.343	0.274	47.5	500

The following table specifies the type and length of each line:

Table B.2: Line data

From bus	**To bus**	**Line type**	**Distance** $[km]$
1	2	OHL	2.82
2	3	UC	3.42
3	4	UC	0.61
4	5	UC	0.56
5	6	UC	1.54
6	7	UC	0.24
7	8	UC	1.67
8	9	UC	0.32
9	10	UC	0.77
10	11	UC	0.33
11	4	UC	0.49
3	8	UC	3.45
12	13	OHL	0.389
13	14	OHL	2.99
14	8	OHL	2.00

In table B.3 the data for the different transformers of the grid is given:

Table B.3: Transformer data [48], [82]

Parameters	Feeder TRF	CHP TRF
Rated Power	25 MVA	3.3 MVA
Rated Voltage HV	110 kV	20 kV
Rated Voltage LV	20 kV	6.3 kV
Copper losses	-	28 kW
No-load losses	-	4 kW

The rated values of the residential loads are specified in table B.4, the apparent power and the power factor are specified for each bus. Additionally the type of load profile used is specified.

Table B.4: Rated power, power factor and profile type of the residential loads of the system

Bus	Apparent Power [MVA]	Power Factor	Load Profile Type
1	15.300	0.98	1
3	0.285	0.97	2
4	0.445	0.97	3
5	0.750	0.97	1
6	0.765	0.97	2
8	0.805	0.97	3
10	0.490	0.97	1
11	0.340	0.97	2
12	15.300	0.98	1
14	9.215	0.97	3

The following table summarizes the rated power and power factor values of the industrial loads:

Table B.5: Rated power and power factor of the industrial loads of the system

Bus	Apparent Power [MVA]	Power Factor
1	5.100	0.98
3	0.265	0.85
7	1.500	0.85
9	2.200	0.97
10	0.080	0.85
12	5.280	0.95
13	0.350	0.85
14	0.390	0.85

Table B.6 specifies the constant impedance and power coefficients that have been used to model each load of the grid. These have been calculated using the values presented in Table 3.2, the rated power of the loads and the type of load.

Table B.6: Constant power and impedance coefficients of the loads of the grid

	Summer		Winter	
Bus	**P [%]**	**Z [%]**	**P [%]**	**Z [%]**
1	75.25	24.75	55	45
3	82.9	17.1	68.91	31.09
4	67	33	40	60
5	67	33	40	60
6	67	33	40	60
7	100	0	100	0
8	67	33	40	60
9	100	0	100	0
10	71.63	28.37	48.42	51.58
11	67	33	40	60
12	75.47	24.53	55.39	44.61
13	100	0	100	0
14	68.37	31.63	42.44	57.56

B.2 Wind Turbine Data and Modeling

In order to adapt the obtained wind speed, measured at 12 meters [72], to the hub height of the chosen wind turbine a conversion method has been applied, as graphically described in Figure B.1.

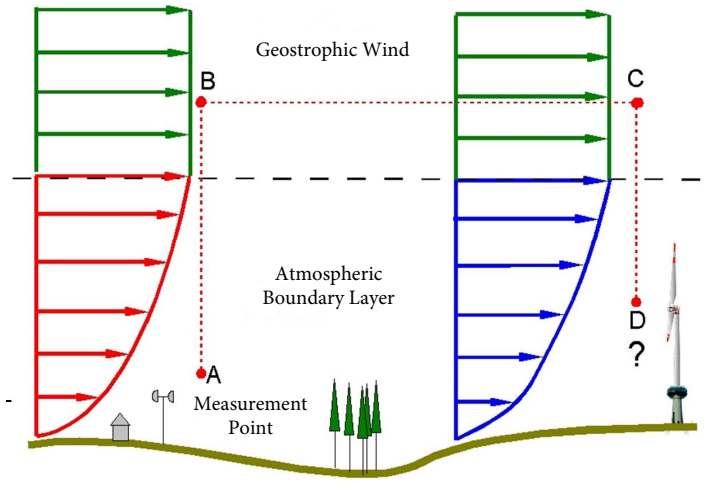

Figure B.1: Wind speed measurement extrapolation to hub height [73]

As observed, the measurement in point A has to be extrapolated to the point B at $1000m$, where the wind is not influenced by the surface objects. From point B to point C the geostrophic wind is assumed to be constant whereas from point C to point D the extrapolation is done in the same way as for points A and B. Theses extrapolations can be expressed with the same equation [83]:

$$v_2(z2) = v_1(z1) \cdot \frac{ln\left(\frac{z_2}{z_0}\right)}{ln\left(\frac{z_1}{z_0}\right)} \tag{B.1}$$

Where v_1 and v_2 are the wind speeds at heights z_1 and z_2, respectively, and z_0 is the roughness length. The measurements were taken in an environment of flat buildings, assuming a z_0 of $1.5m$.

The wind turbines are assumed to be located in the countryside, in a place surrounded with high crops and scattered objects. Therefore, z_0 is assumed to be $0.25m$ [84]. The final conversion is expressed with the following equation:

$$v_2(67m) = v_1(12m) \cdot \frac{ln\left(\frac{1000}{1.5}\right)}{ln\left(\frac{12}{1.5}\right)} \cdot \frac{ln\left(\frac{67}{0.25}\right)}{ln\left(\frac{1000}{0.25}\right)} = v_1(12m) \cdot 2.108 \tag{B.2}$$

B.3 CHP Models and Data

The different elements of the gas turbine model are presented in this section. First, the data of the generator is presented in Table B.7:

Table B.7: Gas turbine generator data

Parameters	Value
Rated power $[MW]$	3.3
Rated voltage $[kV]$	6.3
Stator resistance $[p.u.]$	0.0504
Stator reactance $[p.u.]$	0.1
Synchronous reactance d-axis $[p.u.]$	1.5
Synchronous reactance q-axis $[p.u.]$	0.75
Transient reactance d-axis $[p.u.]$	0.256
Sub transient reactance d-axis $[p.u.]$	0.168
Sub transient reactance q-axis $[p.u.]$	0.184
Transient time constant d-axis $[s]$	0.53
Sub transient time constant d-axis $[s]$	0.03
Sub transient time constant q-axis $[s]$	0.03
Inertia time constant $[s]$	0.54

The block diagram of the gas turbine governor of the CHP is shown in Figure B.2 and its data is summarized in Table B.8. The speed governor is a so called (GAST) which uses a P controller to regulate the speed drop of the CHP.

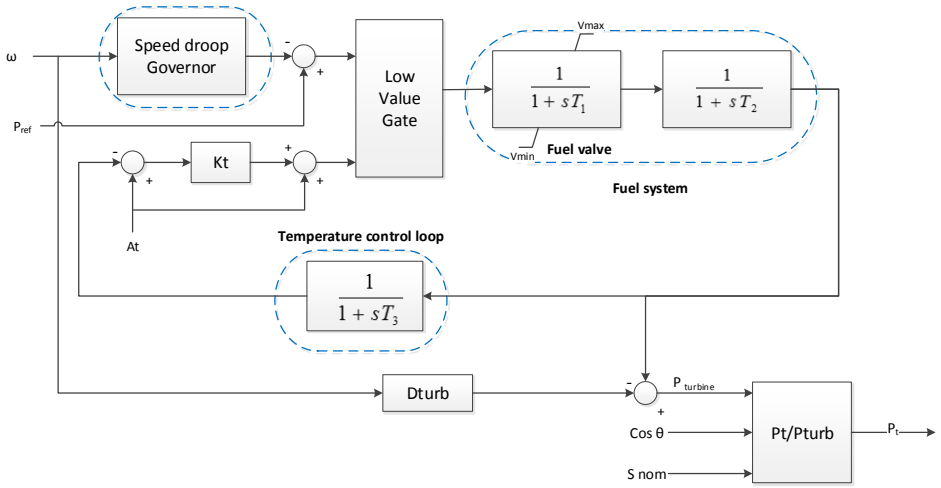

Figure B.2: Block diagram of the GAST governor of the CHP [82]

Table B.8: Gas turbine governor data

Parameters	Value
Speed droop $[p.u.]$	0.05
Controller time constant $[s]$	0.4
Actuator time constant $[s]$	0.1
Compressor time constant $[s]$	3.0
Ambient temperature load limit $[p.u.]$	1.0
Turbine factor $[p.u.]$	2.0
Controller min. output $[p.u.]$	0.0
Controller max. output $[p.u.]$	1.0

Figure B.3 shows the block diagram of the excitation system of the gas turbine, a so called AVRESAC5A, slightly modified to receive the v_{cs} command from the power factor controller.

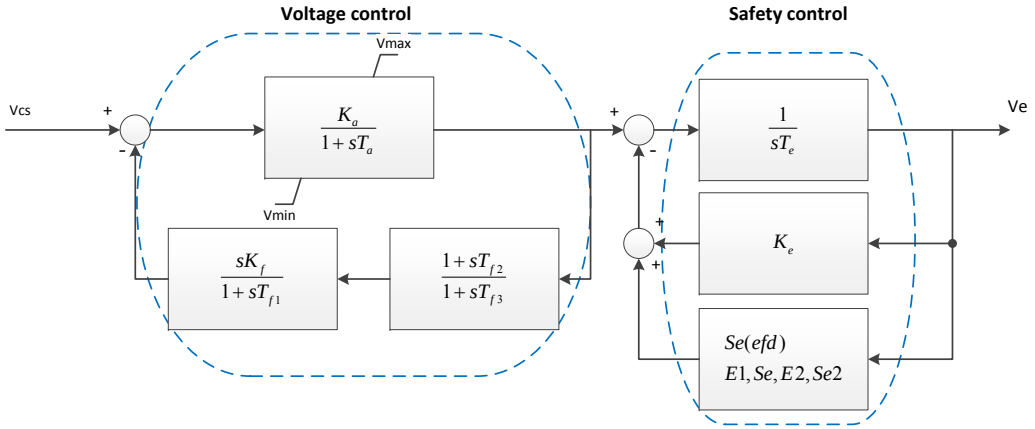

Figure B.3: Block diagram of the excitation system of the CHP [82]

In table B.9 the data of this excitation system is given:

Table B.9: Excitation system data

Parameters	Value
Measurement Delay $[s]$	0.02
Controller Gain $[p.u.]$	200
Controller Time Constant $[s]$	0.03
Exciter Constant $[p.u.]$	1.0
Exciter Time Constant $[s]$	0.8
Stabilization Path Gain $[p.u.]$	0.05
Stabilization Path 1th Time Constant $[s]$	3
Stabilization Path 2th Time Constant $[s]$	0
Stabilization Path 3th Time Constant $[s]$	0
Saturation Factor 1 $[p.u.]$	3.13
Saturation Factor 2 $[p.u.]$	1.73
Saturation Factor 3 $[p.u.]$	4.18
Saturation Factor 4 $[p.u.]$	4
Vmin Controller Output Minimum $[p.u.]$	-20
Vmax Controller Output Maximum $[p.u.]$	20

Figure B.4 shows the implemented power factor controller. According to the actual power factor and the set-point, the reactive power error is measured. This error is forwarded to a PI controller, which determines the excitation voltage set-point v_{cs}. This control has been created from a similar one proposed in [82].

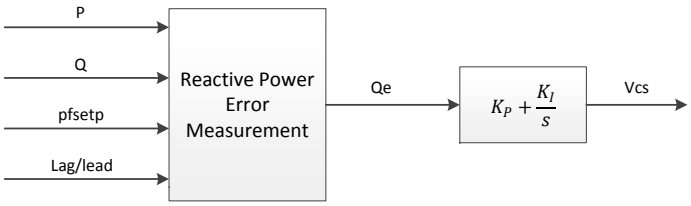

Figure B.4: Block diagram of the power factor controller

The following table shows the estimated number of houses in the buses that include residential loads. This was used to determine the aggregated heat demand.

Table B.10: Estimated number of households in each bus

Bus	nº households
1	5433
3	100
4	156
5	264
6	174
8	129
10	172
11	119
12	5433
14	3239

B.4 Alkaline Electrolyzer Model

The parameters used to model the alkaline electrolyzer are defined in this section. Where Table B.11 defines its general parameters.

Table B.11: General parameters of the alkaline electrolyzer

Parameter	Value
Rated Power $[kW]$	355
Operation Pressure $[bar]$	7
Number of Cells	180
Max. DC voltage $[V]$	342
Min. DC voltage $[V]$	257.4
Max. Operation Temperature $[°C]$	80
C_t $[J/°C]$	$5.38e^6$
$m_{e_{max}}$ $[kg/s]$	1.3
$m_{e_{min}}$ $[kg/s]$	0.01

C Additional Simulations

In this appendix the additional simulations carried out in order to analyze the grid are presented. The following 4 figures present the time sweep simulations carried out in order to determine the worst case scenario and at the same time the hour of the week that is most affected by voltage drop.

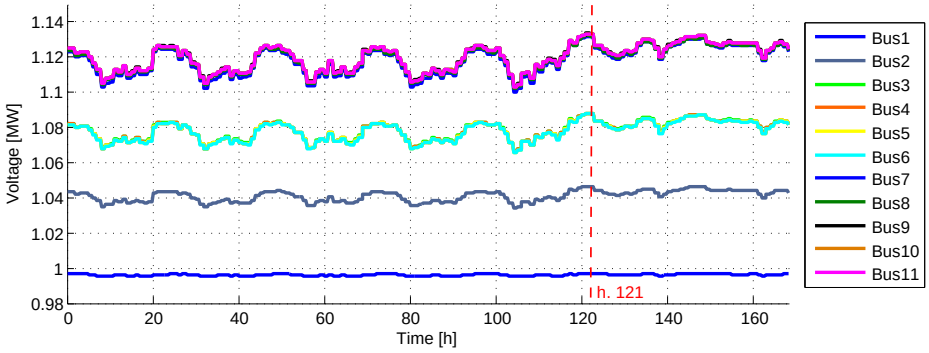

Figure C.1: Time sweep representation of the bus voltages using winter profile at Case 1

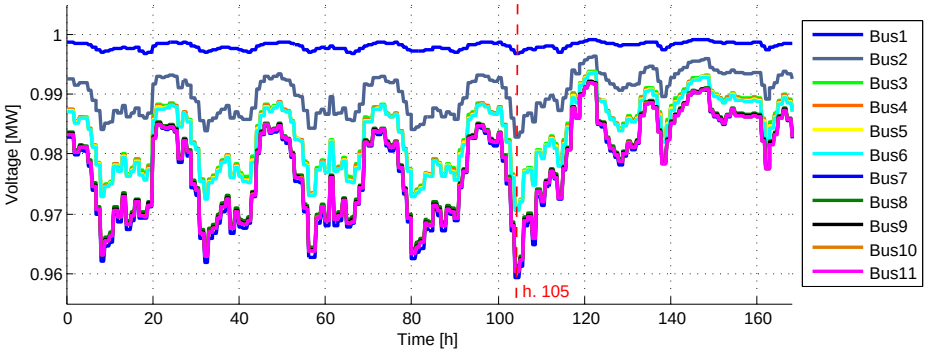

Figure C.2: Time sweep representation of the bus voltages using winter profile at Case 2

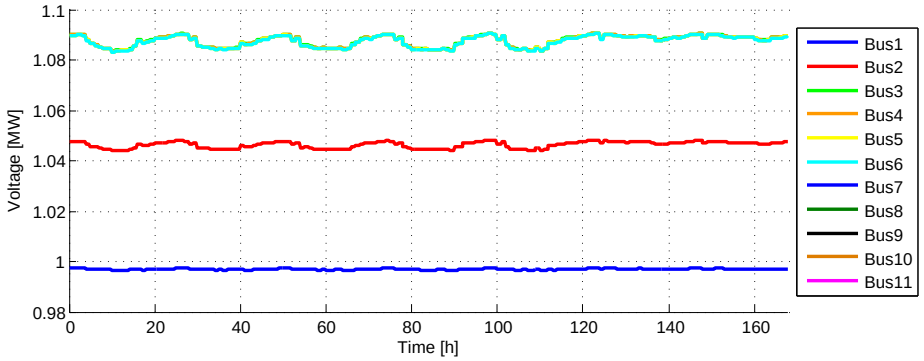

Figure C.3: Time sweep representation of the bus voltages using summer profile at Case 1

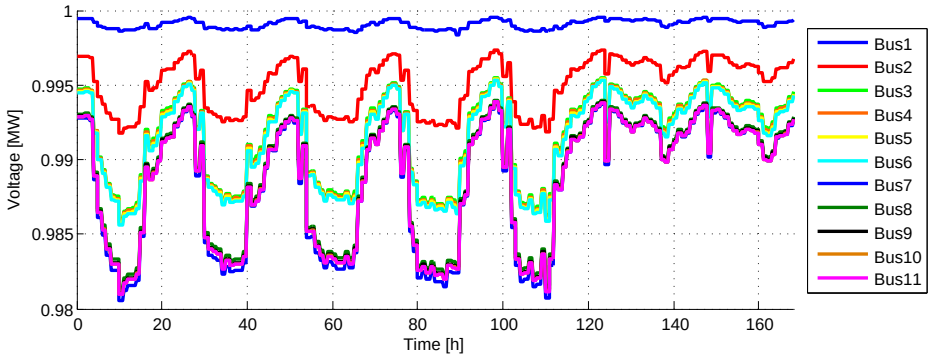

Figure C.4: Time sweep representation of the bus voltages using summer profile at Case 2

D Fuzzy Logic Controller

The equations that defined the membership functions are the following:

$$\mu_{Low} = \begin{cases} 1 & \text{for} \quad price < 200 \\ \frac{price-230}{200-230} & \text{for} \quad 200 \leq price \leq 230 \\ 0 & \text{for} \quad price > 230 \end{cases} \tag{D.1}$$

$$\mu_{Medium} = \begin{cases} 1 & \text{for} \quad price < 200 \\ \frac{price-200}{230-200} & \text{for} \quad 200 \leq price \leq 230 \\ \frac{price-260}{230-260} & \text{for} \quad 230 \leq price \leq 260 \\ 0 & \text{for} \quad price > 260 \end{cases} \tag{D.2}$$

$$\mu_{High} = \begin{cases} 0 & \text{for} \quad price < 230 \\ \frac{price-230}{260-230} & \text{for} \quad 230 \leq price \leq 260 \\ 1 & \text{for} \quad price > 260 \end{cases} \tag{D.3}$$

Bibliography

[1] Danish Government, "Energy strategy 2050," www.ens.dk, 2011, accessed 02-10-2014.

[2] Danish Ministry of Climate, Energy and Building, "Smart grid strategy - the intelligent energy system of the future," www.kemin.dk, 2013, accessed 02-10-2014.

[3] M. Brower, "Wind energy forecasting," www.awstruepower.com, 2011, accessed 02-10-2014.

[4] HyUnder, "Assessment of the potential, the actors and relevant business cases for large scale and long term storage of renewable electricity by hydrogen underground storage in europe," http://www.hyunder.eu/, 2013, accessed 02-10-2014.

[5] E. EASE, "Joint ease/eera recommendations for a european energy storage technology development roadmap towards 2030," http://www.ease-storage.eu/, 2013, accessed 02-10-2014.

[6] C. Baumann, R. Schuster, and A. Moser, "Economic potential of power-to-gas energy storages," in *European Energy Market (EEM), 2013 10th International Conference on the*, May 2013, pp. 1–6.

[7] M. Korpas and T. Gjengedal, "Opportunities for hydrogen storage in connection with stochastic distributed generation," in *Probabilistic Methods Applied to Power Systems, 2006. PMAPS 2006. International Conference on*, June 2006, pp. 1–8.

[8] Øystein Ulleberg, T. Nakken, and A. Eté, "The wind/hydrogen demonstration system at utsira in norway: Evaluation of system performance using operational data and updated hydrogen energy system modeling tools," *International Journal of Hydrogen Energy*, vol. 35, no. 5, pp. 1841 – 1852, 2010. [Online]. Available: http://www.sciencedirect.com/science/article/pii/S0360319909016759

[9] L. Ramirez-Elizondo, G. Paap, and N. Woudstra, "The application of a fuel cell-electrolyzer arrangement as a power balancing set-up in autonomous renewable energy systems," in *Power Symposium, 2008. NAPS '08. 40th North American*, Sept 2008, pp. 1–8.

[10] M. Little, M. Thomson, and D. Infield, "Electrical integration of renewable energy into stand-alone power supplies incorporating hydrogen storage," *International Journal of Hydrogen Energy*, vol. 32, no. 10–11, pp. 1582 – 1588, 2007, {EHEC2005}. [Online]. Available: http://www.sciencedirect.com/science/article/pii/S0360319906005209

[11] H. K. Jacobsen and S. T. Schröder, "Curtailment of renewable generation: Economic optimality and incentives," *Energy Policy*, vol. 49, no. 0, pp. 663 – 675, 2012, special Section: Fuel Poverty Comes of Age: Commemorating 21 Years of Research and Policy. [Online]. Available: http://www.sciencedirect.com/science/article/pii/S030142151200585X

[12] T. Zhou, D. Lu, H. Fakham, and B. Francois, "Power flow control in different time scales for a wind/hydrogen/super-capacitors based active hybrid power system," in *Power Electronics and Motion Control Conference, 2008. EPE-PEMC 2008. 13th*, Sept 2008, pp. 2205–2210.

[13] Energinet.dk, "Danish transmission system ultimo 2014," http://energinet.dk/EN/ANLAEG-OG-PROJEKTER/Generelt-om-elanlaeg/Sider/default.aspx, 2014, accessed 14-10-2014.

[14] Nordic Energy Regulators, "Economic regulation of electricity grids in nordic countries," http://www.nordicenergyregulators.org/wp-content/uploads/2013/02/Economic_regulation_of_electricity_grids_in_Nordic_countries.pdf, 2011, accessed 15-10-2014.

[15] Energinet.dk, "Regulation a: Principles of the electricity market," http://www.energinet.dk, 2007, accessed 17-10-2014.

[16] Nord Pool, "Day-ahead market - elspot," http://www.nordpoolspot.com, 2014, accessed 17-10-2014.

[17] A. P. Houmøller, "The nordic power exchange nord pool and the nordic model for a liberalised power market," http://www.nordpoolspot.com, 2003, accessed 17-10-2014.

[18] Nordic Energy Regulators, "Harmonising the balancing market," http://www.nordicenergyregulators.org, 2010, accessed 17-10-2014.

[19] Energinet.dk, "Regulation c2: The balancing market and balance settlement," http://www.energinet.dk, 2008, accessed 17-10-2014.

[20] D. E. A. Energinet.dk, "Smart grid in denmark 2.0," http://www.energinet.dk, 2012, accessed 17-10-2014.

[21] D. Dansk Energi, "District heating - danish and chinese experiences," http://dbdh.dk/publications/, 2013.

[22] Danish Energy Agency, "Energy statistics 2012," http://www.ens.dk, 2014, accessed 19-10-2014.

[23] U.S. Environmental Protection Agency, "Catalog of chp technologies," http://www.epa.gov/chp/documents/catalog_chptech_full.pdf, 2014, accessed 19-10-2014.

[24] Danish Energy Agency, "Energy statistics 2013," http://www.ens.dk, 2014, accessed 09-01-2015.

[25] C. S.-M. S. N. S. Hans F. Ravn, Jannik Riisom, "Modelling danish local chp on market conditions," http://orbit.dtu.dk/en, 2004, accessed 19-10-2014.

[26] 2G CENERGY®, "2g cenergy®monthly newsletter," http://www.2g-cenergy.com/pdfs/2G-CENERGY-News-Letter-June-2013.pdf, 2013, accessed 19-10-2014.

[27] Danish Energy Agency, "Oil and gas production in denmark 2013," http://www.ens.dk/sites/ens.dk/files/energistyrelsen/Nyheder/2014/oil_and_gas_production_in_denmark_2
2014, accessed 16-10-2014.

[28] Energinet.dk, "Shipping gas in denmark," http://www.energinet.dk/SiteCollectionDocuments/Engelske2008, accessed 16-10-2014.

[29] ——, "Structure of the natural gas system," http://energinet.dk/EN/ANLAEG-OG-PROJEKTER/Generelt-om-gasanlaeg/Sider/Naturgassystemets-opbygning.aspx, 2013, accessed 16-10-2014.

[30] ——, "Illustration of the gas system in denmark," http://energinet.dk/Flash/Forside/UK/index.html?target=gas_net, 2014, accessed 16-10-2014.

[31] Energi Styrelsen, "Gas storage in denmark," http://www.ens.dk/node/1971, 2008, accessed 17-10-2014.

[32] A. Ursua, L. Gandia, and P. Sanchis, "Hydrogen production from water electrolysis: Current status and future trends," *Proceedings of the IEEE*, vol. 100, no. 2, pp. 410–426, Feb 2012.

[33] M. Bodner, A. Hofer, and V. Hacker, "H2 generation from alkaline electrolyzer," *Wiley Interdisciplinary Reviews: Energy and Environment*, 2014.

[34] Øystein Ulleberg, "Modeling of advanced alkaline electrolyzers: a system simulation approach," *International Journal of Hydrogen Energy*, vol. 28, no. 1, pp. 21 – 33, 2003. [Online]. Available: http://www.sciencedirect.com/science/article/pii/S0360319902000332

[35] F. Barbir, "Pem electrolysis for production of hydrogen from renewable energy sources," *Solar Energy*, vol. 78, no. 5, pp. 661 – 669, 2005, solar Hydrogen. [Online]. Available: http://www.sciencedirect.com/science/article/pii/S0038092X04002464

[36] H. Görgün, "Dynamic modelling of a proton exchange membrane (pem) electrolyzer," *International Journal of Hydrogen Energy*, vol. 31, no. 1, pp. 29 – 38, 2006. [Online]. Available: http://www.sciencedirect.com/science/article/pii/S0360319905000868

[37] M. Ni, M. K. Leung, and D. Y. Leung, "Technological development of hydrogen production by solid oxide electrolyzer cell (soec)," *International Journal of Hydrogen Energy*, vol. 33, no. 9, pp. 2337 – 2354, 2008. [Online]. Available: http://www.sciencedirect.com/science/article/pii/S0360319908002255

[38] M. Zahid, J. Schefold, and A. Brisse, "High-temperature water electrolysis using planar solid oxide fuel cell technology: a review," *Hydrogen and Fuel Cells, Fundamentals, Technologies and Applications, Wiley-VCH, Weinheim*, pp. 227–242, 2010.

[39] S. Studer, S. Stucki, and J. D. Speight, *Hydrogen as a Fuel*. Wiley-VCH Verlag GmbH & Co. KGaA, 2008. [Online]. Available: http://dx.doi.org/10.1002/9783527622894.ch3

[40] D. Haeseldonckx and W. D'haeseleer, "The use of the natural-gas pipeline infrastructure for hydrogen transport in a changing market structure," *International Journal of Hydrogen Energy*, vol. 32, no. 10–11, pp. 1381 – 1386, 2007, {EHEC2005}. [Online]. Available: http://www.sciencedirect.com/science/article/pii/S0360319906004940

[41] K. Altfeld and D. Pinchbeck, "Admissible hydrogen concentrations in natural gas systems," www.gas-for-energy.com, 2013, accessed 02-03-2015.

[42] A. Godula-Jopek, *Hydrogen Production: by Electrolysis*. Wiley-VCH, 2015.

[43] BioCat, "Biocat project - power to gas via biological catalysis," http://biocat-project.com, 2012, accessed 20-10-2014.

[44] "Denmark turns excess wind power into gas via hydrogenics tech," *Fuel Cells Bulletin*, vol. 2014, no. 3, pp. 8 – 9, 2014. [Online]. Available: http://www.sciencedirect.com/science/article/pii/S1464285914700823

[45] "Largest power-to-gas facility now operating with hydrogenics tech," *Fuel Cells Bulletin*, vol. 2013, no. 7, pp. 9 –, 2013. [Online]. Available: http://www.sciencedirect.com/science/article/pii/S1464285913702645

[46] E. P. Mainz, "Energie park mainz," http://energiepark-mainz.de/, 2015, accessed 10-05-2015.

[47] I. de Cerio Mendaza, B. Bak-Jensen, and Z. Chen, "Alkaline electrolyzer and v2g system digsilent models for demand response analysis in future distribution networks," pp. 1–8, June 2013.

[48] K. Rudion, A. Orths, Z. Styczynski, and K. Strunz, "Design of benchmark of medium voltage distribution network for investigation of dg integration," in *Power Engineering Society General Meeting, 2006. IEEE*, 2006, pp. 6 pp.–.

[49] T. A. Short, *Electric Power Distribution Handbook*. CRC Press, 2014.

[50] H. L. Willis, *Electrical Transmission and Distribution Reference Book*. Raleigh, 1997.

[51] X. Guo, J. Du, and C. Qi, "Study and application of switching operation of 10kv lines ring network in urban power distribution network," in *Electricity Distribution (CICED), 2012 China International Conference on*, Sept 2012, pp. 1–6.

[52] Insero Energy, "Yearly heat demand of a residential area (confidential)," 2014, accessed 21-02-2015.

[53] L. Zhang, "Comparison of district heating systems used in china and denmark," 2013, accessed 30-03-2015.

[54] S. Varmeværk, "Skagen varmeværk Årsrapport 2013/2014," http://www.skagen-varmevaerk.dk/media/1668229/Regnskab-2013-2014.pdf, 2014, accessed 20-01-2015.

[55] ——, "Skagen varmeværk operation," http://www.emd.dk/desire/skagen/, 2014, accessed 20-01-2015.

[56] G. L. Basso, L. de Santoli, A. Albo, and B. Nastasi, "{H2NG} (hydrogen-natural gas mixtures) effects on energy performances of a condensing micro-chp (combined heat and power) for residential applications: An expeditious assessment of water condensation and experimental analysis," *Energy*, vol. 84, no. 0, pp. 397 – 418, 2015. [Online]. Available: http://www.sciencedirect.com/science/article/pii/S0360544215002893

[57] Energinet.dk, "Gaskvalitet dag for dag," www.energinet.dk, 2015, accessed 21-04-2015.

[58] X. Liu, A. Aichhorn, L. Liu, and H. Li, "Coordinated control of distributed energy storage system with tap changer transformers for voltage rise mitigation under high photovoltaic penetration," *Smart Grid, IEEE Transactions on*, vol. 3, no. 2, pp. 897–906, June 2012.

[59] F. A. Viawan, A. Sannino, and J. Daalder, "Voltage control with on-load tap changers in medium voltage feeders in presence of distributed generation," *Electric Power Systems Research*, vol. 77, no. 10, pp. 1314 – 1322, 2007. [Online]. Available: http://www.sciencedirect.com/science/article/pii/S0378779606002446

[60] C. Reese, C. Buchhagen, and L. Hofmann, "Voltage range as control input for oltc-equipped distribution transformers," in *Transmission and Distribution Conference and Exposition (T D), 2012 IEEE PES*, May 2012, pp. 1–6.

[61] ABB, "Vacuum tap-changers – a logical progression for transformers," http://www.abb.co.uk/cawp/seitp202/25c7292e2d5e19d7c1257b2700515948.aspx, 2014, accessed 01-03-2015.

[62] Energinet.dk, "Teknisk forskrift tf 5.9.1 systemtjenester," www.energinet.dk, 2012, accessed 17-05-2015.

[63] ——, "Technical regulation 3.2.5 for wind power plants with a power output greater than 11 kw," http://www.energinet.dk, 2010, accessed 01-03-2015.

[64] EPA, "Appendix 2 - technical description of the tymien wind farm project," http://www.dnv.com, 2004, accessed 01-03-2015.

[65] Energinet.dk, "Technical regulation for thermal power station units of 1.5 mw and higher," http://www.energinet.dk, 2008, accessed 01-03-2015.

[66] A. Kiprakis and A. Wallace, "Maximising energy capture from distributed generators in weak networks," *Generation, Transmission and Distribution, IEE Proceedings-*, vol. 151, no. 5, pp. 611–618, Sept 2004.

[67] P. Vovos, A. Kiprakis, A. Wallace, and G. Harrison, "Centralized and distributed voltage control: Impact on distributed generation penetration," *Power Systems, IEEE Transactions on*, vol. 22, no. 1, pp. 476–483, Feb 2007.

[68] P. Kundur, *Power Systems Stability and Control*. McGraw-Hill Professional, 1994.

[69] Energinet.dk, "Gaspris guiden," http://gasprisguiden.dk/Home/Companies, 2014, accessed 23-04-2015.

[70] ENS, "Data on operating and decommissioned wind turbines," http://www.ens.dk/node/2233/register-wind-turbines, 2014, accessed 20-01-2015.

[71] Vestas, "V80-2.0mw brochure," http://www.vestas.com/Files/Filer/EN/Brochures/090821_Product-brochure-V80-2.0MW-06-09-EN.pdf, 2014, accessed 20-01-2015.

[72] Aalborg University, "Photovoltaic systems research programme at department of energy technology," www.pv-systems.et.aau.dk, 2013, accessed 20-01-2015.

[73] U. S. Kühn, M., "Windenergienutzung 1," 2011, (in German).

[74] ABB, "Type vrltc™ load tap changer," https://library.e.abb.com/public/173e5fcdb7514c7b85257c900062a3bf/Tech2014, accessed 01-03-2015.

[75] X. Liu, A. M. Cramer, and Y. Liao, "Reactive-power control of photovoltaic inverters for mitigation of short-term distribution-system voltage variability," in *T D Conference and Exposition, 2014 IEEE PES*, April 2014, pp. 1–5.

[76] D. Energi, "Rekommandation 21 - spændingskvalitet i mellemspændingsnet," www.dafu.dk, 2011, accessed 30-04-2015.

[77] M. M. H. H. S. S. E. G.-L. R. S. L. S. X. G. L. G. G. D. F. B.M. Hodge, D. Lew and J. Dobschinski, "Wind power forecasting error distributions: An international comparison," NREL, 2012, accessed 30-03-2015.

[78] J. Mendel, "Fuzzy logic systems for engineering: a tutorial," *Proceedings of the IEEE*, vol. 83, no. 3, pp. 345–377, Mar 1995.

[79] Z. C. Yildiz, "A short fuzzy logic tutorial," Bilkent University, 2010, accessed 30-03-2015.

[80] I. G. S. Peter Thais Bjerregaard, "Impact assessment of integrating thermostatic loads and plug-in electric vehicles in future low voltage distribution grids," AAU digital library, 2013, accessed 17-10-2014.

[81] Energinet.dk, "The danish gas market," http://www.energinet.dk/EN/GAS/Det-danske-gasmarked/Sider/default.aspx, 2013, accessed 19-10-2014.

[82] P. Mahat, "Control and operation of islanded distribution system," http://vbn.aau.dk, 2010, accessed 01-03-2015.

[83] J. T. Robert Gasch, *Wind Power Plants - Fundamentals, Design, Construction and Operation*. Springer, 2012.

[84] Meteorological Resource Center, "Terrain classification in terms of effective surface roughness length," http://www.webmet.com/met_monitoring/663.html, 2002, accessed 20-05-2014.

[85] Vatenfall, "Frontpage image 1," http://powerplants.vattenfall.com/mitte, accessed 20-05-2015.

[86] L. Pipeline, "Frontpage image 2," http://www.leaguepipeline.ca/about-us/, accessed 20-05-2015.

[87] RockPortCap, "Frontpage image 3," http://www.rockportcap.com/our-portfolio, accessed 20-05-2015.